ABSTRACT

SAFAYET, ALI MD. Distributed Voltage Regulation and Grid Connection of Renewable Energy Sources. (Under the direction of Dr. Iqbal Husain).

The installation of renewable energy sources in grid connected distribution network introduces several challenges on power reliability that include voltage regulation and fault protection. When residential renewable energy sources like rooftop solar panels produce more energy than the local load demand, voltage rises and reverse power phenomena occurs. The overvoltage issues can be controlled by proper management of reactive power flow**.** A novel reactive power scheduler algorithm for the distributed voltage regulation with PQ inverters is proposed in this dissertation. Based on the reactive power scheduler, a new approach to achieve voltage regulation in grid connected distribution system through appropriate control of the renewable energy systems has been developed. PQ inverters capable of producing the reactive power are used to either achieve local voltage regulation or deliver the reactive power commanded by the voltage regulator loop located in the upper hierarchy of the grid management system. The proposed PQ scheduler and PQ inverters will work harmoniously in the local distribution controller with minimum communication interface. The proposed control techniques achieve efficient utilization of the PQ inverters with maximum efficiency. Also a reactive power management based on inverter's capacity and sensitivity to the critical bus in a radial low voltage distribution network is presented. This method improves the voltage regulation of distributed system with high penetration of renewable energy sources while utilizing the inverter's reactive power capacity more efficiently.

The control of the real and reactive power for grid connected distributed sources requires accurate phase information of the utility voltage. For large renewable energy systems such as solar and onshore or offshore wind or wave energy there is a need for synchronization with the frequency and phase angle of the single phase or three-phase grid. The most commonly used and easily implementable algorithm for grid synchronization is the phase locked loop (PLL) technique. The power grid in rural distribution side is not clean and typically contaminated with imperfections like harmonics. For three-phase systems, the other imperfection of the grid that needs to be eliminated before feeding the grid voltage to PLL is the voltage unbalance. The proposed algorithm demonstrates a method to eliminate imperfections from both the three-phase and single-phase grid voltage to improve the steady state performance of grid synchronization with high bandwidth PLL.

Along with the distribution system, challenges associated with the transmission of large offshore renewable energy sources like offshore wave park of several hundred megawatt is a challenge for renewable resources. An ocean compressed air energy storage (OCAES) system is being considered as one of the options for utility scale energy storage for off-shore wave energy based renewable power generation. The power transmission requirements for the off-shore renewable energy system with storage has also been addressed in this research.

Distributed Voltage Regulation and Grid Connection of Renewable Energy Sources

by
Ali Md Safayet

A dissertation submitted to the Graduate Faculty of
North Carolina State University
in partial fulfillment of the
requirements for the degree of
Doctor of Philosophy

Electrical Engineering

Raleigh, North Carolina

2015

APPROVED BY:

_____	_____
Dr. Iqbal Husain Committee Chair	Dr. Subhashish Bhattacharya
_____	_____
Dr. Aranya Chakrabortty	Dr. Joseph DeCarolis

DEDICATION

To my mother Aktarun Nahar and father Md. Ashraf Ali who are my best critic and my best supporter in every work.

BIOGRAPHY

Ali Md Safayet received his B.Sc. degree in Electrical and Electronic Engineering (EEE) from Bangladesh University of Engineering and Technology (BUET), Dhaka, Bangladesh, in 2009. He received his Ph.D. degree from the department of Electrical and Computer Engineering at North Carolina State University, Raleigh, NC in 2015.

From 2010 to 2011, he worked as a research assistant at The University of Akron, Akron, OH. During his Ph.D. study he worked for ABB as a graduate intern. His research interests include distributed systems, grid synchronization, transmission and distribution of renewable energy systems.

ACKNOWLEDGMENTS

I would like to express my sincere gratitude to my advisor Dr. Iqbal Husain for his guidance and support throughout the course of this work. I consider myself very lucky for getting the opportunity to work with him. His constant compassionate advice and astute guidance was essential for completion of this work. I am grateful to my committee members, Dr. Subhashish Bhattacharya, Dr. Aranya Chakrabortty and Dr. Joseph DeCarolis for their valuable suggestions and comments. I would like to thank Dr. Yilmaz Sozer for his mentorship and support in my research. I also thank Dr. Poria Fajri for his help in the later part of my PhD.

My sincere gratitude goes toward all the people at the FREEDM System Center for providing a really nice and friendly atmosphere. I specially would like to thank Karen Autry for her help from the very first day that I came to the Center. Also I would like to thank our lab manager Hulgize Kassa for his every suggestion and help in my experimental work.

I would also like to express my gratitude to all friends for their encouragement. I specially would like to thank Rajib Mikail and Mehnaz Akhter Khan for their constant support till now from my first day at United States. They made my life much easier during my toughest days away from home.

My deepest and most gratitude goes to my family members, my mother Aktarun Nahar, my father Md Ashraf Ali and my sister Samira Ishrat Jahan. They have always encouraged and supported me to pursue my goals. Finally, I would like to thank my loving wife Tahmin Tisha for her endless love, support and continued patience. She was always there to encourage me through the good times and bad.

TABLE OF CONTENTS

LIST OF TABLES

LIST OF FIGURES

Chapter 1: Introduction

1.1 Background

Reliability is one of the major issues when developing renewable energy systems for power supply. As the penetration of the renewable energy sources (RES) increases in a distribution system, problems such as over voltage, network overloading, dc current injection, harmonic current emission become important challenges to address. In particular, voltage regulation of the distributed generation system is of significant concern. When the grid connected distributed energy sources (DES) produce more energy than the local load demand, excess power is injected into the network resulting in increased voltage levels. At minimum loading conditions, the overvoltage conditions worsens with high penetration levels of the RES which leads to the reverse power phenomena. For solar PV system, worst case scenario occurs during midday when the penetration level is the highest and load demand is the lowest. Also, the rapid change in the energy production from RES causes an oscillation in the grid voltage. For example, the irradiance to solar panels changes rapidly as clouds pass over the PV panels. Any frequency and voltage events in the grid would cause all the inverters to trip and an unwanted transient phenomenon occurs on the grid voltages at its various nodes [1].

The amount of reactive power injected into the network affects the gird node voltages, and it is possible to regulate the voltage through reactive power compensation. Control devices such as step voltage regulator (SVR) and static VAR compensator (SVC) are used to regulate the voltage [2]. The lagging reactive power is usually compensated by introducing leading reactive power devices into the utility, which is achieved by adding capacitors and generators

that can produce variable voltage levels. Also, Static Synchronous Compensator (STATCOM) can be used at the distribution voltage level [3]-[6] although equipment cost is a major concern of using STATCOM.

Another important aspect of renewable energy systems is the grid synchronization. The increasing demand of integrating single-phase or three-phase renewable energy sources (RES) like solar PV system, offshore or onshore wind and wave energy systems, storage of fuel cells or hybrid vehicles to the utility grid requires proper estimation and synchronization of frequency and phase angle of the grid voltage. Also, the control of the real and reactive power for grid connected distributed sources requires accurate phase information of the utility voltage.

The most commonly used and easily implementable algorithm for grid synchronization is the phase locked loop (PLL) technique [11]. The basic algorithm of the PLL used in power system applications is realized in the synchronous reference frame (SRF) [9], [12] where grid voltage is decomposed in synchronously rotating *d-q* reference frame. The conventional SRF based PLL (SRF-PLL) works perfectly with a grid that has no imperfections such as harmonics, unbalanced voltage or frequency fluctuation. In reality, the power grid is not as clean and is typically contaminated with imperfections. The challenge is to implement a robust and fast PLL for operation in distorted utility conditions [13].

Most popular renewable technologies lend themselves to local small-scale and even domestic distributed generation. But development of the renewable energy technology has gradually moved from small scale distributed sources towards the large scale production such

as off-shore wind and wave energy to meet high energy demand all over the world. Renewable energy sources on the generation side also have a strong impact in utility grid. In the past few years off-shore power generation has received substantial interest from various researchers. Beside off-shore wind energy, ocean wave energy has significant opportunity and could be utilized to meet the world's increasing energy demand [25]-[28]. Wave energy has benefits over solar or wind energy systems. Waves are more available and more predictable with better demand matching. Also, energy density is higher and wave energy converters can extract more energy with smaller volume and reduced cost. However, there are a number of technical and economic challenges in considering grid connection of large wave park [29]. Some of these challenges include intermittency of wave generated power, storage system, transmission of energy from offshore wave park to the onshore grid, voltage distortion, reactive power requirement, implication of grid code requirements etc. As a part of a large multi-disciplinary team, the challenges of power transmission, grid connection and storage system for an offshore wave park at North Carolina coast have been investigated for the ocean energy program through the UNC Coastal Studies Institute.

1.2 Research Motivation

Research focusing on distributed voltage regulation attributes to controlling the reactive power injection into the network to regulate the voltage within allowable range. High installation and equipment cost of conventional voltage regulating devices such as SVC, AVR or STATCOM brings the focus of research towards the control of distributed sources to produce reactive power. Power electronic inverter associated with the RES can produce

reactive power after meeting the demand of real power for the system. The active power is produced to extract the maximum energy from the RES and reactive power is produced on demand by utility to regulate the voltage.

One of the fundamental problems of regulating voltage of distribution system consisting of several distributed sources and loads is the reactive power management of the sources. The total current producing capacity of an inverter is limited by its kVA rating. Inverters have to produce the real power commanded from maximum power point tracking (MPPT) and rest of its capacity can be utilized for reactive power production. As the real power command varies with the environmental changes, the inverter's capacity of producing reactive power is also varying. This instantaneous capacity has to be considered by the control algorithm so that inverter can be operated within its limit and utilizing its reactive power most efficiently. Typically distributed system consists of several RES and it is not practical to use communication among the inverters. Therefore a central management is required to distribute total required reactive power among the inverters using minimum communication. In this research, a reactive power scheduler has been proposed which can detect the reactive power production capacity of the inverters and produce reference reactive power for voltage regulation without any communication among the inverters.

In a grid connected radial distribution system, the critical bus is an important one which is defined as the farthest bus of a radial distribution feeder from the grid tie point. The grid tie point is called the point on common coupling (PCC). With high penetration of solar PV units or other renewable energy sources, the highest voltage rise occurs at the critical bus as it sees

the highest line impedance from its location to the PCC. Another important aspect for voltage regulation of a radial distribution system is the voltage sensitivity of different bus to the critical bus. Voltage sensitivity determines the impact of real and reactive power generation at any bus on the critical bus voltage. Along with the inverter's current carrying capacity, another constraint that has to be considered for reactive power management is its power factor. The owner of the DES has to maintain a minimum power factor limit given by the grid operators. A central reactive power management system is proposed in this dissertation for radial distribution system which incorporates voltage sensitivity and power factor management for overvoltage prevention during high PV penetration.

Proper control of active and reactive power is highly dependent on the phase and frequency tracking of grid voltage. The common technique for grid synchronization is phase locked loop. Conventional SRF-PLL cannot appropriately track the phase and frequency when the grid is weak. Usually distribution systems have non-linear loads connected to the PCC which are the main sources of grid harmonics. As the number of power electronic systems increases in the utility grid, the harmonics in the grid voltage become more pronounced. Three-phase grid may have unbalanced voltage which worsens the performance of SRF-PLL. The estimated phase by SRF-PLL in presence of impurity contains high error in steady state. This steady state error can be reduced by reducing the bandwidth (BW) of the PLL loop filter. But dynamic performance of PLL is degraded with lower bandwidth. So there is a tradeoff between steady state performance and dynamic performance in choosing BW of the PLL. If the sources of steady state error that include harmonics and voltage unbalance can be eliminated before feeding the voltage measurement into PLL, the BW of the loop filter can be increased since

the steady state error will not be an issue for phase estimation. Higher BW will improve the dynamic performance in the presence of frequency fluctuation. Several methods have been proposed to improve to PLL performance in distorted utility conditions. In one approach, active filters (band pass, band stop, low pass, notch and adaptive notch) are used to remove harmonics at a preselected cutoff frequency knowing the harmonics and unbalanced voltage pattern [14]-[18]. However, the method is complex, may not eliminate the harmonics completely, and suffer from long computation time, filtering delay and sensitivity to the frequency variations. Decoupled double synchronous reference frame has been used to remove the negative sequence voltage caused by unbalanced grid voltage using two oppositely rotating synchronous reference frame [20]-[21], but this method does not consider the harmonic effect. This led to an alternative approach of PLL to eliminate harmonics and unbalanced voltage effect for phase estimation in this dissertation.

1.3 Contributions

The key contributions of the dissertation are listed as follows:

1. A novel reactive power scheduler (RPS) is proposed for distributed voltage regulation. The RPS can detect reactive power production capacity of each inverter in a distributed system without any communication among the inverters.
2. Reference reactive power generation algorithm has been proposed for the distributed inverters in such a way that all inverters operate in equally stressed condition based on their capacity.

3. A Central Reactive Power Management System (CRPMS) is proposed for overvoltage prevention of radial distribution system during high penetration of DES.
4. Proposed CRPMS addresses the limitations of existing reference reactive power generation method for voltage regulation. It considers voltage sensitivity of different buses on critical bus and power factor constraint.
5. An improved and robust phase locked loop algorithm for synchronization of renewable energy sources with weak grid containing voltage harmonics and unbalanced voltage which may be the case for rural distribution system is presented.
6. A detailed concept of system design, power transmission and grid connection of a 200MW off-shore wave-park has been presented. Some challenges associated with power transmission, grid connection and storage of off-shore renewable energy sources have been addressed.

1.4 Dissertation Outline

Chapter 2: The basic concepts of distributed voltage regulation with reactive power produced by the distributed sources are explained in this chapter. The impact of power generation from renewable energy sources in the distribution system is discussed. The effects of environmental change on inverter's reactive power production capacity are explained. The motivation for adopting RPS for coordinating inverters associated with the RES are discussed.

The algorithm and operating principal of RPS are presented in this chapter. The application of RPS for a residential and grid connected distribution system is studied; the real and reactive power control of PQ inverter is explained; special scenarios such as real power curtailment for

RPS are discussed; the impact of RPS on voltage regulation in case of low demand and high generation of RES are illustrated through simulations. At the end, experimental results for a grid connected system are presented.

Chapter 3: Along with inverters' rating there is usually a power factor constraint for inverters connected to a distributed system and it is not desired for any distributed load or source to operate at power factors below a certain limit which will result in the consumer being penalized by the grid operator. In a radial distribution system, the farthest bus is considered as the critical bus as the sensitivity to the change of real and reactive power for this bus is the highest among all the buses in the system. In this chapter, an improved reactive power management is proposed based on the inverters' reactive power capacity and sensitivity of the bus that has distributed sources and load.

Chapter 4: The development of a reactive power scheduler for voltage regulation of grid connected distributed energy system led to the challenges of grid connection for the RES which is addressed in this chapter. The challenges of grid connection for the RES are presented; the basic concept and current research of the most commonly used and easily implementable algorithm for grid synchronization method, phase locked loop (PLL), are also presented. The performance degradation of PLL in phase angle or frequency tracking in the presence of grid impurity is discussed. A modified cascaded block is proposed in this chapter which can eliminate the effects of unbalanced voltage and harmonics present in the grid. The proposed method can eliminate the grid harmonics/unbalanced voltage effects using a few trigonometric operations on the sampled grid voltage without using any external filter. The improved

performance of the PLL is shown by simulation. The experimental verification of the proposed algorithm is also presented.

Chapter 5: This chapter discusses the concept of system design, power transmission and grid connection of an off-shore wave energy park. State of the art for energy storage of off-shore power generation at utility scale is studied. Then, the viability of the ocean compressed air energy storage (OCAES) system which is one of the recently proposed forms of energy storage for off-shore power is discussed. The challenges of power transmission and grid connection of a large wave energy park are presented. Approaches to mitigate these challenges are addressed using the simulation results of a 200MW wave energy park which incorporates the design criteria for RPS and advanced PLL method proposed earlier.

Chapter 6: The conclusions of this dissertation are presented in this chapter. In addition, the proposed future work is outlined in this chapter.

Chapter 2: Reactive Power Scheduler for Distributed Voltage Regulation

2.1 Introduction

Grid connected distributed energy sources (DES) like rooftop photovoltaic (PV) systems, electric or hybrid vehicles, fuel cells, storage devices, wind power systems are considered as the most prominent and rapidly growing technologies in the power distribution system. The implementation of DES in low voltage (LV) distribution system can reduce the transmission and distribution line losses and ratings. But the installation of DES in distribution network incorporates some challenges on power reliability which are primarily voltage regulation and fault management. For example, PV installation capacity in LV grid connected systems is limited due to the voltage rise concerns associated with high PV penetration and low consumer demand. There is a possibility of reverse power phenomena and overvoltage in LV distribution feeder during high generation of solar PV systems with low demand situations. Reverse power phenomena is more likely to occur with the solar PV systems during midday. Any frequency and voltage events in the grid would cause all the inverters to trip and a transient behavior would appear on the voltage profile of the system. Voltage flicker is another issue as the penetration of DES increases. A rapid change in the energy production from DES causes an oscillation in the grid voltage. For example, the irradiance to solar panels changes rapidly as clouds pass over the PV panels. The transient in the power production from the solar panels cannot be compensated by the rotating machine type generators to stabilize the system voltage.

As the amount of reactive power flowing in the utility affects the voltage, it is possible to regulate the voltage through reactive power compensation. Reactive power capability of the inverters is limited by the inverters' rating and maximum current carrying capacity of semiconductor switches. The inverters are operated to produce as much real power as possible which is determined by the maximum power point tracking (MPPT) algorithm. In this case, the rest of the current capacity can be used for reactive power. The fundamental problem for reactive power management is to determine which inverter should produce how much reactive power. In this chapter, a novel approach to schedule reactive power for different distributed generators is presented. By incremental perturbation of reference reactive power, the reactive power production capacity of each inverter can be detected. Minimum communication is required between the inverters and the scheduler for this method. The total reference reactive power needed to keep the voltage at a desired value is then divided among the inverters according to their capacity ratio.

2.2 Distributed Voltage Regulation

To transmit the power from primary substation to distribution network as shown in Fig. 2.1, the voltage at primary substation ($V_{substation}$) should be higher than the voltage at distribution side ($V_{distribution}$) considering the voltage drop across transmission line or cable. As the distribution bus moves further from substation, the voltage drop increases due to the longer transmission cable. The voltage difference between $V_{substation}$ and $V_{distribution}$ can be approximated by (2.1) as shown in Fig. 2.2.

$$\Delta V = V_{substation} - V_{distribution}$$

$$= IRcos(\theta) + IXsin(\theta)$$

$$= \frac{R * V_{substation} Icos(\theta) + X * V_{substation} Isin(\theta)}{V_{substation}}$$

$$So,\ \Delta V = \frac{RP+XQ}{V_{substation}} \tag{2.1}$$

where P and Q are real and reactive power, respectively flowing from grid side to the distribution side. The allowable range of the distribution side voltage depends on the grid code or Electricity Supply Regulations. It is distribution network operator's responsibility to ensure that distribution side voltage at any bus remains within the permissible range. Considering the voltage drop across transmission line, the substation voltage is maintained at higher level using automatic voltage regulator (AVR), on-load tap-changing transformer and line-drop compensator so that distribution side voltage is maintained within the allowable range [25].

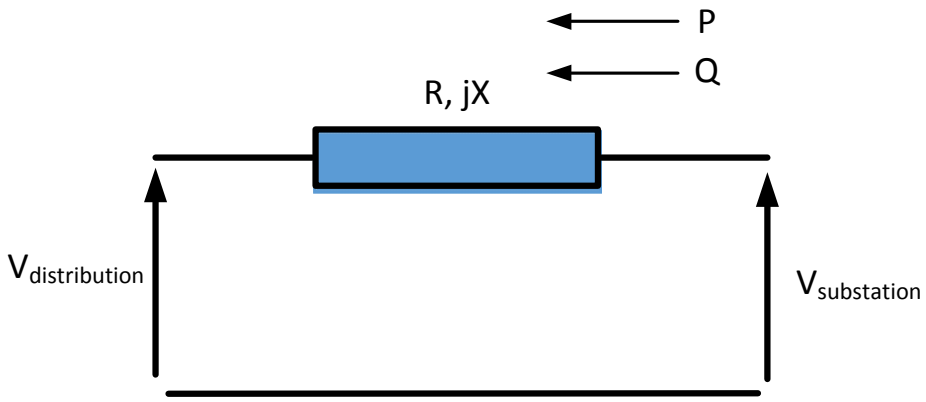

Figure 2.1. Simplified diagram of grid connected distribution system

When DESs are connected to the distribution system, some of the load is supported by these local generation. The amount of power generated by DES depends on the availability of the sun or wind; this reduces the amount of power coming from the grid. According to (2.1), when

real power (P) coming from the substation decreases, the voltage difference ΔV between substation and distribution side also decreases if the reactive power Q remains unchanged. Therefore, real power penetration at a distribution bus from DES results in the increase of voltage level at that bus. The bus voltage keeps increasing with the increase of DES penetration. When DES produce more energy than the local load demand, voltage at the distribution side becomes higher than the substation voltage and reverse power flow towards the substation occurs. This voltage rise issues can be counteracted by the reactive power absorption as XQ in (2.1) which compensates the change in RP. As the amount of real power generation from RES varies with the change of environmental condition, the amount of reactive power required to regulate the voltage must be adjusted accordingly.

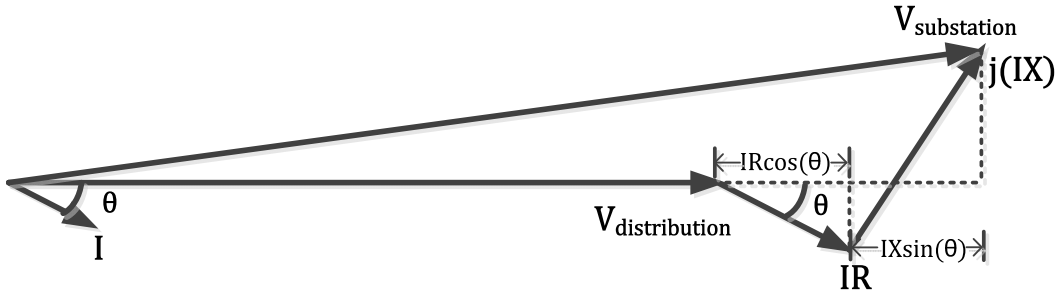

Figure 2.2. Phasor diagram of distribution system

The reactive power compensation needs dynamic control capability to regulate the voltage. Control devices such as step voltage regulator (SVR) and static VAR compensator (SVC) have been used to regulate the voltage [2]. The lagging reactive power is usually compensated by introducing leading reactive power devices into the utility, which is achieved by adding capacitors and generators that can produce variable voltage levels. However, with minimum

load conditions and high penetration, the reverse power conditions cannot be alleviated by the SVRs. Moreover, installation of SVC or SVR is expensive. A Static Synchronous Compensator (STATCOM) can be used at the distribution voltage level [3]-[6], but is not very common due to equipment cost.

Several methods have been proposed in literature for distributed voltage regulation. The most straightforward approach is to upgrade the existing distribution network by larger cables to reduce the impedance [33], [34]. But this approach is not economically feasible. Historically capacitor bank has been used for VAR support from substation to maintain distribution side voltage within a desired level. But optimal placement of these capacitor bank is still a topic of research [98] – [100]. The application of online tap changing transformer has been discussed in [26] and [27]. However, capacitor banks and tap changing transformer are not fast enough to compensate the voltage fluctuation due to the transient events such as cloud passing over the PV panel [101] – [102]. Also determining proper control setting for online tap changer is challenging and especially during high penetration of DES [28]-[29]. The power electronic inverter associated with the DES would have the active (P) and reactive power (Q) production capability. The active power is produced to extract maximum energy from renewable sources and reactive power is produced on demand by the utility grid. DES inverter has the capability to cope with rapid and random fluctuations of environmental change. Typically voltage source converter associated with DES takes few milliseconds to react for a voltage deviation while online tap changer takes few seconds to react. The coordinated control with tap changing transformer and DES is discussed in [30]. Tap changing transformer works as master during normal operating condition but during fault ride through and over voltage situation DES works

as master as tap change needs longer time to react. When DES hits the limit, tap changer is also used. However according to [104], one of the main reasons of why the distributed generators (DGs) are not allowed to control voltage with tap changing transformer is that it can destabilize the automatic tap changing controller.

The application of energy storage during high penetration of DES is also a way for voltage regulation [31]. The storage can be coordinated with DES inverter where excess energy of DES can be stored in storage and DES will absorb reactive power when storage reaches to its limit. However, when DES absorbs more reactive power, storage capacity decreases. As mentioned above, due to high R/X ratio of the cables in distribution system, real power has significant effect on distribution bus voltage. Therefore, real power control is also an effective way to regulate the voltage in distribution network [35], [36]. Real power curtailment during high penetration of DES does not require reactive power compensation device or increased ratings of power electronic devices to compensate reactive power. But when there are several distributed sources owned by different owners, the equal opportunity of real power management has to be ensured in real power curtailment. The end users' loss of benefits from real power curtailment should be strongly considered in this approach. The characteristics of fairness of power management have been considered as an important research area this time [37], [38], [39].

A vehicle-to-grid reactive power support (V2GQ) strategy for optimal coordinated voltage regulation with high penetration of DES is proposed in [103]. The proposed algorithm employs plug-in electric vehicles (PEVs), DES and on-load tap changer (OLTC) to satisfy PEV

charging demand and grid voltage requirements with relaxed tap operation, and minimum DG active power curtailment. A corrective control based on Model Predictive Control has been proposed in [105] to correct voltages out of limits by applying optimal changes of the control variables. The control objective proposed in this paper is such that if some of the voltages fall in the undesirable region, the controller will use the minimum control actions to bring these voltages within the acceptable limits. As the voltages are in the undesirable region (0.98pu-1.02pu), not in emergency yet, the controller will only use the cheapest control variables. If some bus voltages operate in the unacceptable region, outside of the emergency limits (0.94pu-1.06pu), the controller will use all of the available (cheap and expensive) control variables until the undesirable region is reached. The reactive power output of the DES and OLTC are considered as the cheap controls while the active power output of a DG unit is considered as an expensive control and should not be requested unless emergency conditions are encountered. However this paper does not consider the end user's loss of benefits from active power curtailment and delayed response of OLTC.

A real power curtailment method is proposed in [40] for overvoltage prevention caused by reverse power flow. This paper is based on a precise active power limit prediction using the dynamic Thevenin equivalent. However, effectiveness of this approach is significantly impacted by the accuracy of Thevenin equivalent parameters.

Considering the facts stated above reactive power compensation is mostly used method for voltage support at distribution network. It is straightforward to take benefit of producing as much real power as possible. Developing a renewable energy system with integrated power

electronics and intelligent control that has the reactive power capability can accomplish the tasks of voltage regulation more elegantly and efficiently at a much reduced cost. A proper reactive power management is a prime necessity of distributed voltage regulation using inverters' reactive power capacity.

Communication among the inverters in a distribution system consists of several DES is a major factor for reactive power management. The need for global communication systems seriously limits the benefits of coordinated control to small distributed systems [41]. Centralized approach of voltage regulations can ensure optimization of reactive power management but it requires a robust communication structure. On the other hand distributed voltage regulation approach which coordinates DES to provide proper voltage regulation can accomplish the task with less communication requirements [103]. A two way communication based distributed voltage regulation for smart distribution feeders has been proposed in [106]. Power line communication (PLC) has been considered for communication of this scenario as it is the only technology that has a deployment cost comparable to wireless, since the lines are already there. Also wireless communication for smart grid has been discussed in [107]. An advanced communication architecture named SunWave Communicator is presented by Petra Solar in [108]. It features two way communication to each smart energy device connected to it, allowing both individual and system monitoring and control.

A novel reactive power scheduler has been presented in this chapter for PQ inverters for voltage regulation. PQ inverters were used for voltage regulation previously [8]. In this chapter, a novel way to schedule reactive power for different distributed generators is

presented. By incremental perturbation of reference reactive power, the reactive power production capacity of each inverter can be detected. There will be no communication among the inverters at distribution system in this method. The total reference reactive power needed to keep the voltage at a desired value is then divided among the inverters so that all inverter are equally loaded with real and reactive power without getting over stressed. In this way a balanced sharing of reference reactive power is ensured in the system. This will increase the inverters' life and ensure equal utilization of all inverters owned by distributed users.

2.3 System Structure

The basic representation of a single renewable energy source connected to the PCC and the utility grid is shown in Fig. 2.3. The current delivered to the utility grid is given by

$$i = \frac{V_s e^{j\delta} - V_g e^{j0}}{jX_L} = \frac{V_s cos\delta + jV_s sin\delta - V_g}{jX_L} = \frac{V_s sin\delta}{X_L} + j\left(\frac{V_s cos\delta - V_g}{X_L}\right) \quad (2.2)$$

where V_s and δ are the magnitude and phase of the DES inverter, and V_g is the magnitude of the grid voltage. The total power delivered to the grid can be represented as

$$S = P + jQ = V_g i^* = \frac{V_s V_g sin\delta}{X_L} - jV_g\left(\frac{V_s cos\delta - V_g}{X_L}\right) \quad (2.3)$$

For small phase angle δ, the reactive power flow to the grid is

$$Q = \frac{V_s - V_g}{X_L} V_g \quad (2.4)$$

Therefore, $V_s - V_g$ can be controlled by adjusting Q.

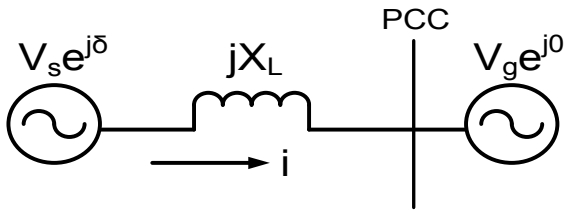

Figure 2.3. Interface between DES and the grid

2.3.1 Distribution System Structure

The substation associated with a distribution system may have several distributed sources and load. Any bus in a residential distribution feeder may consist of several residential sources like roof-top solar panel, electric/hybrid vehicle and storage devices. The difference between the desired voltage and the dynamic voltage of a certain bus will determine the total reference reactive power (Q_{ref_total}) for the inverters in that bus. A PI controller can be used to calculate the Q_{ref_total} from the voltage error [7]. A central scheduler will take Q_{ref_total} command from the substation as input and will produce reference reactive power (Q_{i_ref}) for the i^{th} inverter based on inverter's reactive power capacity.

Fig. 2.4 shows the distribution system structure for the proposed scheduler. The system has a central master scheduler for several substations which is responsible for determining the total reference reactive power for each substation. The scheduler located at the substation monitors the voltage error at different nodes and PCC, and the reactive power production capacity of all the inverters. Based on those inputs, the scheduler decides the total reference reactive power for the substation.

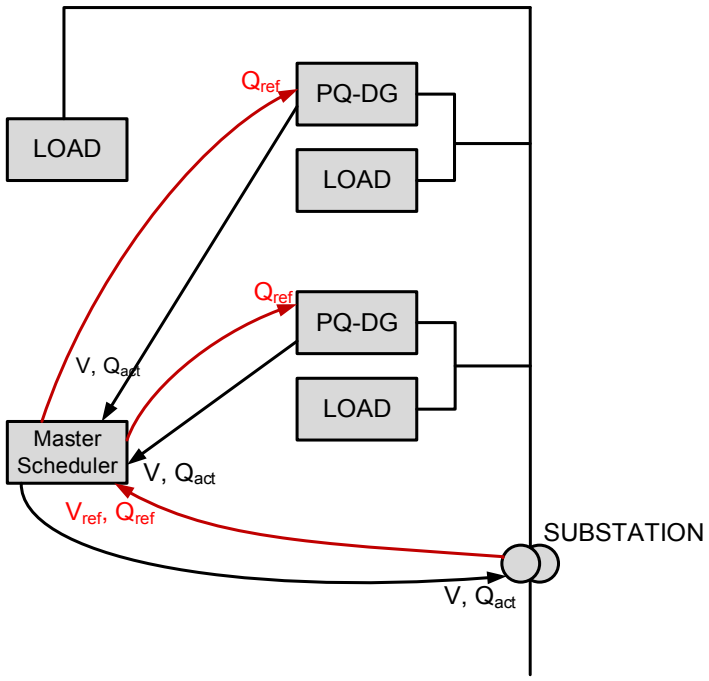

Figure 2.4. Overview of distribution system

2.3.2 Control Structure

The control is implemented in the *d-q* reference frame. The dynamics of power and current controls are much faster with *d-q* reference frame controller as the control variables are decoupled from the utility power angle θ. Also, the *d-q* reference frame enables the separation of active power and reactive power components. The single phase current produced by the inverter can be converted to two phase rotating reference frame components i_d and i_q by Park's Transformation [9] shown in (2.5).

$$\begin{bmatrix} i_q \\ i_d \end{bmatrix} = \frac{2}{3}\begin{bmatrix} cos\varphi & -sin\varphi \\ sin\varphi & cos\varphi \end{bmatrix}\begin{bmatrix} i_\alpha \\ i_\beta \end{bmatrix} \tag{2.5}$$

where, i_q and i_d are the direct axis and quadrature axis current respectively, φ is the estimated phase angle by phase-locked loop.

$i_\alpha = I_m cos\theta_i$; In phase component of single phase current.

$i_\beta = I_m \cos(90^0 + \theta_i) = -I_m sin\theta_i$; Out of phase component of single phase current.

Similarly, single phase voltage can be converted to two phase rotating reference frame components v_d and v_q as shown in (2.6)

$$\begin{bmatrix} v_q \\ v_d \end{bmatrix} = \frac{2}{3}\begin{bmatrix} cos\varphi & -sin\varphi \\ sin\varphi & cos\varphi \end{bmatrix}\begin{bmatrix} v_\alpha \\ v_\beta \end{bmatrix} \quad (2.6)$$

where,

$v_\alpha = V_m cos\theta_v$; In phase component of grid voltage

$v_\beta = V_m \cos(90^0 + \theta_v) = -V_m sin\theta_v$; Out of phase component of grid voltage.

From (2.5) and (2.6),

$$v_q = V_m \cos(\theta_v - \varphi) \quad (2.7)$$

$$v_d = -V_m \sin(\theta_v - \varphi) \quad (2.8)$$

$$i_q = I_m \cos(\theta_i - \varphi) \quad (2.9)$$

$$i_d = -I_m \sin(\theta_i - \varphi) \quad (2.10)$$

Using (2.7) to (2.10), real power $P = V_m I_m \cos(\theta_v - \theta_i)$ and reactive power $Q = V_m I_m \sin(\theta_v - \theta_i)$ can be expressed as

$$P = v_d i_d + v_q i_q \quad (2.11)$$

$$Q = v_d i_q - v_q i_d \quad (2.12)$$

If the estimated phase φ is locked with grid voltage phase θ_v, v_d shown in (2.8) is zero. Then (2.11) and (2.12) can be rewritten as

$$P = v_q i_q \tag{2.13}$$

$$Q = -v_q i_d \tag{2.14}$$

So, the real power can be controlled by controlling i_q and reactive power can be controlled by controlling i_d.

The common voltage in the utility grid can be controlled mostly by controlling the amount of reactive power inserted into the grid. The approach to the problem uses a multi loop control perspective. The outer voltage control, having multipoint sensors, regulates the common grid voltage and sets the command for the amount of reactive power required from the distributed energy sources. The inner control loop can be part of the inverter of the distributed energy sources. The inverters would produce the amount of reactive power commanded by the outer voltage control loop. Fig. 2.4 shows the power flow and information flow structures in the substation. The substation has a distributed energy system with PQ inverters. The central controller receives a reactive power or voltage profile from the upper hierarchy in the distribution system. The central controller reports back the voltage and actual reactive power (Q_{act}) to the upper hierarchy. The master scheduler distributes the reactive power command if it receives reactive power command from the upper hierarchy. If the scheduler receives a voltage profile, it would have to achieve closed loop voltage control itself. Actual voltage and reactive power produced from the individual points in the substation are received to proceed with the voltage control.

In order to run the RES at the maximum power extraction condition, the operating voltage and current should be adjusted for a given environmental condition. Maximum Power Point Tracking (MPPT) algorithm dictates the real power demand, i.e. i_q for the inverters. After meeting the real power demand, the inverter has capacity of i_d for reactive power as

$$i_d = \sqrt{{I_a}^2 - {i_q}^2} \tag{2.15}$$

where, I_a is the rated current limit of the inverter. The difference between the desired voltage and the dynamic voltage at the PCC will determine the total reference reactive power (Q_{ref_total}) for the inverters. The phase angle of the utility voltage needs to be determined using methods such as the phase-locked loop (PLL). A PWM control scheme can be used for generating the inverter gate signals for current regulation. Fig. 2.5 shows the overall control structure of the PQ inverters.

Since there is a limit on the phase current based on the capacity of the inverter, the distribution between i_d and i_q should be adjusted appropriately to run the inverter within its limit. MPPT determines the amount of i_{q_ref} to deliver as much active power as possible by the renewable energy source. The block "i_{d_ref} $scheduler$" in Fig. 2.5 converts the reference reactive power from the scheduler to i_{d_ref}. The "i_{q_ref} $prioritizer$" block checks if the inverter is capable of producing this i_{d_ref}. If it is not capable then it would reduce the i_{d_ref} in favor of i_{q_ref}. If an inverter produces its full capacity of i_d, then it will be labeled as saturated inverter since it cannot produce additional reactive power.

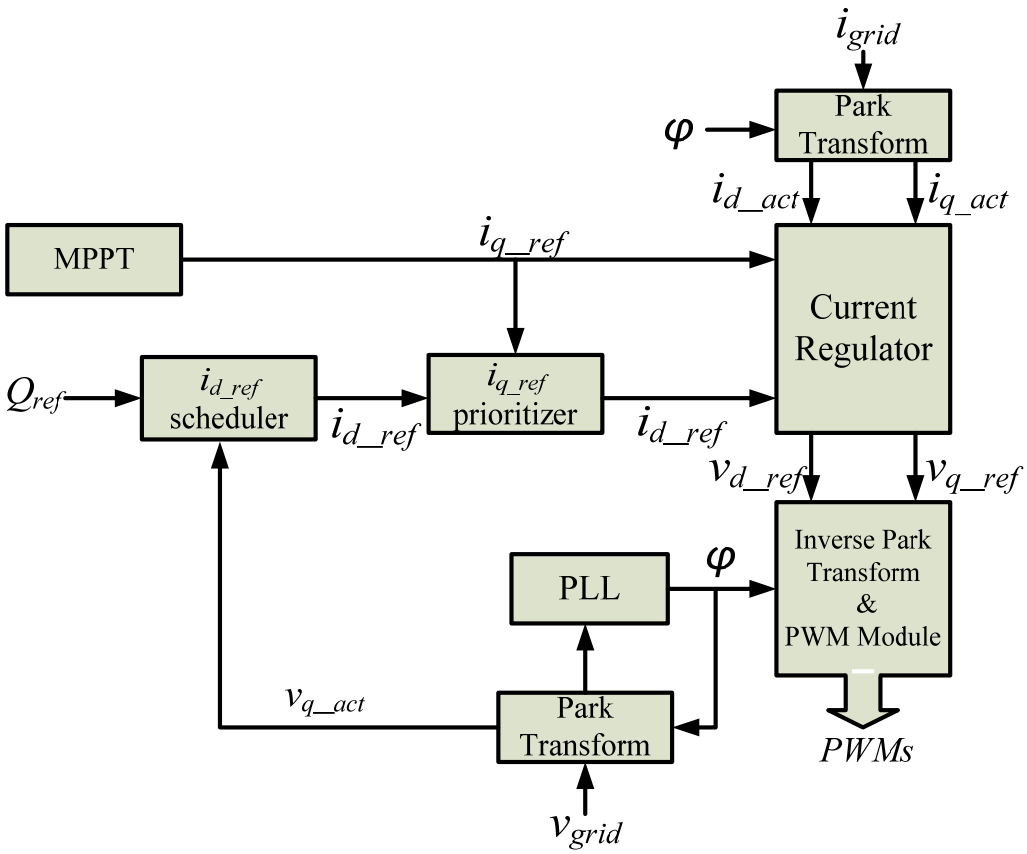

Figure 2.5. Overall control structure of PQ inverter

2.4 Reactive Power Scheduler

The reactive power scheduler produces the reference reactive power for different inverters based on their capacities with minimum level of communication with the inverters. It takes the information of actual reactive power Q_{act} produced by inverters and generates reference reactive power for all the inverters. The information of the inverter's rating or total current carrying capacity is not required to be loaded in scheduler. Scheduler only requires the information of total number of DES operating in the system. The change in environmental condition such as sun irradiance may change the real power command for the inverters. An

increase in real power command results in a decrease of reactive power production capacity and vice versa. When an inverter does not have the capacity to produce reactive power then other inverters will share the required reference reactive power demand and produce reactive power based on their capacity. A reactive power capacity detection algorithm is proposed for the scheduler based on the response of the individual inverters to reactive power commands from the scheduler. The reactive power capacity of the individual PQ inverters is detected through a scheduler perturbation technique with small transition from the normal state.

The PQ scheduler either delivers the total reference reactive power Q_{ref_total} required to regulate voltage through closed loop control or gets it from the outer scheduler that resides in the upper hierarchy in the distribution system. At the beginning of operation, the scheduler distributes Q_{ref_total} among all inverters equally. Periodically the scheduler gets into the perturbation state and checks if the reactive power capacity of any inverter is at the limit.

2.4.1 Perturbation State

During the perturbation state, the reference reactive power of one inverter is increased by a Δ% of its steady state value at each cycle and it is checked if the inverter is saturated or not. If the difference between actual reactive power Q_{act} of present cycle of any inverter and Q_{act} of previous cycle of that inverter is below a threshold value then that inverter is considered saturated as Q_{act} does not increase with the incremental perturbation of reference reactive power. The threshold value is very small number. The reference reactive power of the other inverters are decreased at the same time such that Q_{ref_total} and Q_{act_total} remains the same during the perturbation state. The reactive power capacity Q_{cap} of an inverter is obtained in

the cycle when an inverter gets saturated. After reaching at saturation point, reference reactive power of the perturbed inverter is the decreased to the value from where the perturbation was started. Then perturbation of another inverter is started and capacity of that inverter is detected in the similar way. Fig. 2.6 shows the state machine of the proposed capacity detection and scheduling algorithm. Perturbation state is completed when the capacities of all the inverters are detected and then scheduler moves into the normal state. Usually perturbation state takes few seconds depending on number of inverters to be perturbed to detect the reactive power capacity of all inverters. The scheduler repeats the perturbation algorithm at a certain frequency based on the probability of changes in the environmental conditions.

2.4.2 Normal State

When the capacity of all the inverters are detected, the scheduler redistributes the total reference reactive power among the inverters in the normal state based on their ratio of capacity as shown in (2.16) so that none of the inverters are over stressed from producing/absorbing reactive power.

$$Q_i = \frac{Q_{i,cap}}{\sum_{i=1}^{n} Q_{i,cap}} * Q_{ref,total} \tag{2.16}$$

Normal state of the inverter is much longer than the perturbation state. The duration of the normal state is typically 30 seconds to few minutes depending on the environmental condition of a particular area so that the real power reference does not change to frequently during this state.

Scheduler moves between perturbation state and normal state periodically and change the reference reactive power set point for different inverters based on their capacity. In this way, no communication is required among the inverters. The scheduler only takes actual reactive power produced or absorbed by different inverter and the voltages at different node.

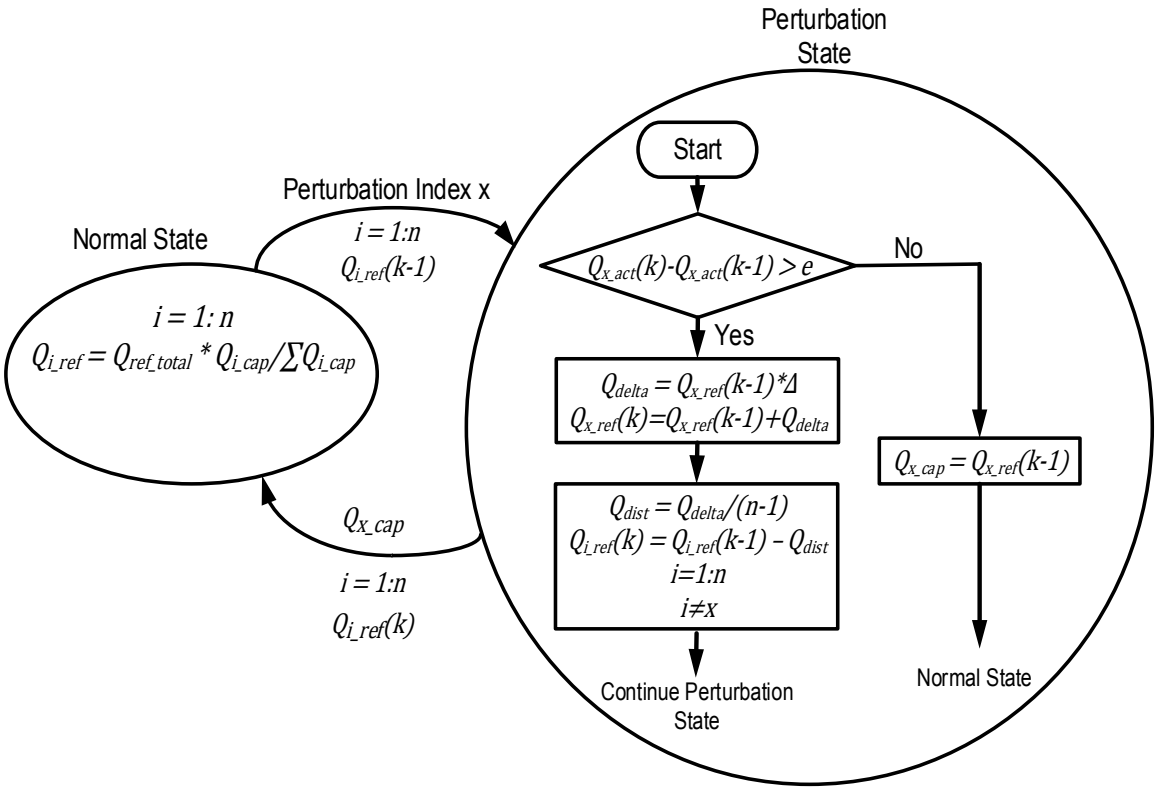

Figure 2.6. State diagram of the reactive power scheduler

2.5 Simulation Results

The reactive power scheduler algorithm presented in section 2.4 has been simulated using MATLAB/Simulink. The scheduler periodically enters in the perturbation state and normal

state. Same grid connected distribution system has been used in both simulation and experiment to verify effectiveness of the scheduler in voltage regulation.

2.5.1 Distribution Network

The grid connected distribution system used for simulation and experimental verification of the proposed RPS is shown in Fig. 2.7. The system consists of three identical DES with a capacity of 1 kVA each and a distributed load connected to the bus closest to the grid. The nominal voltage of the system is 120 V rms. The voltage, power and line parameters for this system are summarized in Table 2.1. The objective is to regulate the voltage across the load. ANSI C84.1 [109] expects equipment to operate at service voltages between 95% and 105% of the nominal value. Therefore, total reference reactive power is generated by the RPS according to (2.1) to maintain the load bus voltage between 114 V and 126 V. This section shows the simulation results while experimental verification using the same system is presented in the next section.

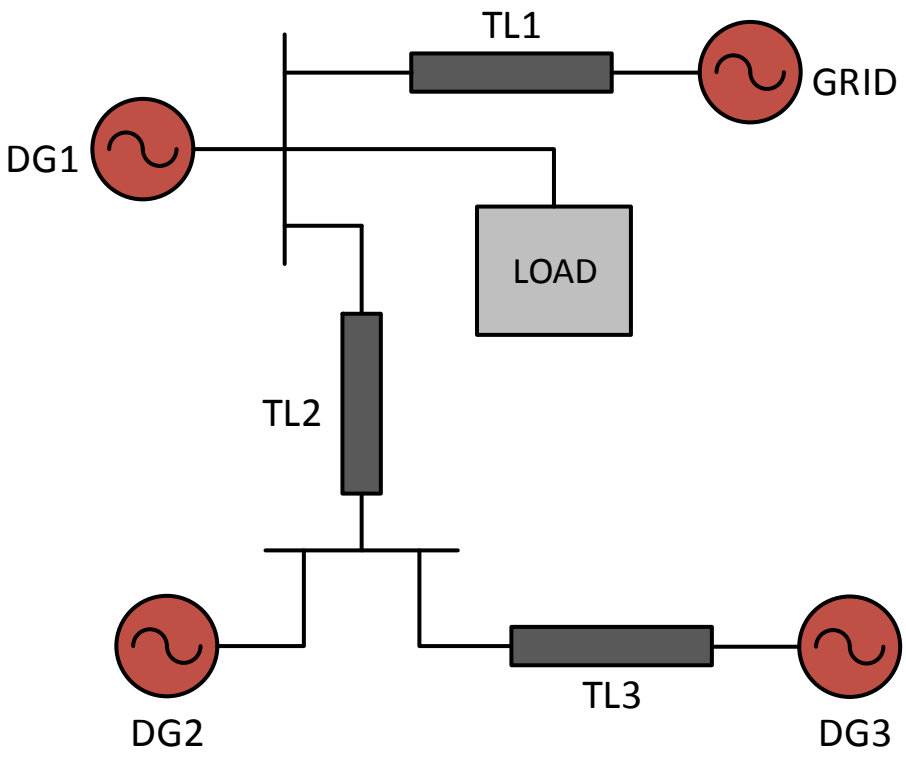

Figure 2.7. Grid connected distribution system

Table 2.1. Distribution system parameters

Nominal voltage	120 V	
Inverter rating	1 kVA	
Maximum Load	1 kW	
Line impedance	(0.38 + j0.26) ohm/km	
Line length	TL1	3 km
	TL2	1 km
	TL3	1 km

2.5.2 Scheduler Algorithm and Distributed Voltage Regulation

In this sub-section simulation results for RPS and effect of RPS on distributed voltage regulation will be presented. Initially, RPS equally distributes the total reference reactive power among the inverters. If any inverter in the system exceeds its capacity, that inverter is operated at maximum reactive power and the deficiency of reactive power from the saturated inverter is equally distributed among the other inverters in the next operating cycle. The RPS periodically changes between perturbation state and normal state and updates its commands in each period to compensate for a change in the load profile or environmental conditions. In this simulation it is assumed that the RPS update period is 0.5 sec. Therefore, every 0.5 sec RPS goes into the perturbation state. In perturbation state the reactive power capacity of each inverter in the system is detected and in the normal state a reference reactive power for each inverter is generated based on the detected reactive power capacity.

Fig. 2.8 shows the generated i_q value which represents the real power generation of each inverter. From 0 to 0.8 sec the reference i_q for the three inverters are assumed to be 6.2, 6.8 and 8.1 A respectively. The real power generation is changed for all inverters at 0.8 sec to resemble a change in the environmental conditions such as a cloud passing over PV of inverter 2 which was previously assumed to be on PV of inverter 1 since it had the lowest value of i_q. At this time reference i_q for the three inverters is considered to be 7.5, 6.2 and 6.8 A respectively. At 1.38 sec there is another change in real power generation for inverter 1 and i_q for this inverter increases to 9.6A resembling high solar irradiation on PV1.

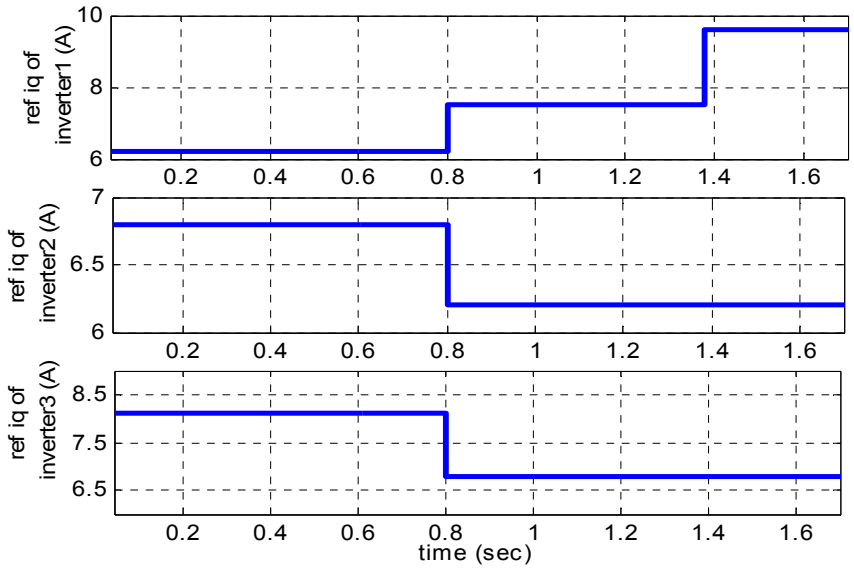

Figure 2.8. Reference i_q for different distributed inverters

Fig. 2.9 shows the i_d command from RPS to each inverter for reactive power control and the detected capacity at the end of the perturbation state for each inverter. The first perturbation state starts at 0.4 sec and ends at 0.5 sec as shown in Fig. 2.9. Also Fig. 2.9 shows the reactive power capacities represented as i_d capacities of the three inverters in this perturbation state which are 7.846, 7.332 and 5.864 A respectively. Total reference i_d required for voltage regulation in this stage is calculated by the RPS to be 11.5 A. In normal state this total reference i_d is distributed among the inverters according to (2.14) and (2.16). Therefore in normal state reference i_d for the three inverters are 4.288, 4.007, and 3.205 A respectively. As the three inverters are identical, the inverter which is producing higher real power has the least reactive power capacity and vice versa. As the update time period of RPS is 0.5 sec, second perturbation state starts at 0.9 sec and ends at 1.0 sec. Once again the change in reactive power capacity is detected in this perturbation state as a result of a change in the real power generation. Reactive power capacities measured as i_d capacities of three inverters in the second perturbation state

are 6.614, 7.846 and 7.332 A respectively. Consequently, in the following normal state the total required i_d of 10.858 A is distributed among the three inverters by the RPS as 3.296, 3.909, 3.653 A respectively. Before the third perturbation state, which is started from 1.4 sec and ends at 1.5 sec, inverter 1 becomes saturated with reactive power due to the high penetration of real power and it operated at $i_d = 2.8\,A$ which is its maximum capacity with $i_q = 9.6\,A$. During the third perturbation state its capacity is detected as 2.8 A and total reference reactive power is readjusted for three inverters in similar way.

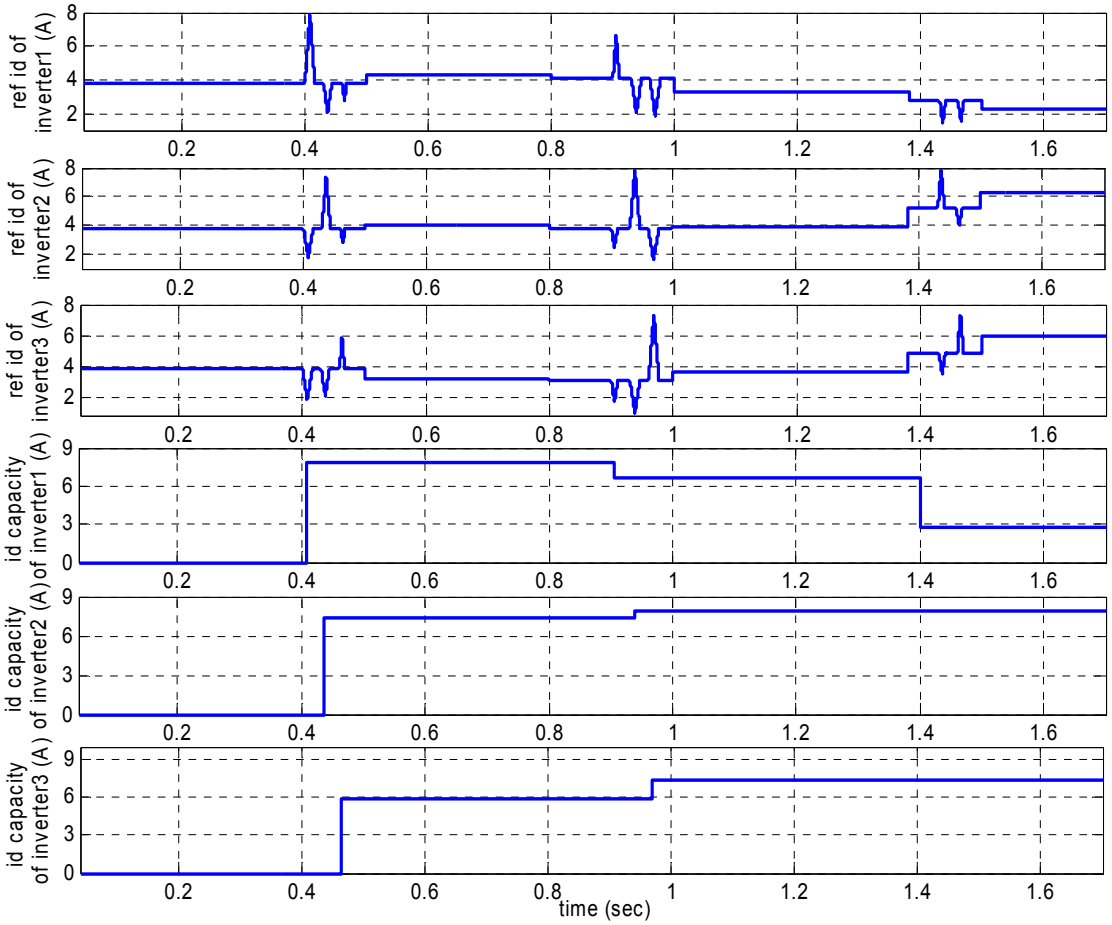

Figure 2.9. Reference i_d for each inverter and i_d capacity detection for different inverters

Fig. 2.10 shows the resulting voltage across the load with and without the RPS. It can be seen from Fig. 2.10 that when the RPS is present, the voltage across the load is maintained below 126 V rms at all times even during the time when inverter 1 is producing the highest real power after 1.38 secs. The RPS is able to track reactive power capacity of all inverters and it can identify if there is any saturated inverter. The reference reactive power is generated for each inverter based on detected capacity so that no inverter is over stressed by reactive power generation and voltage is maintained within the allowable range.

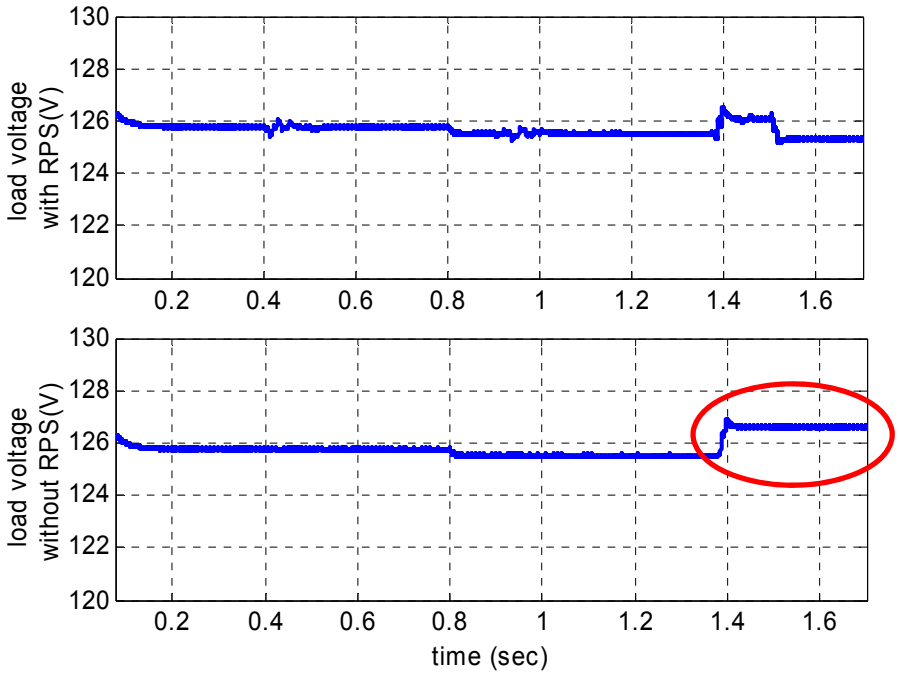

Figure 2.10. Load voltage with and without RPS

However, when RPS was not present, total reference reactive power is equally distributed among the inverters. Therefore, the system was unable to identify that the inverter 1 being saturated and redistribute reference reactive power command for inverter 2 and 3 during that time. As a result, load voltage increases and exceeds the allowable upper limit of 126 V after

1.38 secs. Also equal sharing of total reference reactive power regardless of their capacity limit sets an extra stress on the inverters with low capacity such as on inverter 3 from 0 to 0.8 sec. Simulation results are summarized in Table 2.2.

Table 2.2. Summary of simulation results

<table>
<tr><td rowspan="2">Time (sec)</td><td colspan="3">i_q (A)</td><td colspan="3">i_d capacity (A)</td><td colspan="3">i_d (A)</td><td colspan="2">Voltage</td></tr>
<tr><td>i_{q1}</td><td>i_{q2}</td><td>i_{q3}</td><td>$i_{d,cap1}$</td><td>$i_{d,cap2}$</td><td>$i_{d,cap3}$</td><td>i_{d1}</td><td>i_{d2}</td><td>i_{d3}</td><td colspan="2">1.048pu</td></tr>
<tr><td>0 – 0.4</td><td>6.2</td><td>6.8</td><td>8.1</td><td>N/A</td><td>N/A</td><td>N/A</td><td></td><td></td><td></td><td colspan="2">1.048pu</td></tr>
<tr><td>0.4 – 0.5</td><td colspan="10">PERTURBATION STATE</td></tr>
<tr><td>0.5 – 0.8</td><td>6.2</td><td>6.8</td><td>8.1</td><td rowspan="2">7.846</td><td rowspan="2">7.332</td><td rowspan="2">5.864</td><td>4.288</td><td>4.007</td><td>3.205</td><td colspan="2">1.048pu</td></tr>
<tr><td>0.8 – 0.9</td><td>7.5</td><td>6.2</td><td>6.8</td><td>4.049</td><td>3.784</td><td>3.026</td><td colspan="2">1.048pu</td></tr>
<tr><td>0.9 – 1.0</td><td colspan="10">PERTURBATION STATE</td></tr>
<tr><td>1.0 – 1.4</td><td>7.5</td><td>6.2</td><td>6.8</td><td>6.614</td><td>7.846</td><td>7.332</td><td>3.296</td><td>3.909</td><td>3.653</td><td colspan="2">1.045pu</td></tr>
<tr><td>1.4 – 1.5</td><td colspan="10">PERTURBATION STATE</td></tr>
<tr><td rowspan="2">1.5 – 1.9</td><td rowspan="2">9.6</td><td rowspan="2">6.2</td><td rowspan="2">6.8</td><td rowspan="2">2.8</td><td rowspan="2">7.846</td><td rowspan="2">7.332</td><td rowspan="2">2.258</td><td rowspan="2">3.322</td><td rowspan="2">5.908</td><td>With RPS</td><td>1.044pu</td></tr>
<tr><td>Without RPS</td><td>1.054pu</td></tr>
</table>

2.6 Experimental Verification

The experimental work using the same distribution network shown as in Fig. 2.7 is presented in this section. Three inverters are considered for experimental demonstration of the advantages of a PQ inverter equipped with reactive power scheduler algorithm. The experimental setup of the grid connected system is shown in Fig. 2.11. The dc bus voltage of

the inverter is 170V. Considering the rating of the devices for experimental setup, the nominal voltage is scaled down to 90V rms. The current rating of inverter 1 and inverter 2 are considered as 4 A and of inverter 3 as 3.2A. In the first experiment, system was tested with only real power generated by the inverters. The real power component of the inverter current i_q for three inverters are 1.9, 1.9 and 2.0 A, respectively. The load voltage in this condition is 95.7V which is 6.33% higher than the nominal value. This condition is shown in Fig. 2.12. In the next experiment, RPS is incorporated and real power penetration from the three inverters are considered to be the same as in the last condition. In the perturbation state of RPS reactive power capacity of the three inverters represented by i_d capacity are detected as 3.52, 3.52 and 2.52 A respectively. Total reference reactive power required to regulate the voltage is determined by (2.1) and calculated reference i_d is 2.43 A. In normal state RPS generates reference reactive power for each inverter and divides total reference reactive power among the inverters based on their reactive power capacity ratio. Therefore, reference i_d for the inverters generated by RPS in normal state are 0.89, 0.89 and 0.64 A, respectively. Fig. 2.13 shows the voltage across the load and current generated by the inverters. It can be seen that the load voltage is 91.8V which is 2.1% higher than the nominal voltage. The rms value of the inverter currents are determined as follows.

$$i_{a1,rms} = \frac{\sqrt{i_{q1}^2 + i_{d1}^2}}{\sqrt{2}} = \frac{\sqrt{1.9^2 + 0.89^2}}{\sqrt{2}} \cong 1.5 \tag{2.17}$$

$$i_{a2,rms} = \frac{\sqrt{i_{q2}^2 + i_{d2}^2}}{\sqrt{2}} = \frac{\sqrt{1.9^2 + 0.89^2}}{\sqrt{2}} \cong 1.5 \tag{2.18}$$

$$i_{a3,rms} = \frac{\sqrt{i_{q3}^2 + i_{d3}^2}}{\sqrt{2}} = \frac{\sqrt{2.0^2 + 0.64^2}}{\sqrt{2}} \cong 1.5 \tag{2.19}$$

The load voltage and inverter current wave shapes shown in Figs. 2.12 and 2.13 are zoomed in Fig. 2.14(a) and 2.14(b) respectively for better demonstration of the effect of reactive power from RPS. Fig. 2.14 shows. The inverter currents are lagging from the load voltage because of the line inductance and filter inductance between the inverters and load. Therefore, peaks of the currents from three inverters are shifted to the right of the peak of load voltage in Fig. 2.14(a) when there is no reactive power. When inverters absorb reactive power commanded from RPS the current waveforms shifted to the left from its original position which is shown in Fig. 2.14(b).

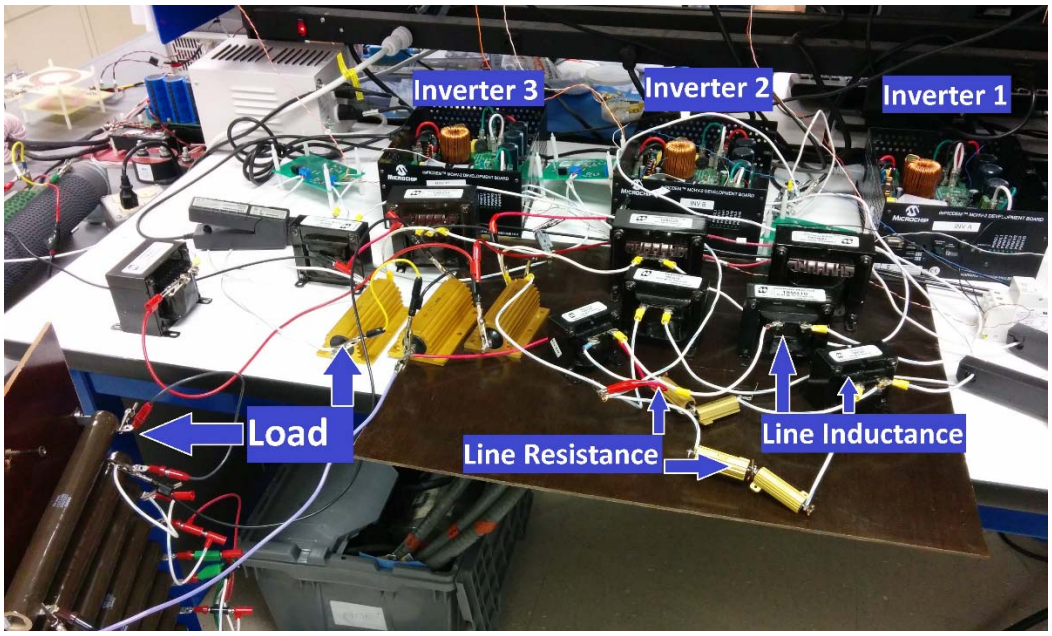

Figure 2.11. Experimental setup

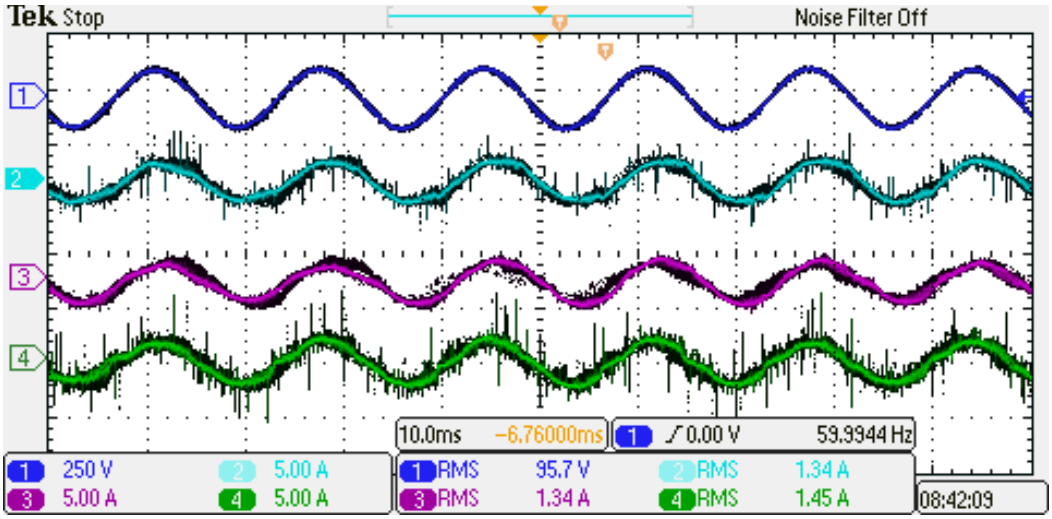

Figure 2.12. Load voltage and inverter current without RPS. Ch.1: load voltage (95.7V rms), Ch.2: inverter 1 current (1.34A rms), Ch.3: inverter 2 current (1.34A rms), Ch.4: Inverter 3 current (1.45A rms)

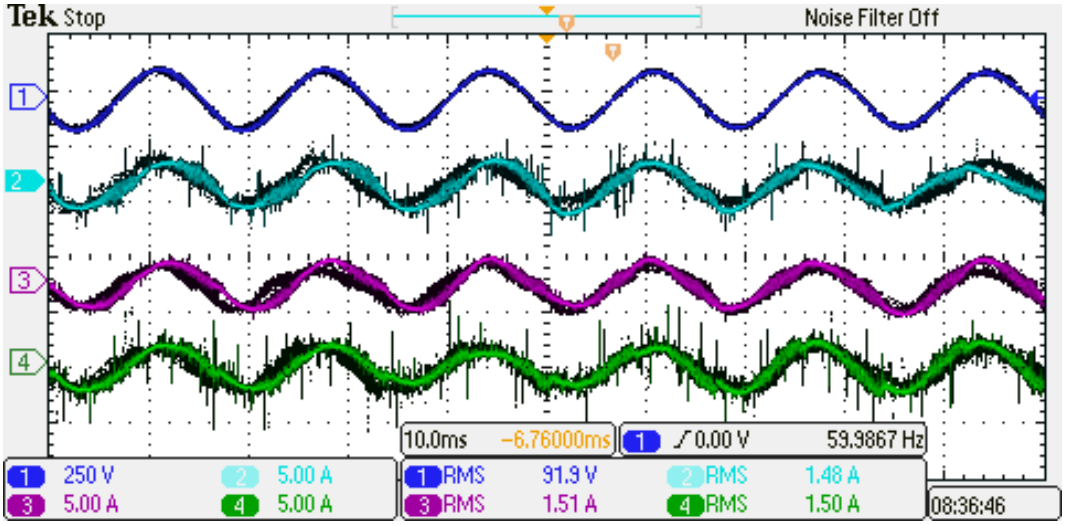

Figure 2.13. Load voltage and inverter current with RPS. Ch.1: load voltage (91.9V rms), Ch.2: inverter 1 current (1.48A rms), Ch.3: inverter 2 current (1.51A rms), Ch.4: Inverter 3 current (1.50A rms)

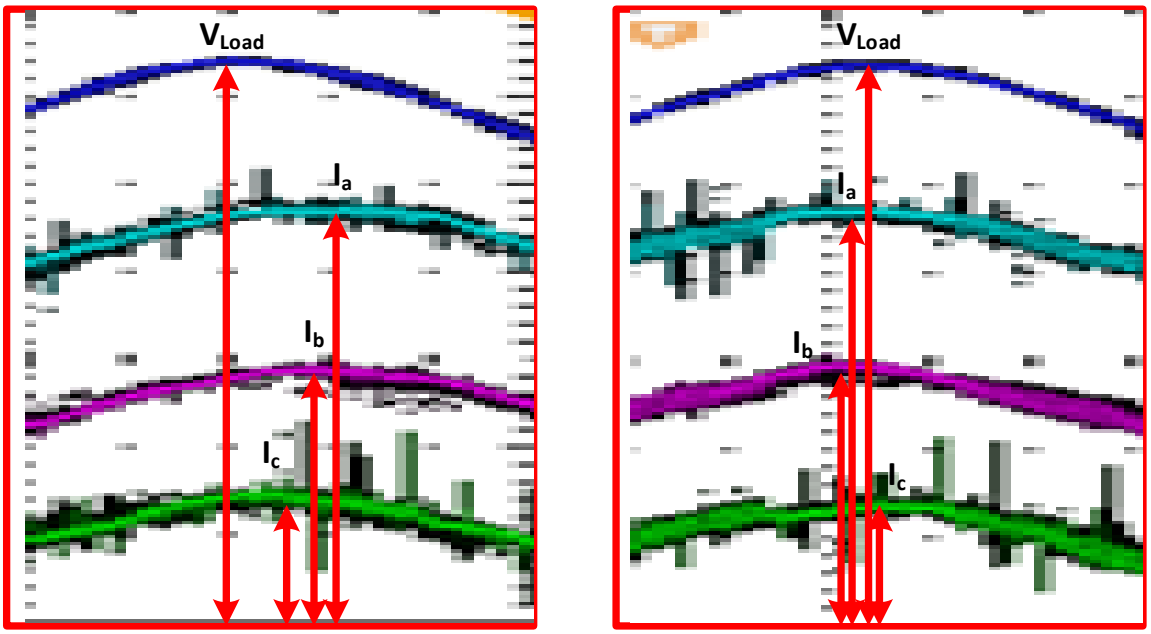

Figure 2.14. Load voltage and inverter current zoomed in to half cycle. (a) Without RPS, (b) first experiment with RPS

In the next experiment, it is considered the real power penetration by the three inverters are changed to resemble the change in environmental condition. The reference i_q for three inverters are 1.5, 2.0 and 2.0 A respectively. Inverters' rating are same as it was in previous experiments. Reactive power capacities of the three inverters represented by i_d capacity are detected in perturbation state as 3.71, 3.46 and 2.52 A, respectively. As the real power penetration from inverter 1 decreases in this case, higher reactive power capacity is detected for this inverter. Similarly, inverter 2 has higher real power penetration and has lower reactive power capacity. Real power generated by inverter 3 is unchanged from the previous condition, therefore its reactive power capacity remains same. Total reference i_d is determined as 1.04A to regulate the voltage within specified limit. The reference i_d for three inverters generated by

RPS based on the i_d capacities of the inverters are 0.4, 0.372 and 0.27 A, respectively. The rms value of the inverter currents can be determined using the same equations shown in (2.17) – (2.19). Fig. 2.15 shows the load voltage and rms current of the inverters for this condition. It can be seen that the load voltage is 91.8V and voltage rise is regulated to 2% of the nominal value. Also load voltage and inverter currents are zoomed in Fig. 2.16. It can be seen from this figure that the current peaks are at different position compared to Fig. 2.14(b) because the inverters are absorbing different amount of reactive power for the changed condition. Experimental results are summarized in Table 2.3.

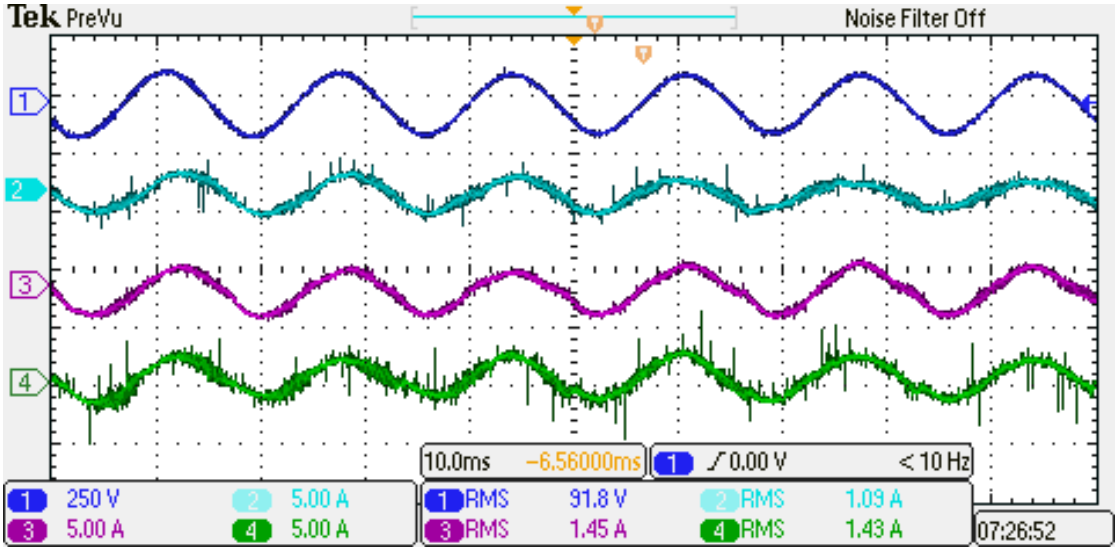

Figure 2.15. Load voltage and inverter current with RPS for change in environmental condition. Ch.1: load voltage (91.8V rms), Ch.2: inverter 1 current (1.09A rms), Ch.3: inverter 2 current (1.45A rms), Ch.4: Inverter 3 current (1.43A rms)

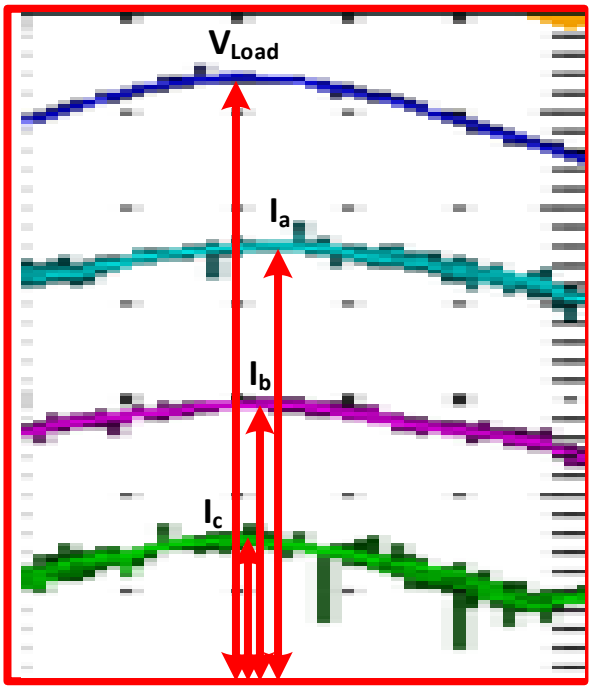

Figure 2.16. Load voltage and inverter current zoomed in to half cycle for second experiment with RPS for change in environmental condition

Table 2.3. Summary of experimental results

Experiment	Inverter	Ref i_q (A)	$i_{d,cap}$ (A)	Capacity ratio	Ref i_d (A)	i_{peak} (A)	i_{rms} (A)	Load voltage (pu)
1st experiment (without RPS)	Inverter 1	1.9	No RPS	No RPS	No RPS	1.9	1.34	1.0633
	Inverter 2	1.9	No RPS		No RPS	1.9	1.34	
	Inverter 3	2.0	No RPS		No RPS	2.0	1.45	
2nd experiment (with RPS)	Inverter 1	1.9	3.52	1:1:0.716	0.89	2.1	1.5	1.021
	Inverter 2	1.9	3.52		0.89	2.1	1.5	
	Inverter 3	2.0	2.52		0.64	2.1	1.5	
3rd experiment (with RPS and changed condition)	Inverter 1	1.5	3.71	1:0.93:0.76	0.4	1.55	1.09	1.02
	Inverter 2	2.0	3.46		0.37	2.034	1.43	
	Inverter 3	2.0	2.5		0.27	2.018	1.43	

2.7 Contribution

- A novel reactive power scheduler has been proposed for distributed voltage regulation.
- The reactive power capacity of distributed sources, which may vary with the change of environmental condition, can be detected periodically by the proposed RPS.
- The balanced way of generating reference reactive power for different distributed sources using RPS has been presented. In this way, inverters associated with the DES share reactive power based on its dynamic reactive power capacity detected by RPS. Therefore, total

reference reactive power for voltage regulation is distributed among the inverters without overstressing any inverter.

- RPS ensures equal usage of the inverters owned by users of distributed systems and increase the inverters' life by reducing the stress.
- The task of voltage regulation of the distributed system has been accomplished using no global communication among the inverters.

2.8 Conclusion

The voltage at distributed system can be regulated using proper management of reactive power from the distrubted inverters. The concept of PQ inveters and the utilization of their reactive power production capacity for grid management is shown. The reactive power production capacity of the inverters is detected considering dynamic changes in the operating conditions and without any additional sensor elements. Inverters are operated such that all of them work harmoniously to produce the total commanded reactive power with minimum stress on each of them.

Chapter 3: Power Management for Overvoltage Prevention with High PV Penetration in a Radial Distribution System

3.1 Introduction

Grid connected photovoltaic (PV) systems are considered as the most prominent and rapidly growing technology among the renewable energy sources. The implementation of rooftop PV in distribution network improves the efficiency of providing electric power to the consumer. Along with the benefits of reducing transmission line loss and cost, customer owned PV has the advantages of upgradeability and decrease of dependence on fossil fuel. But the intermittent nature of solar irradiation imposes some challenges on power reliability. PV installation capacity in low voltage (LV) grid connected systems is limited due to the voltage rise concerns associated with high PV penetration and low consumer demand. As mentioned in the previous chapter, there is a possibility of reverse power phenomena and overvoltage in LV distribution feeder during high generation of solar PV systems and low demand situations. The management of real power curtailment for overvoltage prevention of grid connected distributed sources has been discussed in [37], [39]. There are several options available to address the overvoltage situation, although not all of them are attractive. An adaptive active power control strategy for large grid-connected PV power plants has been presented in [40] to maintain PV terminal voltages within a specified range. This chapter is focused on the improvement of reactive power management for voltage regulation of a low voltage distribution system incorporating inverters associated with PV or other renewable energy sources (RES) that can absorb or produce reactive power. This chapter introduces the critical

bus concept with the previously mentioned reactive power scheduler algorithm and addresses the power factor issue in voltage regulation using reactive power capacity of the inverters.

A reactive power scheduler was proposed in the previous chapter where reactive power capability of the inverters was limited by their rating and maximum current carrying capacity of semiconductor switches. The inverters are operated to produce as much real power as possible which is determined by the maximum power point tracker (MPPT). In this case, the rest of the current capacity can be used for reactive power production. However, along with inverters' rating there is usually a power factor constraint for inverters connected to a distributed system and it is not desirable for any distributed load or source to operate at power factors below a certain limit. Operating below the limit will result in the consumer being penalized by the grid operator. This limit varies with a country's grid code [96].

The fundamental problem for reactive power management is to determine which inverter should produce how much reactive power. The objective of voltage regulation is to regulate all the bus voltages in a distribution feeder within a range by effectively utilizing the reactive power capability of the inverters such that no inverter is overstressed or violates its power factor and total current carrying capacity limitations. However, uncoordinated reactive power generation or absorption by the inverters may cause additional losses. Therefore, efficient use of inverter's reactive power capability is a desirable feature for the PV inverter which is addressed in this chapter.

In a radial distribution system shown in Fig. 3.1, the farthest bus from the grid tie point is considered as the critical bus. With the high penetration of PV sources, maximum voltage rise occurs at the critical bus. Therefore, the objective of the voltage regulation of a radial

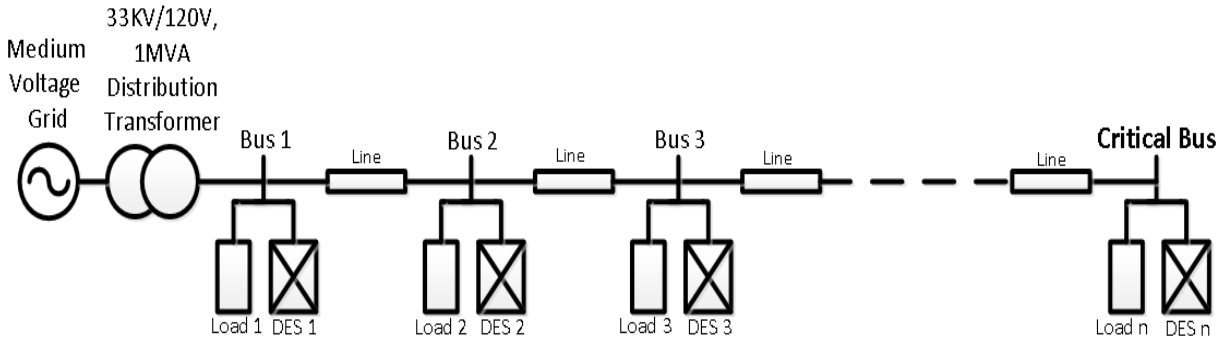

Figure 3.1. Radial distribution network

distribution system is to keep the critical bus voltage within its limits. ANSI C84.1 [109] expects equipment to operate at service voltages between 95% and 105% of the nominal value. The sensitivity of other inverters' real and reactive power on the critical bus voltage is important to determine reference reactive power of the other inverters [96]-[97]. The proposed method in [97] produces a reference reactive power for the inverters such that the power factor (PF) of the inverters with higher voltage rise is lower while making sure that the PF of each inverter does not go below a certain limit. Therefore, during high PV generation the reference reactive power for the critical bus inverter will be higher and may go beyond its capacity which is not addressed in this approach. A central scheduler of reactive power has been proposed in the previous chapter [110] which can detect the reactive power production capacity of different distributed sources without any communication among the inverters. However, in this approach, the critical bus and PF limitations are not considered by the scheduler. A reactive power management algorithm has been proposed in [111] for microgrids with high penetration of single phase induction motors in fault induced islanding case. Two states for reactive power generation have been proposed in the method where DES produce maximum reactive power

in the maximum reactive power (MRP) state, and voltage is supported by providing a reactive power from DES based on sensitivity in the sensitivity-based distributed Q compensation (SBDQC) state which is calculated by an optimization algorithm. However, with this approach the MRP state does not consider the PF constraint, which may be acceptable for few cycles during fault situation, but should be considered during normal operation of the DES.

In this chapter, an improved reactive power management system for radial distribution system is proposed which regulates the bus voltages within the permissible limit during high penetration of PV by utilizing the inverter's reactive power capacity more efficiently [113]. The proposed method considers the sensitivity of reactive power of the inverters at different location relative to the critical bus. This method enables other inverters close to the critical bus to effectively utilize their capacity which can reduce the inverter KVA rating when considering highest penetration during the year.

3.2 Voltage Sensitivity

Voltage sensitivity analysis provides the most efficient way to determine reference reactive power for the distributed inverters [97]. Voltage sensitivity matrix is derived by solving the power flow equation shown in (3.1) and (3.2). The solution is given by (3.3).

$$P_i = \sum_{j=1}^{n} |V_i||V_j|Y_{ij} \cos(\theta_{ij} + \delta_j - \delta_i) \tag{3.1}$$

$$Q_i = \sum_{j=1}^{n} |V_i||V_j|Y_{ij} \sin(\theta_{ij} + \delta_j - \delta_i) \tag{3.2}$$

$$\begin{bmatrix} \Delta\delta \\ \Delta V \end{bmatrix} = \begin{bmatrix} S_{\delta P} & S_{\delta Q} \\ S_{VP} & S_{VQ} \end{bmatrix} \begin{bmatrix} \Delta P \\ \Delta Q \end{bmatrix} \tag{3.3}$$

where P_i and Q_i are the active and reactive powers from bus i, $Y_{ij}\angle\theta$ is the admittance between bus i and j, V_i and V_j are voltage magnitude, δ_i and δ_j are voltage phase angles, $S_{\delta P}$ and $S_{\delta Q}$ are the sensitivities of the bus angles to the change in real and reactive powers, and S_{VP} and S_{VQ} are the sensitivities of the bus voltages to the change in real and reactive powers, respectively. The voltage sensitivity matrix shown in (3.3) is derived by solving two non-linear equations shown in (3.1) and (3.2) using Newton-Raphson method. The system Jacobian matrix is updated in each iteration and inverse of this Jacobian matrix results the sensitivity matrix. The real and reactive power variations of the inverters located farther from the grid tie point will have a higher impact on the critical bus voltage. Therefore, inverters closer to the n^{th} bus in Fig. 3.1, i.e., $(n-1)^{th}$ inverter, would have a higher impact on the critical bus voltage than that of inverter 1 or 2. Therefore, when DES produces more real power than the local load demand, the critical bus voltage increases more than other bus voltages. As a result, the critical bus inverter and other inverters close to it should be operated with lower PF to regulate the voltage below the permissible limit.

3.3 Reference Reactive Power Generation

Reference reactive power generation method for the inverters in the system should be based on sensitivity of the inverters. In the $cos\varphi(P)$ method shown graphically in Fig. 3.2(a), reference reactive power is produced based on inverter's real power generation [96]. In this method, with an increase of real power generation, PF of the inverter decreases. However, when both generation and local load demand is high, inverters may not need to operate at lower PF as the voltage rise will be lower in this case. Moreover, this method generates location free

reference reactive power which does not consider the sensitivity of the inverter. Fig. 3.2(b) shows the $Q(V)$ method where sensitivity of the inverter is considered in reference reactive power generation. Inverters with higher voltage deviation are operated with lower reactive power in this method. Inverters close to the grid absorb negligible, sometimes zero, reactive power as the voltage rise is very small in these inverters. As a result, the total amount of reactive power absorption in the system may be lower compared to the $cos\varphi(P)$ method. On the other hand, sometimes the critical bus voltage may rise over the permissible limit without other inverters contributing to support the critical bus voltage. One way so solve this problem may be through the use of communication among the inverters to switch from $Q(V)$ method to $cos\varphi(P)$ method. However, this is not considered as an efficient solution. The $cos\varphi(P,V)$ shown in Fig. 3.2(c) combines the previous two methods to generate reference reactive power for the inverters [96]. The lower limit of the PF C_2 of each inverter is varied with the voltage and PF is varied with the real power generation. In this way, other inverters can also support the critical bus voltage by absorbing reactive power without communication among the inverters. However, during high penetration of PV at the critical bus, PF is fixed at the lowest value of 0.9. As a consequence, the ratio of real and reactive power ($tan\varphi$) is also fixed during high penetration which results in high reference reactive power for the critical bus. As the inverter's reactive power capacity is limited by its rating, and with high real power generation, this capacity being even lower, at some stage the reference reactive power may go beyond the inverter's reactive power capacity. One way to address this situation is to set the inverter's current rating based on the highest yearly power generation and demand profile of the area, which results in an increase in the inverter cost.

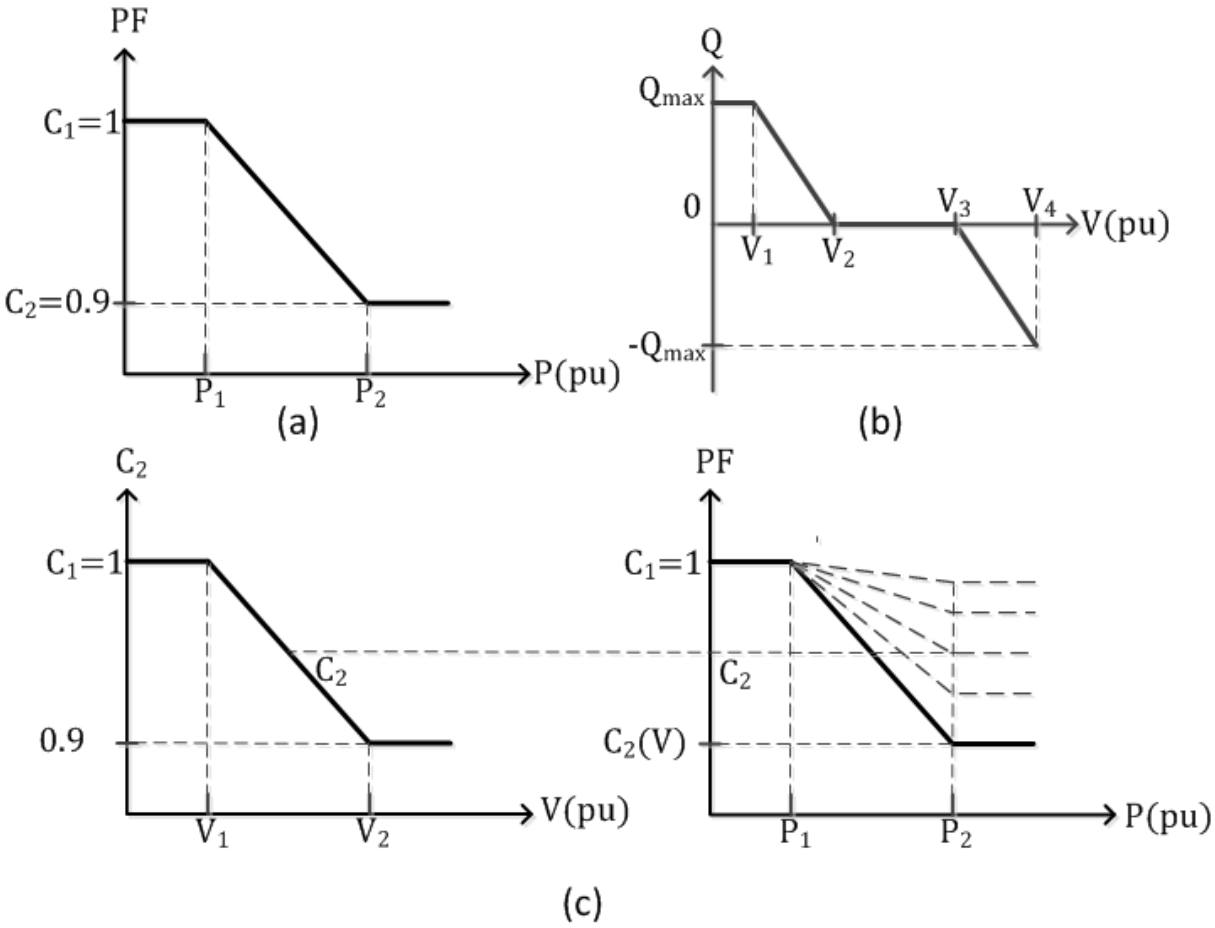

Figure 3.2. (a) $cos\varphi(P)$ method, (b) Q(V) method, (c) $cos\varphi(P,V)$ method

In the perturbation state of RPS described in the previous chapter, reactive power capacity is detected by small incremental perturbation of reactive power and in the normal state inverters are operated with reference reactive power set by the scheduler based on the ratio of the inverter's capacity. In this way, inverters have communication only with the scheduler and no communication is required among them. However, the downside of this method is that it does not consider the critical bus voltage and sensitivity of the inverters. Scheduler considers only the capacity of the inverter and total reference reactive power required by the system.

3.4 Proposed Method for Reference Reactive Power Generation

The objective of the proposed reference reactive power generation method is to regulate the critical bus voltage by effectively utilizing reactive power generation capacity of other inverters with high voltage sensitivity to the critical bus while maintaining sufficient PF requirements. A central reactive power management system (CRPMS) similar to the one used as reactive power scheduler in previous chapter is incorporated in the $cos\varphi(P,V)$ method to overcome the limitations stated in the previous section. In this method, the inverters do not have any communication among them.

Usually during high penetration of PV with low consumer demand, the critical bus inverter requires high reactive power absorption to bring down the critical bus voltage and maintain it within acceptable limits. With the increase of the real power penetration, reference reactive power for the inverter increases if the load demand remains fixed. However, during high penetration period, inverter's reactive power capacity decreases as most of its volt-amp capacity is utilized to produce real power. As a result when a high reference reactive power is generated for the critical bus inverter during high penetration, the inverter may not have the capacity of absorbing that reference reactive power. With $cos\varphi(P,V)$ method, other inverters' reactive power absorption is lower than the critical bus inverter as the voltage rise in other buses is less than that of the critical bus. Therefore, when critical bus inverter is saturated with reactive power, other inverters reactive power capacity can be utilized to regulate the critical bus voltage.

If the n^{th} bus in a radial distribution feeder is considered as a critical bus as shown in Fig.3.1, then n^{th} inverter associated with the n^{th} distributed energy source (*DES n*) has the highest sensitivity of reactive power to the voltage at the critical bus. The $(n-1)^{th}$ inverter will have the next highest sensitivity to the critical bus voltage and similarly sensitivity of each inverter becomes lower as it gets closer to the grid and farther from the critical bus.

When the critical bus inverter is saturated with reactive power during high penetration of PV, $cos\varphi(P,V)$ method no longer remains a viable option for voltage regulation at this bus. In the proposed method, for this situation, the CRPMS partially disregards the $cos\varphi(P,V)$ method and generates new reference reactive power for all inverters. When critical bus inverter reaches its capacity, it requires support from other inverters to regulate the voltage within allowable range. The CRPMS detects this support requirement. In this case, critical bus inverter absorbs as much reactive power that its capacity allows after meeting the real power command. The $(n-1)^{th}$ inverter is first considered by CRPMS to provide support for the critical bus inverter since it has the next highest sensitivity to the critical bus voltage. The new reference reactive power for $(n-1)^{th}$ inverter is set so that it is operated at PF $= 0.9$ which is the highest reactive power it can provide within allowable PF range. If $(n-1)^{th}$ inverter is incapable of absorbing reactive power at 0.9 PF or if its maximum possible reactive power is not sufficient to regulate the critical bus voltage, CRPMS will consider the next inverter with the highest sensitivity to operate at PF $= 0.9$ and support the critical bus inverter. All other inverters will be operated under $cos\varphi(P,V)$ method in this case. By using this method, unutilized reactive power capacity of the distributed inverters can be effectively used without

increasing the current rating of the critical bus inverter. Fig. 3.3 shows the flow diagram of the proposed reference reactive power generation method.

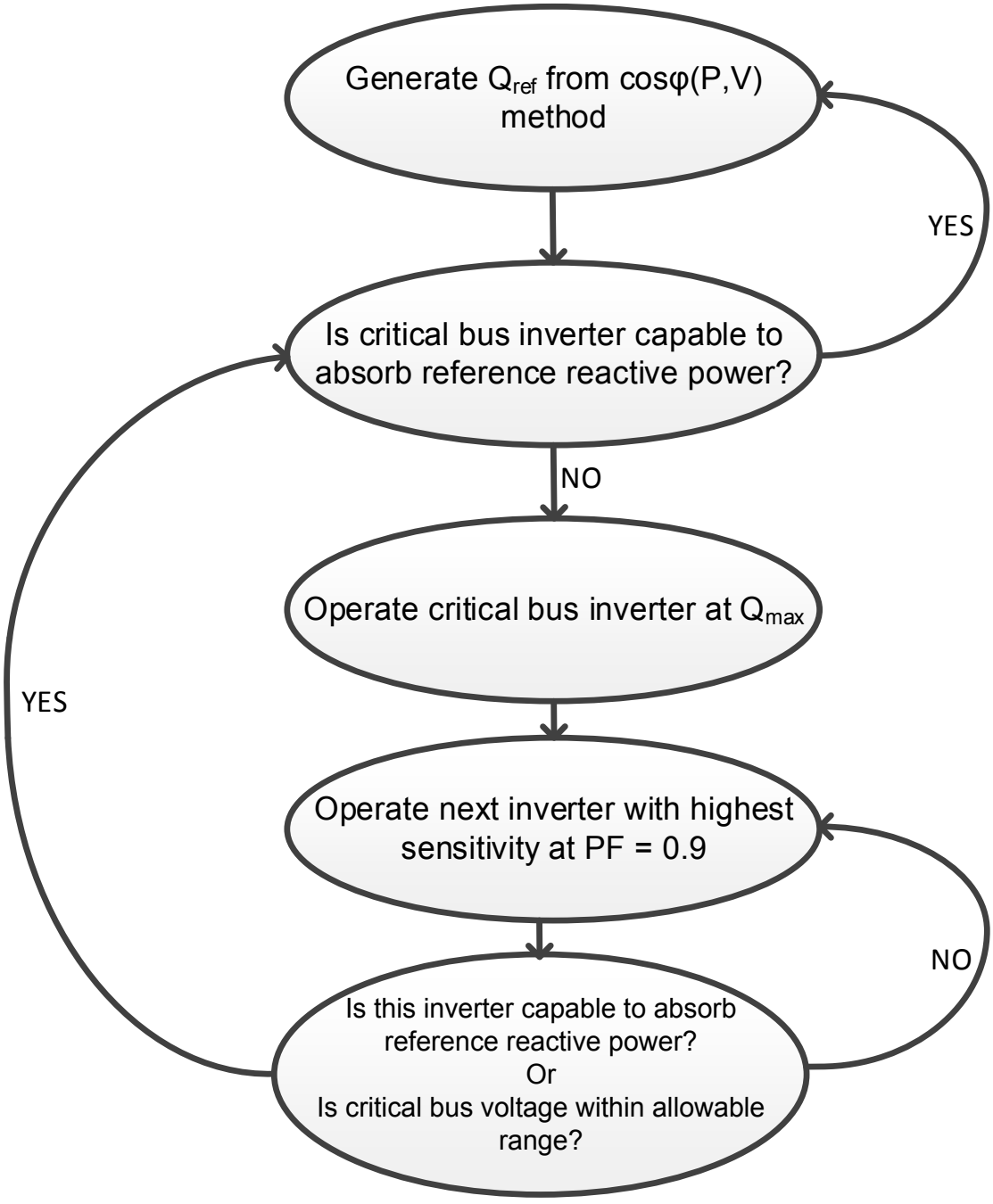

Figure 3.3. Proposed Central Reactive Power Management System

3.5 Simulation Results

A small distribution system has been considered which consists of three distributed inverters and loads at different bus locations of the feeder. The one line diagram of the system is shown in Fig. 3.4. Bus 3 is the critical bus for this system as it is the farthest one from the grid tie point. The voltage, power and line parameters for this simulation are summarized in Table 3.1. The lower limit of the PF is considered as 0.9 in this simulation. The allowable voltage range is between 95% and 105% of the nominal value according to [109] and the nominal voltage is 120 VAC. Therefore, the allowable range for service voltage at which utility delivers power to each home is 114 – 126 V.

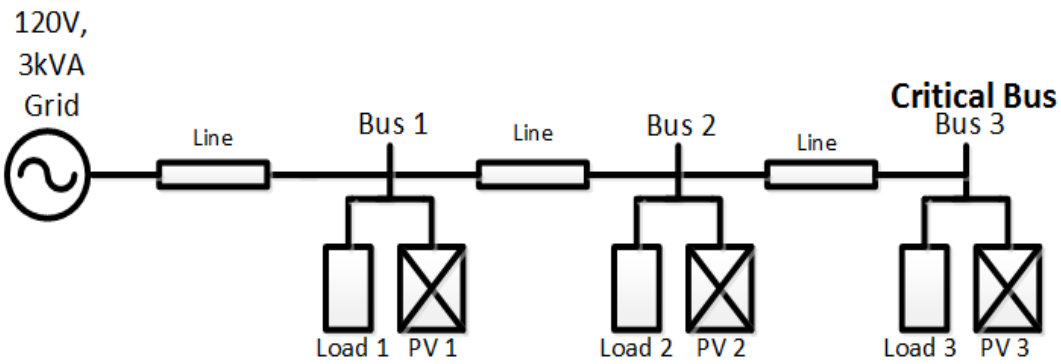

Figure 3.4. One line diagram of radial distribution feeder for simulation

Table 3.1. Radial feeder parameters

Base voltage	120V
Base power	3 KVA
Line impedance	(0.1581 + j0.1121) pu
Each load	200 W

Since in this configuration bus 3 is the critical bus, PV3 is considered as the DES at critical bus. The control of the distributed inverters is implemented in the *d-q* reference frame since this enables the separation of active power and reactive power components. The park transformation used for the conversion of single phase current produced by the inverter to two phase rotating reference frame components i_q and i_d is shown in (3.4).

$$\begin{bmatrix} i_q \\ i_d \end{bmatrix} = \frac{2}{3}\begin{bmatrix} cos\varphi & -sin\varphi \\ sin\varphi & cos\varphi \end{bmatrix}\begin{bmatrix} i_\alpha \\ i_\beta \end{bmatrix} \tag{3.4}$$

where i_α and i_β are in phase and 90^0 out of phase component of single phase current respectively and φ is the estimated phase angle by phase-locked loop. By this conversion, real and reactive power can be controlled by controlling i_q and i_d, respectively. The rated current limit for the distributed inverters are considered as 8A.

Fig. 3.5 shows the real power variation of PV3 commanded by MPPT of the respective PV with the change of solar insolation and different bus voltages of the radial distribution feeder. The change in real power is shown as the change of i_q. The bus voltages are shown in per unit (pu) based on nominal voltage 120V. All the inverters are operated in $cos\varphi(P,V)$ method at

normal operation. A change in PV penetration occurs at bus 3 at 0.3 second. From 0.3 second to 0.6 second the critical bus $i_q = 6A$ which is 2.5 times higher than the local load demand. It can be seen that the critical bus voltage (at bus 3) during this time increases to 4% of its nominal value. At 0.6 second, the penetration of PV3 is further increased to 3.3 times of the local load demand with an $i_q = 7.9A$. In this case reactive power capacity of the PV3 inverter measured by i_d capacity is 1.26 A but the reference reactive power generated by $cos\varphi(P,V)$ method for this inverter is 3.77 A. Therefor PV3 inverter does not have the capacity of absorbing reference reactive power calculated by the $cos\varphi(P,V)$ method. As a result the critical bus voltage rises to over 5% of its nominal value which is beyond the allowable range. After 1.0 second PV penetration decreases which brings the critical bus voltage down to allowable range.

Figs. 3.6 and 3.7 show the effect of incorporating the proposed CRPMS for voltage regulation during high PV penetration. Fig. 3.6 shows the comparison between generated reference reactive power by $cos\varphi(P,V)$ method and the proposed method. As seen in Fig. 3.5, support is required for PV3 inverter to regulate the voltage at bus 3 from 0.6 to 1.0 second when PV3 penetration is high and $cos\varphi(P,V)$ method is not sufficient enough to keep the critical bus voltage within allowable range. Fig. 3.6 shows that when reactive power support is required from PV2, which is the next DES with the highest sensitivity after PV3, the calculated reference i_d of PV2 and PV3 from the $cos\ \varphi(P,V)$ method are 1.45 A and 3.77 A respectively. Since voltage rise in bus 2 is lower than the voltage rise at bus 3, reference i_d generated for PV2 inverter is lower compared to the PV3 inverter. The i_d capacity during this time for these two inverters are 7.86 A and 1.26 A respectively. Therefore while PV3 inverter

is saturated with its capacity while PV2 inverter is underutilized with low reference reactive power generated by $cos\varphi(P,V)$ method.

In the CRPMS method reference i_d of PV3 inverter is reduced to 1.26 A during high penetration time which is the maximum available reactive power Q_{max} for PV3. Also PV2 inverter is operated at PF 0.9 for which reference i_d for this inverter is calculated as 2.9 A. In this way reactive power capacity of PV2 inverter is utilized when critical bus inverter is saturated. Fig. 3.7 verifies that the critical bus voltage remains within allowable range i.e., the voltage rise is not over 5% for the same high penetration of PV3 with the proposed reactive power management. Table 3.2 summarizes the simulation results.

Table 3.2. Summary of simulation results

Time (sec)	**PV3 Ref i_q**	**PV3 i_d Capacity**	**Ref i_d**			
			***cosφ*(*P*,*V*) method**		**CRPMS**	
			PV2	PV3	PV2	PV3
0.3-0.6	6A	5.29A	1.18A	1.5A	1.18A	1.5A
0.6 -1.0	**7.9A**	**1.26A**	**1.45A**	**3.77A**	**2.9A**	**1.26A**
1.0-1.6	6A	5.29A	1.18A	1.5A	1.18A	1.5A

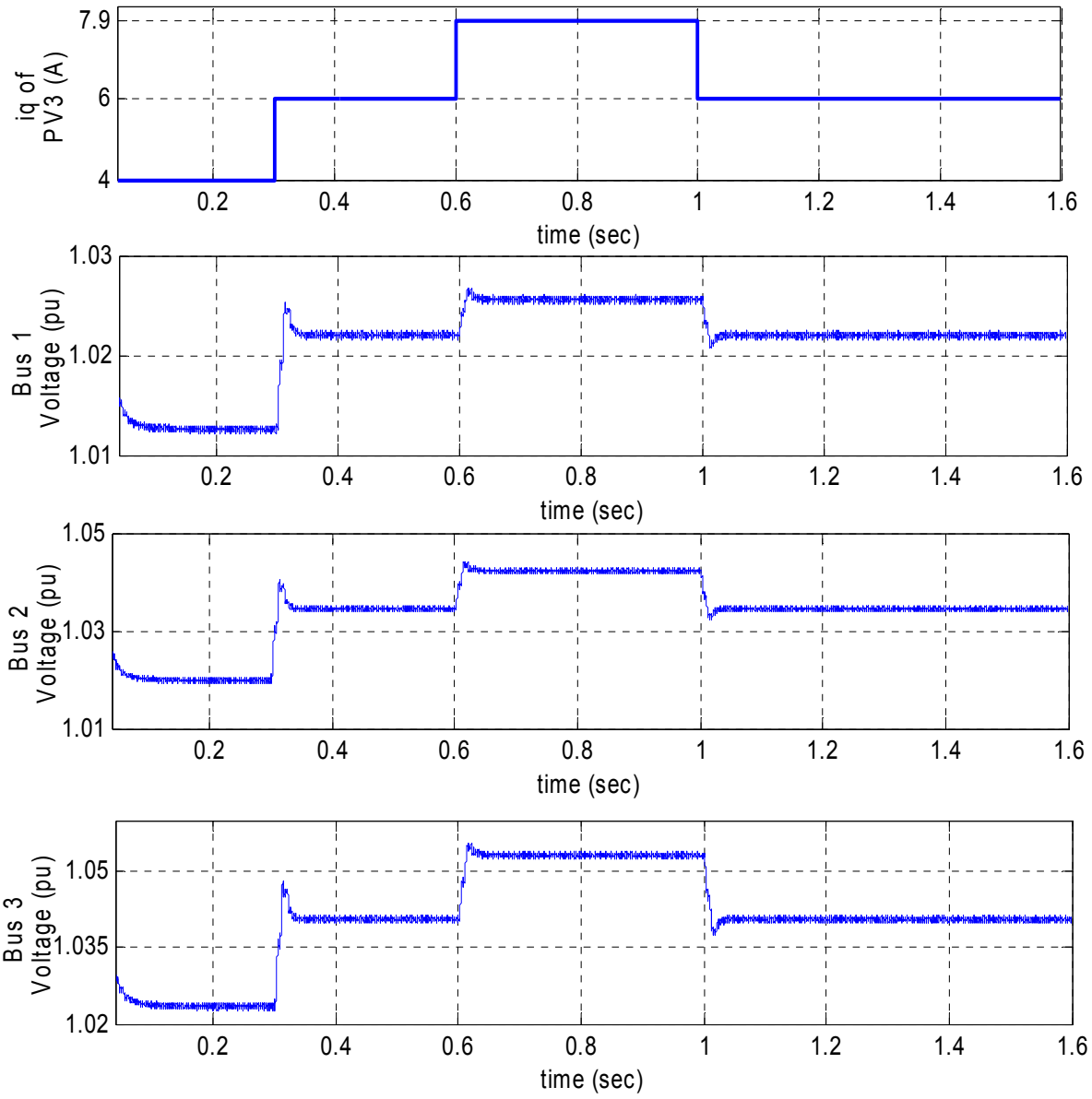

Figure 3.5. Real power command measured by i_q of PV3 and different bus voltages with $cos\varphi(P,V)$ method

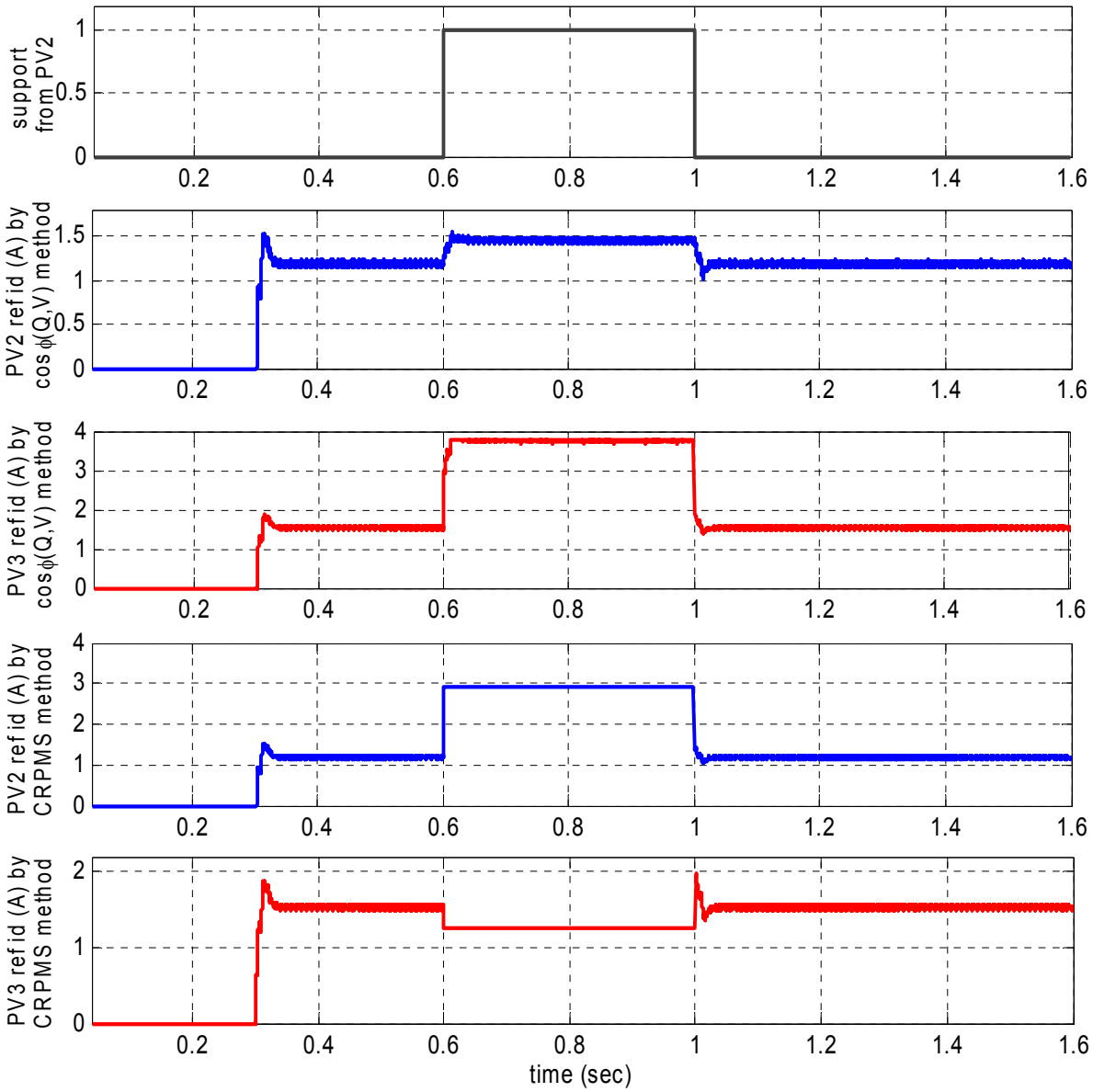

Figure 3.6. Reference reactive power measured by i_d for PV2 and PV3 calculated by $cos\varphi(P,V)$ method and proposed CRPMS

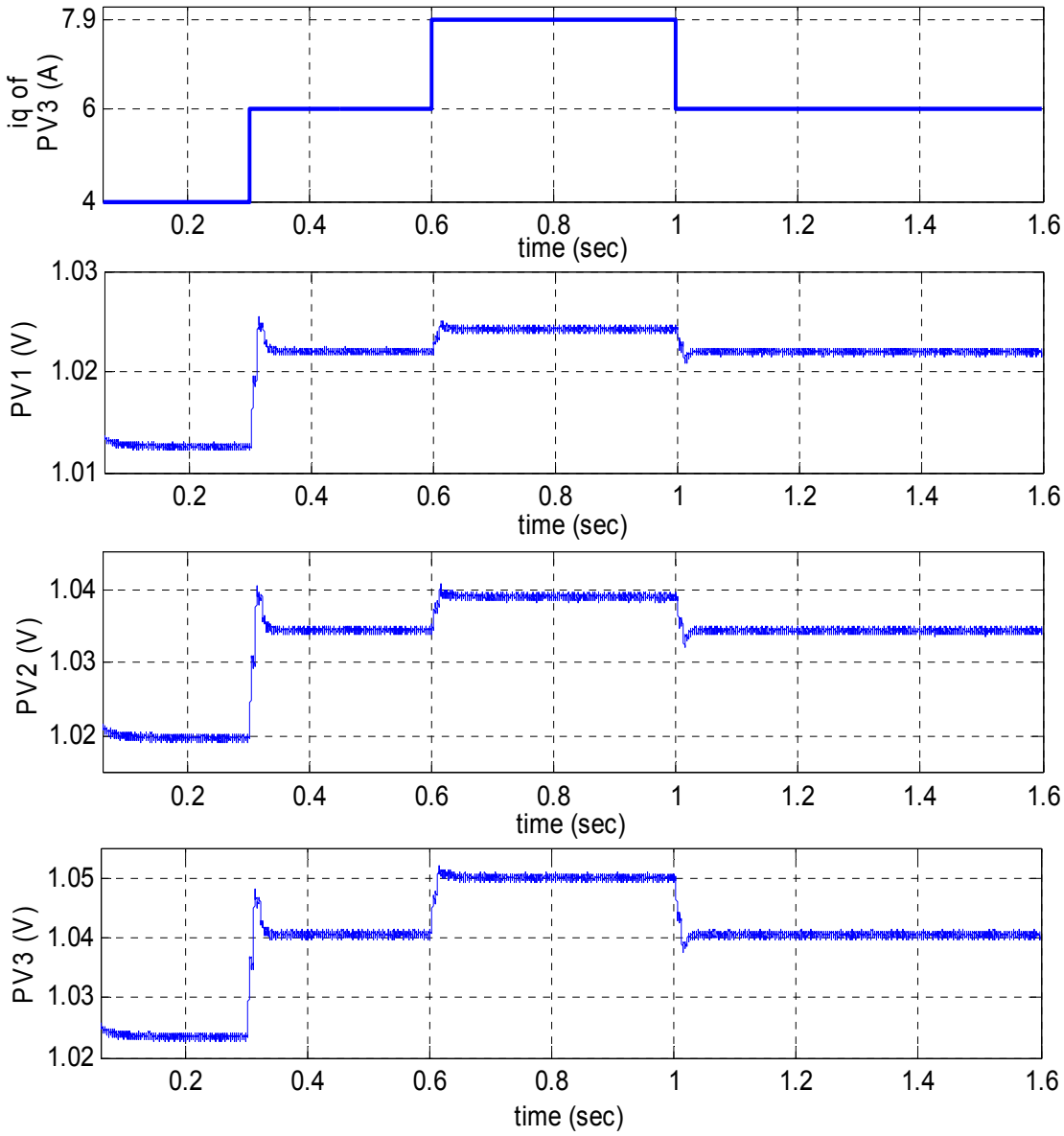

Figure 3.7. Real power command measured by i_q of PV3 and different bus voltages with the proposed CRPMS

3.6 Experimental Results

The same radial distribution network shown in Fig. 3.4 for simulation work is used for experimental validation of the proposed algorithm. The experimental setup is shown in Fig. 3.8 which is implemented with three distributed inverters and loads at different bus location. Three inverters have been connected to the grid for parallel operation. Considering the ratings of the devices for experimental setup, the nominal voltage is scaled down to 90V rms.

The inverters are operated in $cos\varphi(P,V)$ method in the first experiment. The real power produced by the critical inverter which is PV3 is 3.3 times higher than its local load demand. Also the closest inverter to the critical bus which is PV2, produces real power 1.5 times higher than its local load demand to resemble a high PV penetration with low load demand situation. The current ratings of each inverter is considered to be 4A. The experimental results for this case are shown in Fig. 3.9. It can be seen from the results that the critical bus inverter (PV3) is not capable of absorbing reactive power commanded by $cos\varphi(P,V)$ method in this scenario since it is producing high real power. Therefore, the critical bus voltage (97.1V) increases by 7.89% of the nominal voltage which is beyond the allowable range.

In the second experiment, the inverters are operated by the proposed CRPMS method. Fig. 3.10 shows the voltages and currents of bus 3 and bus 2 for the CRPMS method. In this method, PV2 is operated at 0.9 PF and critical bus inverter is operated at maximum reactive power with 0.98 PF. It can be seen from the results that the bus 3 voltage is 94.4 now. The voltage rise at critical bus is maintained at 4.89% of the nominal value which is within the allowable range.

Table 3.3 summarizes the real and reactive power components of the inverter currents, and the voltage increase for both methods.

Table 3.3. Summary of experimental results

Method	Parameter	PV3	$PV2$
$cos\varphi(P,V)$	Current rating i_a	4A	4A
	i_q	3.95A	2A
	i_d capacity	0.63A	3.46A
	i_d reference	0.88A	0A
	Voltage rise	7.89%	6.67%
CRPMS	Current rating i_a	4A	4A
	i_q	3.95A	2A
	i_d capacity	0.63A	3.46A
	i_d reference	0.63A	0.968A
	Voltage rise	4.89%	3.78%

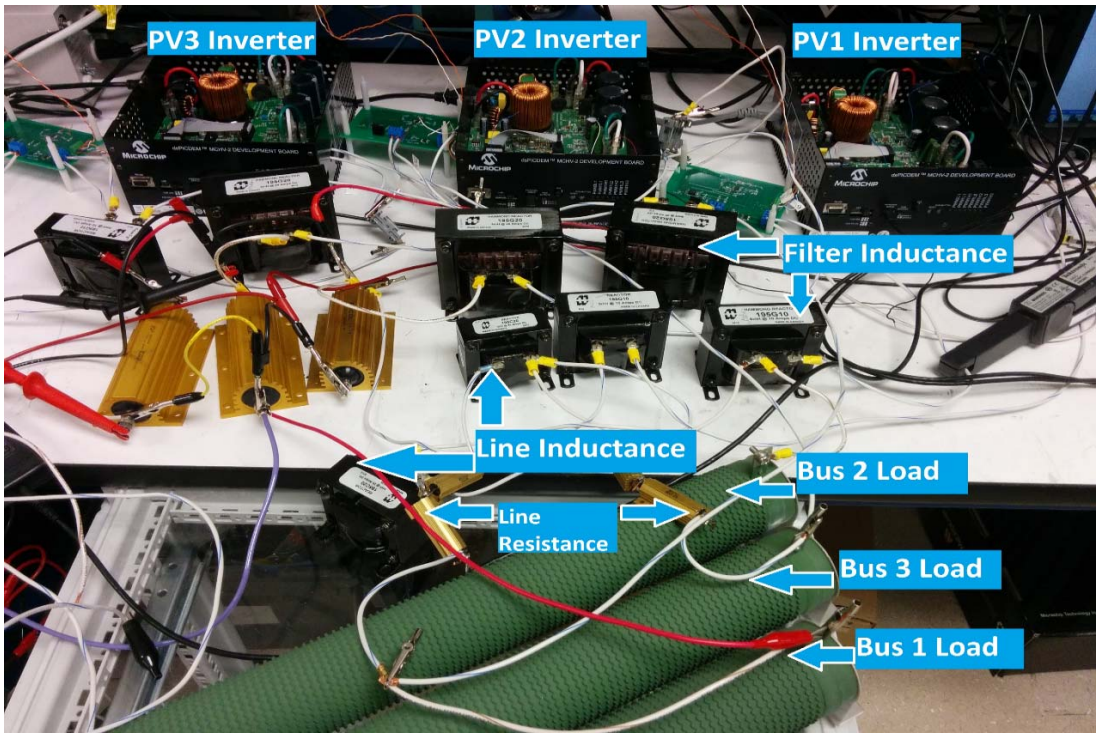

Figure 3.8. Experimental setup

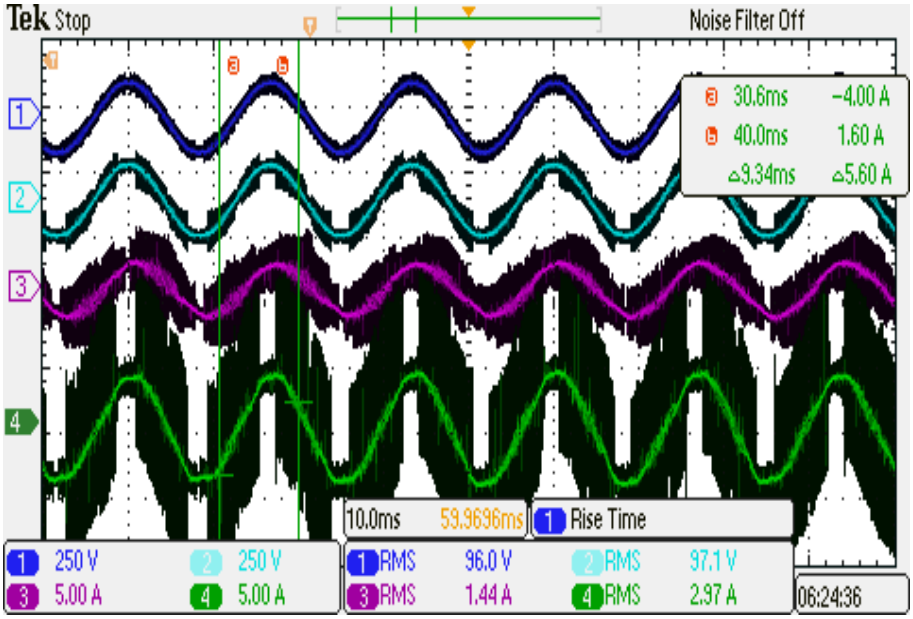

Figure 3.9. Bus voltages and inverter currents by $cos\varphi(P,V)$ method. Ch.1: bus 2 voltage (96 V rms). Ch.2: critical bus voltage (97.1 V rms). Ch.3: PV2 current (1.44A rms). Ch.4: PV3 current (2.97A rms)

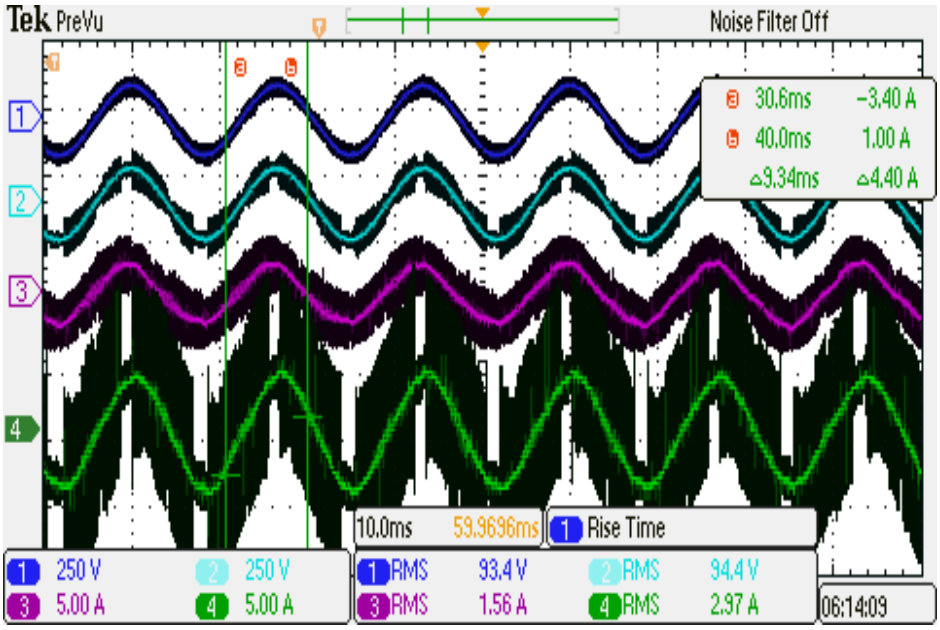

Figure 3.10. Bus voltages and inverter currents by CRPMS method. Ch.1: bus 2 voltage (93.4V rms). Ch.2: critical bus voltage (94.4V rms). Ch.3: PV2 current (1.56A rms). Ch.4: PV3 current (2.97A rms)

3.7 Contribution

- A Central Reference Reactive Power Management System has been proposed for voltage regulation of the radial distribution system during high PV penetration.
- The CRPMS addresses the limitations of the existing methods and improves the voltage regulation of distribution system with distributed energy sources.
- The proposed CRPMS considers not only the inverters total current capacity but also the power factor constraint given by the grid operator.

- Effective utilization of reactive power capacity of the inverters at buses with high sensitivity to critical bus has been ensured during high penetration of distributed PV inverters.
- The improvement of the voltage regulation compared to existing method has been presented both in simulation and experiments.

3.8 Conclusion

A new method of CRPMS has been proposed in this chapter which addresses the limitations of the existing methods and improves the voltage regulation of a radial distribution system during high penetration of DES. This method is based on inverters capacity and sensitivity to the critical bus and allows effective utilization of reactive power capacity of the inverters with high sensitivity to the critical bus. Simulation and experimental results are presented to validate the improvement of voltage regulation by the proposed CRPMS

Chapter 4: Grid Synchronization in Presence of Grid Impurity

4.1 Introduction

The increasing demand of integrating single phase or three-phase renewable energy sources (RES) like distributed solar systems, electric or hybrid vehicles, storages, offshore or onshore wind and wave energy systems to the utility grid requires proper estimation and synchronization of frequency and phase angle of the utility voltage. The control of the real and reactive power for grid connected distributed sources requires accurate phase information of the utility voltage. Therefore, voltage regulation algorithm for grid connected distributed system using reactive power control presented in last two chapters is highly dependent on the accurate estimation of phase angle of grid voltage. Also the operation of different power electronic devices and drives for motor control application is highly dependent on the accuracy of phase estimation. The most commonly used and easily implementable algorithm for grid synchronization is the phase locked loop (PLL) technique [11]. The basic structure of the PLL used in power system applications is realized in synchronous reference frame (SRF) [9], [12]. The conventional three-phase SRF based PLL (SRF-PLL) works perfectly with a grid that has no imperfections such as harmonics, unbalanced voltage or frequency fluctuation. In reality the power grid is not as clean and typically contaminated with imperfections. The challenge is to implement a robust and fast PLL for operation in distorted utility conditions [13].

The harmonics in the grid voltage are considered as disturbances by the phase-locked loops (PLLs) whose effect should be eliminated [42]. An accurate estimation for the grid phase is

needed to estimate the harmonics, but the existence of harmonics on the grid voltage deteriorates the phase estimation accuracy. If the utility grid has significant amount of harmonics, PLL suffers from steady state error in phase estimation. The estimated phase or frequency has oscillations in this case.

Three-phase utility grid has another imperfection along with voltage harmonics and that is unbalanced voltage. Voltages of three phases may get unbalanced by magnitude or by phases. The steady state performance also suffers from unbalanced voltage effect of the grid. Along with the steady state performance, dynamic performance of PLL is equally important. The dynamic performance of PLL worsens in case of any frequency fluctuation. Poor dynamics of PLL may result in instability in the system and cause severe damage to the power electronic devices.

This chapter demonstrates a simple and robust technique to eliminate both the harmonics and unbalance effect of the grid voltage to improve the steady state performance with high PLL bandwidth. The approach is to first eliminate the harmonics or unbalanced voltage effect present in the grid. Then, the harmonic-free signal can be used by the PLL to estimate the phase of the grid voltage. The theoretical basis of the algorithm along with the simulation and experimental results are presented in this chapter.

4.2 PLL Grid Synchronization

The objective of the PLL is to detect the instantaneous phase angle of the grid voltage. The phase angle is the integral of instantaneous angular frequency of the grid voltage. The phase

angle information is required for synchronization of DES inverter to the grid. Also the operation of current controller to regulate real and reactive power at the reference value as presented in chapter 2 uses the grid voltage phase angle and frequency information to generate reference voltage for space vector PWM in digital signal processor (DSP). If the PLL output is erroneous, the control over real and reactive power will not be accurate enough which may lead to voltage oscillation, over voltage scenario, distortion of inverter output current or instability of the system. Therefore PLL plays an important role in grid connected distributed energy system.

Figs. 4.1(a) and 4.1(b) show the block diagram of single phase and three-phase SRF-PLL respectively. Accuracy of the phase estimation depends on the bandwidth (BW) of the loop filter shown in Fig. 4.1. If the utility grid has significant amount of harmonics and/or voltage unbalance, PLL suffers from steady state error in phase estimation. The estimated phase or frequency has oscillations in this case. Lower BW loop filter improves the steady state error, but worsens the dynamic performance in case of any frequency fluctuation. Thus, there is a tradeoff between steady state error and dynamic performance when PLL is used for a polluted grid. If the sources of steady state error that include harmonics and voltage unbalance can be eliminated before feeding the voltage measurement into PLL, the BW of the loop filter can be increased since the steady state error will not be an issue for phase estimation. Higher BW will improve the dynamic performance in the presence of frequency fluctuation.

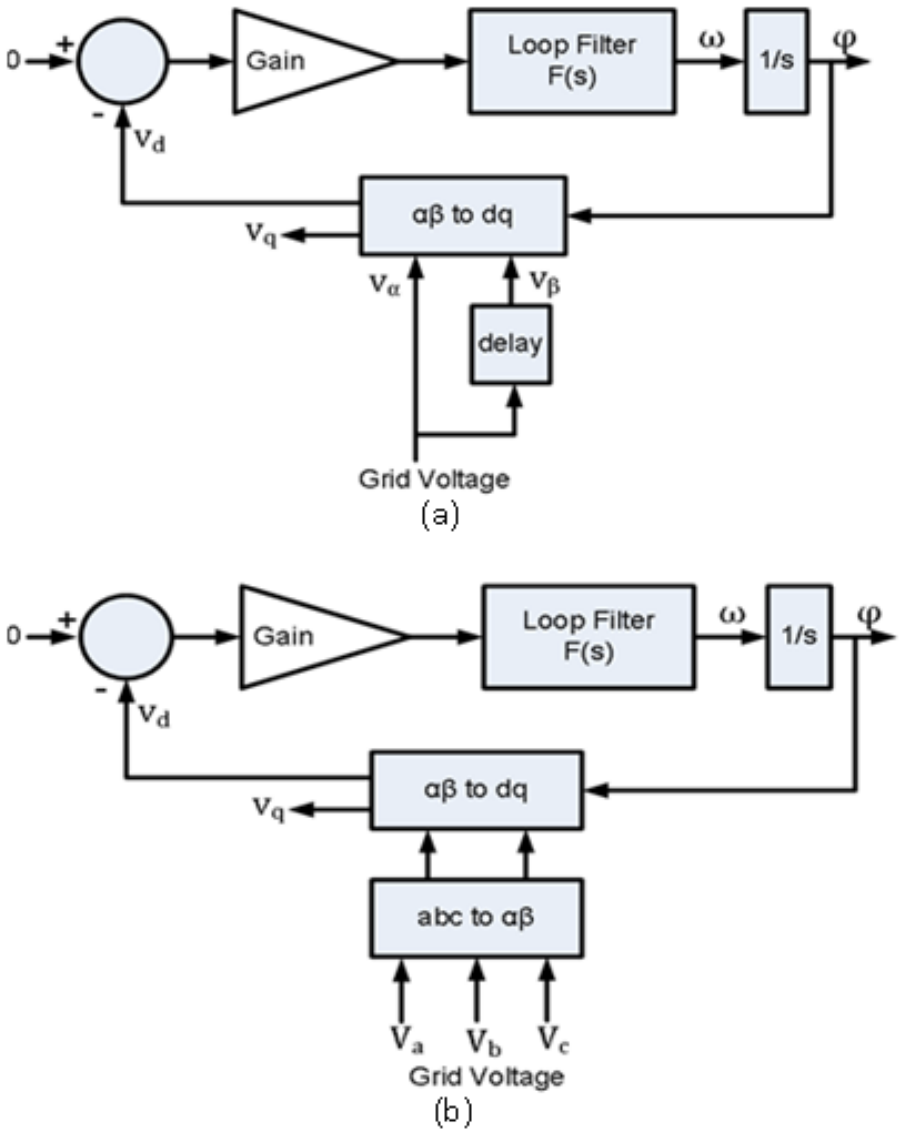

Figure 4.1. (a) Single phase SRF-PLL (b) Three-phase SRF-PLL

Several methods have been proposed to improve to PLL performance in distorted utility conditions. In one approach, active filters (band pass, band stop, low pass, notch and adaptive notch) are used to remove harmonics at a preselected cutoff frequency knowing the harmonics and unbalanced voltage pattern [14]-[18]. The approach used in [44]–[46] uses a group of bandpass filters whose outputs are sinusoidal signals synchronized with the grid voltage

harmonics. However, for effective harmonic injections, the harmonics needed to be estimated in the *dq* rotating reference frame. Therefore, developing harmonic estimators that give their outputs in the *dq* reference frame is required for this approach. Also, the method using filter is complex, may not eliminate the harmonics completely and suffer from long computation time, filtering delay and sensitivity to the frequency variation. Delayed signal cancellation method is used for the same purpose, but negative sequence current and a large cascaded system is required for the implementation [19]. Decoupled double synchronous reference frame has been used to remove the negative sequence voltage caused by unbalanced grid voltage using two oppositely rotating synchronous reference frame [11]-[12], but this method does not consider the harmonic effect. In [43], one PLL block per harmonic is used, but redundancies are involved in this approach when the frequency of each harmonic is estimated independently.

The objective of proposed approach is to operate PLL at high bandwidth of loop filter. As mentioned previously, the existence of the harmonics and unbalanced voltage in the grid disturbs the phase estimation. However, elimination of harmonics and unbalanced voltage effect from the input of PLL ensures accurate phase estimation. There is no requirement to use a special PLL algorithm. The proposed algorithm will be presented in the following sections.

4.3 Single Phase PLL

4.3.1 Single Phase SRF-PLL Structure

The basic structure of the single phase PLL is shown in Fig. 4.1(a). For single phase system, the grid voltage is decomposed into two phase stationary reference frame by using a memory

block [42]. One of the two phase voltages v_α is equal to the grid voltage v_g, and other voltage is previous ¼-period value of v_g multiplied by (-1). So the stationary frame voltages can be expressed as

$$v_\alpha = V_m \cos(\theta) \tag{4.1}$$

$$v_\beta = -V_m \sin(\theta) \tag{4.2}$$

where, V_m is the peak value and θ is the actual phase angle of the grid voltage. Then voltages are converted from stationary reference frame to synchronously rotating reference frame by the following Park Transformation,

$$\begin{bmatrix} v_q \\ v_d \end{bmatrix} = \begin{bmatrix} cos\varphi & -sin\varphi \\ sin\varphi & cos\varphi \end{bmatrix} \begin{bmatrix} v_\alpha \\ v_\beta \end{bmatrix} \tag{4.3}$$

where, φ is the estimated phase angle by PLL and v_q and v_d are quadrature and direct axis voltage respectively. Replacing (4.1) and (4.2) in (4.3), v_q and v_d can be expressed as

$$v_q = V_m \cos(\theta - \varphi) \tag{4.4}$$

$$v_d = -V_m \sin(\theta - \varphi) \tag{4.5}$$

When estimated phase φ of PLL is equal to the actual phase θ, direct axis voltage v_d is equal to zero. Therefore v_d is compared to zero and error is passed through the loop filter to estimate the grid frequency ω as shown in Fig. 4.1(a). Hence, the PLL frequency $\hat{\omega}$ and phase φ can track the utility frequency ω and phase angle θ, respectively, by the proper design of the loop filter. The loop filter can be a proportional-integral (PI) type controller which can be given as

$$F(s) = K_p \frac{1+s\tau}{s\tau} \tag{4.6}$$

where, K_p is the proportional gain and K_p/τ is the integral gain. The loop filter and integrator together forms a second order system. The linearized model [12] of the SRF-PLL is shown in Fig. 4.2. The transfer function of this second order closed loop system can be derived as

$$H(s) = \frac{F(s)V_m}{s+F(s)V_m} \tag{4.7}$$

The transfer function given in (4.7) can be rewritten in the generalized second order system format as

$$H(s) = \frac{2\xi\omega_n s+{\omega_n}^2}{s^2+2\xi\omega_n s+{\omega_n}^2} \tag{4.8}$$

Comparing (4.7) and (4.8), the bandwidth is $\omega_n = \sqrt{\frac{K_p V_m}{\tau}}$, and the damping ratio is $\xi = \frac{K_p V_m}{2\omega_n} = \frac{\sqrt{\tau * K_p * V_m}}{2}$. The settling time to within 2% of the final value is $T_s = \frac{3.9}{\xi\,\omega_n}$.

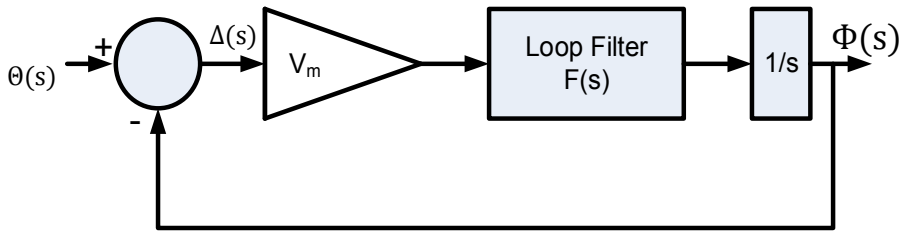

Figure 4.2. Linearized model of SRF-PLL

4.3.2 Single Phase SRF-PLL in Polluted Grid

The single phase grid voltage could be contaminated by higher order even or odd harmonics. The error between estimated phase and actual phase of the grid voltage is significantly high in presence of harmonics. Bandpass filters can be used to attenuate the harmonics in the grid

voltage signal, but these filters may not remove the harmonics completely and their implementation could be computationally demanding. Therefore, an efficient method is required that eliminates the higher order harmonic effects from the sampled single-phase grid voltage using simple arithmetic operations. The single-phase grid voltage v_g that is distorted by up to the n^{th} order harmonics can be written as

$$v_g(t) = V_1 \sin(\omega t + \phi) + \sum_{k=2}^{n} V_k \sin(k\omega t + \phi_k) \tag{4.9}$$

where V_k, $k\omega$, and ϕ_k are the magnitude, frequency, and phase of the k^{th} harmonic component.

4.3.3 Harmonic Elimination Method

In this sub-section a harmonic elimination method has been proposed with some simple arithmetic operation. The following operation can be used for elimination of all even harmonic components:

$$v_{g0}(t) = v_g(t) - v_g\left(t - \frac{\pi}{\omega}\right) \tag{4.10}$$

$$= V_1 \sin(\omega t + \phi) + \sum_{k=2}^{n} V_k \sin(k\omega t + \phi_k) - V_1 \sin\left(\omega\left(t - \frac{\pi}{\omega}\right) + \phi\right) - \sum_{k=2}^{n} V_k \sin\left(k\omega\left(t - \frac{\pi}{\omega}\right) + \phi_k\right)$$

$$= V_1 \sin(\omega t + \phi) + \sum_{k=2}^{n} V_k \sin(k\omega t + \phi_k) + V_1 \sin(\pi - \omega t - \phi) + \sum_{k=2}^{n} V_k \sin(k\pi - k\omega t - \phi_k)$$

Since k is an even number, $V_k \sin(k\pi - k\omega t - \phi_k) = -V_k \sin(k\omega t + \phi_k)$. Then,

$$v_{g0}(t) = 2V_1 \sin(\omega t + \phi) + \sum_{k=2}^{n} V_k \sin(k\omega t + \phi_k) - \sum_{k=2}^{n} V_k \sin(k\omega t + \phi_k)$$

$$v_{g0}(t) = 2V_1 \sin(\omega t + \phi)$$

Therefore, there is no even harmonic component in $v_{go}(t)$ after the single operation of (4.10) and fundamental component can be recovered from the grid voltage contaminated by even harmonics of any order.

No single operation like the one in (4.10) exists to remove all odd harmonics. In fact, every single odd harmonic needs a separate operation. In the following discussion, the derivation is only devoted to the odd harmonics. Let us define $v_{g0-(i_1,i_2,i_3\ldots\ldots,i_n)}$ as the processed $v_{g0}(t)$ after removing $i_1^{th}, i_2^{th}, i_3^{th} \ldots\ldots, i_n^{th}$ odd harmonics. The proposed operation to remove the h^{th} harmonic (h being an odd number) is given by

$$v_{g0-(h)}(t) = v_{g0}(t) + v_{g0}\left(t - \frac{\pi}{h\omega}\right) \tag{4.11}$$

$$= V_1 \sin(\omega t + \phi) + V_h \sin(h\omega t + \phi_h) + V_1 \sin\left(\omega\left(t - \frac{\pi}{h\omega}\right) + \phi\right) + V_h \sin\left(h\omega\left(t - \frac{\pi}{h\omega}\right) + \phi_h\right)$$

$$= V_1 \sin(\omega t + \phi) + V_h \sin(h\omega t + \phi_h) + V_1 \sin\left(\omega t - \frac{\pi}{h} + \phi\right) - V_h \sin(\pi - h\omega t - \phi_k)$$

$$= V_1 \sin(\omega t + \phi) + V_h \sin(h\omega t + \phi_h) + V_1 \sin\left(\omega t - \frac{\pi}{h} + \phi\right) - V_h \sin(h\omega t + \phi_k)$$

$$= V_1 \sin(\omega t + \phi) + V_1 \sin\left(\omega t - \frac{\pi}{h} + \phi\right)$$

Here V_h is the amplitude of h^{th} harmonic component. After the operation of as shown in (4.11), h^{th} harmonic component goes away from $v_{g0}(t)$. Accordingly, to remove different harmonics, the following operations can be used:

$$v_{g0-(3)}(t) = v_{g0}(t) + v_{g0}\left(t - \frac{\pi}{3\omega}\right) \tag{4.12}$$

$$v_{g0-(3,5)}(t) = v_{g0-(3)}(t) + v_{g0-(3)}\left(t - \frac{\pi}{5\omega}\right) \tag{4.13}$$

$$v_{g0-(3,5,7)}(t) = v_{g0-(3,5)}(t) + v_{g0-(3,5)}\left(t - \frac{\pi}{7\omega}\right) \tag{4.14}$$

$$v_{g0-(3,5,7,9)}(t) = v_{g0-(3,5,7)}(t) + v_{g0-(3,5,7)}\left(t - \frac{\pi}{9\omega}\right) \tag{4.15}$$

After removing m numbers of odd harmonics from the sampled grid voltage, the processed signal becomes

$$v_{g0-(3,5,7,\ldots,2m+1)}(t) = 2^m\left(\prod_{k=1}^{m} cos\frac{\pi}{4k+2}\right) * V_1 \sin\left(\omega t + \phi - \sum_{k=1}^{m}\frac{\pi}{4k+2}\right) \tag{3.16}$$

This signal represents the fundamental component of $v_{g0}$with some gain and a phase lag. To recover the original phase, the phase obtained by the PLL should be corrected by adding an amount of $\sum_{k=1}^{m}\frac{\pi}{4k+2}$ phase shift to it. The harmonic elimination block diagram is shown in Fig. 4.3.

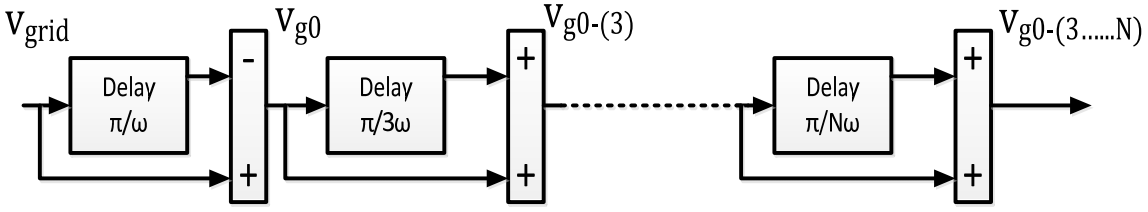

Figure 4.3. Harmonic elimination block

4.4 Three-Phase PLL

4.4.1 Three-Phase SRF-PLL Structure

Three-phase PLL structure is shown in Fig. 4.1(b). Three-phase grid voltage is converted to two phase stationary reference frame voltage v_α and v_β by the following transformation.

$$\begin{bmatrix} v_\alpha \\ v_\beta \end{bmatrix} = \frac{2}{3}\begin{bmatrix} 1 & -\frac{1}{2} & -\frac{1}{2} \\ 0 & -\frac{\sqrt{3}}{2} & \frac{\sqrt{3}}{2} \end{bmatrix}\begin{bmatrix} V_m\cos(\theta) \\ V_m\cos(\theta - \frac{2\pi}{3}) \\ V_m\cos(\theta + \frac{2\pi}{3}) \end{bmatrix} \tag{4.17}$$

where, V_m is the peak value and θ is the actual phase angle of the grid voltage. After simplification of (4.17), v_α and v_β can be expressed as

$$v_\alpha = V_m \cos(\theta) \tag{4.18}$$

$$v_\beta = -V_m \sin(\theta) \tag{4.19}$$

The expression of v_α and v_β for three-phase system shown in (4.18) and (4.19) is same as the expression for single phase system shown in (4.4) and (4.5). Therefore transformation from stationary reference frame to synchronously rotating reference frame and loop filter design is same as shown for single phase PLL in section 4.4.1.

4.4.2 Modified SRF-PLL for Polluted grid

Three-phase grid voltage may contain another impurity along with voltage harmonics and that is voltage unbalance. This section will demonstrate the modified structure of SRF-PLL in presence of harmonics and unbalanced voltage. The typical non-linear loads connected to the point of common coupling (PCC) are three phase full bridge line frequency rectifiers. For this

kind of loads, the even and triplen harmonics are negligible and they can be considered to be zero [14], [22]-[23]. Instead of a balanced set of harmonic free grid voltage, let us consider the grid voltage as follows

$$\begin{bmatrix} v_a \\ v_b \\ v_c \end{bmatrix} = \begin{bmatrix} V_1 cos\theta - V_5 \cos(5\theta) + V_7 \cos(7\theta) - V_{11} \cos(11\theta) + \cdots \\ (1+\beta)\left(V_1 \cos\left(\theta - \frac{2\pi}{3}\right) - V_5 \cos\left(5(\theta - \frac{2\pi}{3})\right) + \cdots \right. \\ (1+\gamma)\left(V_1 \cos\left(\theta + \frac{2\pi}{3}\right) - V_5 \cos\left(5(\theta + \frac{2\pi}{3})\right) + \cdots \right. \end{bmatrix} \quad (4.20)$$

When θ approaches φ, it can be assumed that $(\theta - \varphi)$ is a small quantity. Let $(\theta - \varphi) = \delta$ and $(\theta + \varphi) = 2\theta$. After transforming (4.20) from three phase to synchronously rotating reference frame, v_d becomes

$$v_d = E_g \delta \left(\frac{3+\gamma+\beta}{3}\right) + E_g E_{pu} \cos(2\theta - \Psi) + \sqrt{\frac{3}{2}}(V_5 + V_7) \cos\left(6\theta + \frac{\pi}{2}\right) + \sqrt{\frac{3}{2}}(V_{11} + V_{13}) \cos\left(12\theta + \frac{\pi}{2}\right) + \cdots \quad (4.21)$$

where $E_g = \sqrt{\frac{3}{2}} V_1$

$$E_{pu} = \sqrt{\left(\frac{(\gamma-\beta)}{2\sqrt{3}}\right)^2 + \left(\frac{(\gamma+\beta)}{2\sqrt{3}}\right)^2}$$

$$\Psi = tan^{-1}\left(\frac{(\gamma+\beta)}{\sqrt{3}(\gamma-\beta)}\right)$$

Therefore, the disturbance in the grid voltage pollutes the direct axis voltage as shown in (4.21). Equating (4.21) to zero, it can be shown that

$$\varphi = \theta + \frac{3}{3+\gamma+\beta} E_{pu} \cos(2\theta - \Psi) + \frac{(V_5+V_7)}{V_1} \cos\left(6\theta + \frac{\pi}{2}\right) + \frac{(V_{11}+V_{13})}{V_1} \cos\left(12\theta + \frac{\pi}{2}\right) + \cdots \quad (4.22)$$

Therefore, it can be concluded that the estimated phase has a certain amount of ripple if the grid voltage is not ideal. In other words, the voltage v_d will have harmonic components of the order 2, 6, 12 etc. The odd harmonic terms existing in the three phase voltages appear as even harmonic terms in dq reference frame. Thus, 5th and 7th harmonics in three-phase grid voltage bring 6th harmonic term in (4.22). Similarly, 11th and 13th harmonics in (4.20) appear as 12th harmonic in (4.22), and so on. Unbalanced three-phase voltage is responsible for 2nd harmonic component in d axis voltage, and hence, in the estimated phase in (4.22). Thus, if even harmonic terms do not exist in grid voltage, then there will be no odd harmonic component in v_d. Even harmonic components can be eliminated from v_d by a minimum number of cascaded even harmonic elimination blocks [112]. If all the even harmonics can be removed from (4.21) and feed it into PLL, then effects of voltage unbalance and grid voltage harmonics will be eliminated, and accordingly the phase can be tracked with higher BW for better dynamic performance.

4.4.3 Even Harmonic Elimination Algorithm

Odd and even harmonic elimination method for single phase PLL has been presented in section 4.4.3 where even harmonics can be eliminated using only one network and there is no need for any cascaded system. However, for odd harmonics individual harmonic elimination blocks in a cascaded set-up need to be used. This is advantageous for three phase SRF-PLL in polluted grid since the direct-axis voltage, and hence, the estimated phase contains only the even harmonic components as shown in the previous section. However, unlike the single-phase system scenario, a DC component $E_g\delta\left(\frac{3+\gamma+\beta}{3}\right)$ has to be recovered from the even harmonics

instead of the fundamental sinusoidal component. The even harmonic elimination (EHE) block has been modified from the previous section to accommodate this.

Let v_{gd} represent the dc and the even harmonics up to n^{th} order which can be written as

$$v_{gd}(t) = v_{dc} + \sum_{k=2}^{n} V_k \cos(k\omega t + \rho_k) \tag{4.23}$$

where *k* is an even numbers up to *n*. The first block of modified EHE can be represented as

$$v_{gd0}(t) = 0.5\left[v_{gd}(t) + v_{gd}\left(t - \frac{\pi}{2\omega}\right)\right] \tag{4.24}$$

$$= 0.5\left[v_{dc} + \sum_{K=2}^{n} V_k \cos(k\omega t + \rho_k) + v_{dc} + \sum_{K=2}^{n} V_k \cos\left(k\omega\left(t - \frac{\pi}{2\omega}\right) + \rho_k\right)\right]$$

$$v_{gd0}(t) = 0.5\left[2v_{dc} + \sum_{K=2}^{n} V_k \cos(k\omega t + \rho_k) + \sum_{K=2}^{n} V_k \cos(k_1\pi - (k\omega t + \rho_k))\right] \tag{4.25}$$

here $k_1 = \frac{k}{2}$. If k_1 is an odd number, 2nd and 3rd terms of (4.25) are eliminated and only the dc term remains. But if $k_1$is an even number, v_{dc} cannot be recovered. For negligible even and triplen harmonics in the grid, (4.24) cannot eliminate the grid harmonics of order $(6k \pm 1)$ where $k = 2, 4, 6\ldots$ i.e., even numbers, since these grid harmonics appear as even multiples of 6th harmonic in v_d. Usually, 11th, 13th or other higher order $(6k \pm 1)^{th}$ harmonics are not dominant in the grid, but for generalization two additional harmonic elimination blocks cascaded with (4.24) are required to remove these higher order harmonics from (4.21). These blocks are represented by (4.26) and (4.27).

$$v_{g1}(t) = 0.5\left[v_g(t) + v_g\left(t - \frac{\pi}{12\omega}\right)\right] \tag{4.26}$$

$$v_{g2}(t) = 0.5\left[v_g(t) + v_g\left(t - \frac{\pi}{24\omega}\right)\right] \tag{4.27}$$

Odd multiples of 12th harmonics presented in (4.21) are removed by (4.26) and odd multiples of 24th harmonics are removed by (4.27). If the EHE algorithm expressed in (4.24), (4.26) and (4.27) is applied to (4.21), the DC quantity $E_g\delta\left(\frac{3+\gamma+\beta}{3}\right)$ can be extracted. PLL can track θ with higher BW that ensures better dynamic performance when the two main sources of steady state error in phase estimation, grid voltage harmonics and voltage unbalance, have been eliminated from v_d. Fig. 4.4 shows the block diagram for SRF-PLL with harmonics and unbalanced voltage effect elimination where D_1, D_2 and D_3 represent the blocks for (4.24), (4.26) and (4.27), respectively.

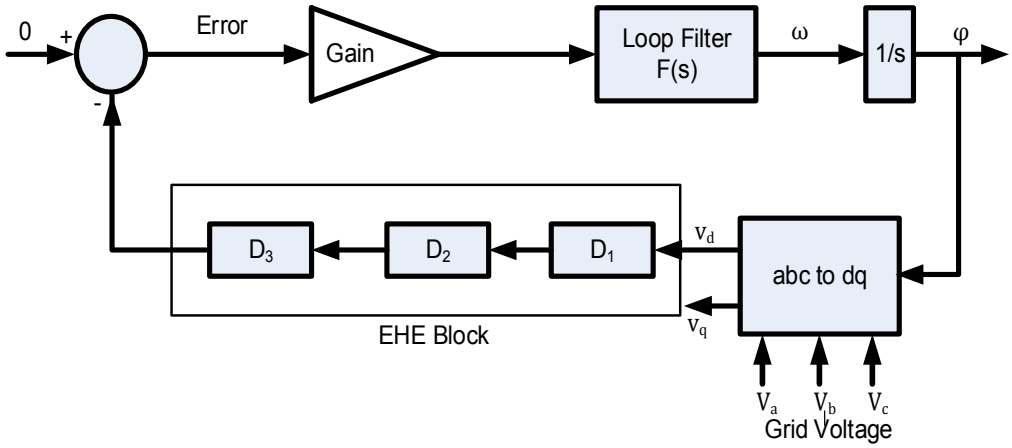

Figure 4.4. Modified SRF-PLL with harmonics and unbalanced voltage elimination

Table 4.1 lists the appropriate harmonic elimination block required to remove a particular grid voltage harmonics. Grid harmonics up to 37th order are considered in Table 4.1 for generalization, although it is unlikely to get harmonics of that high order in the three-phase grid voltage; higher order harmonics beyond the 37th order are ignored.

Table 4.1. Harmonic elimination block for grid harmonics

Possible harmonics		$k_1 = \frac{k}{2}$	**Elimination block**
Three phase	v_d **(k)**		
5^{th} and 7^{th}	6^{th}	3	D1
11^{th} and 13^{th}	12^{th}	6	D2
17^{th} and 19^{th}	18^{th}	9	D1
23^{rd} and 25^{th}	24^{th}	12	D3
29^{th} and 31^{st}	30^{th}	15	D1
35^{th} and 37^{th}	36^{th}	18	D2

4.5 Simulation Results

The proposed method of harmonics and unbalanced voltage effect elimination has been simulated in MATLAB/Simulink. In the following sub-sections, the improvement in SRF-PLL performance has been presented in presence of impurity in grid voltage.

4.5.1 Single Phase PLL

The single-phase grid voltage considered is given by

$$V_g = 70\cos(\omega t) - 10\sin(\omega t) - 14\cos(3\omega t) - 40\sin(3\omega t) + 1.8\cos(5\omega t) \qquad (4.28)$$

The fast Fourier transform (FFT) components of this signal are shown in Fig. 4.5. In Fig. 4.6, the harmonic elimination block output is compared with the original voltage. Fig. 4.6 shows that the proposed harmonic elimination method is quite effective in eliminating the higher order harmonics.

The effect of the harmonic elimination in the PLL operation is shown in Fig. 4.7, where the harmonic elimination algorithm is activated at 0.8 s. The existence of the harmonics causes ripple in the PLL frequency estimation, but after the elimination algorithm is enabled; the frequency estimation becomes accurate at 377 rad/s.

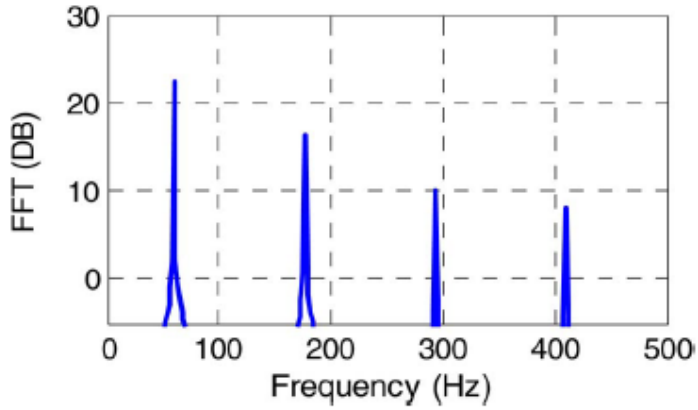

Figure 4.5. FFT analysis for the grid voltage

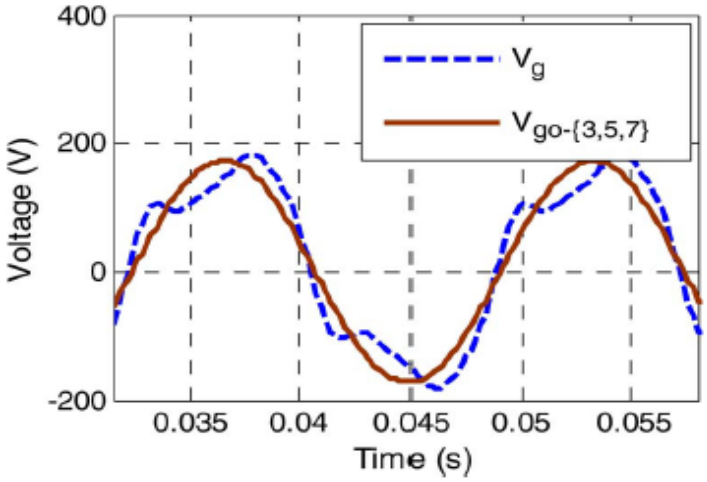

Figure 4.6. Simulation results for the harmonic elimination

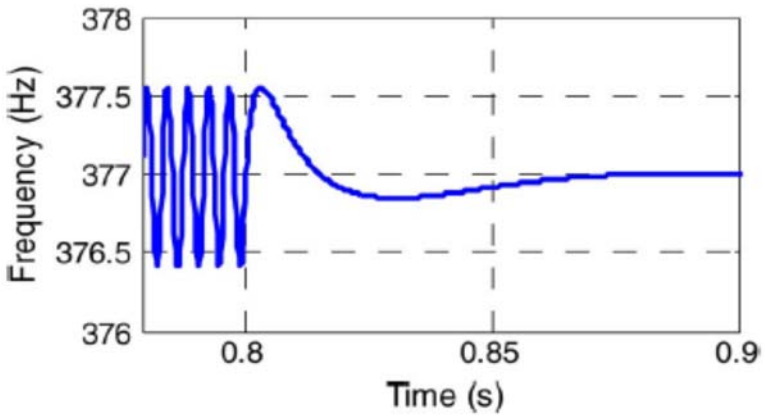

Figure 4.7. Simulation results for the harmonic elimination effect on frequency estimation.

4.5.2 Three-Phase PLL

The performances of the PLL for two different bandwidths are shown in Figs. 4.8 and 4.9. For both cases, damping ratio ξ is chosen as 0.707. The bandwidths are chosen as 188 rad/s and 377 rad/s respectively. The peak of the utility voltage is considered as 170V. The comparison of results in Figs. 4.8 and 4.9 shows that the dynamic performance is better with higher BW.

Figs. 4.10 and 4.11 shows the error between actual frequency and estimated frequency when the three phase grid voltages are unbalanced. The voltages of phase *b* and *c* are 110% and 90% of the phase *a,* respectively. The phase estimation error, and hence, the estimated phase contains 2^{nd} order harmonics as discussed in section 4.4.3. Also, the results show that the phase estimation error increases with BW. The phase estimation error for BW of 188 rad/s is almost 50% less than that of BW of 377 rad/s.

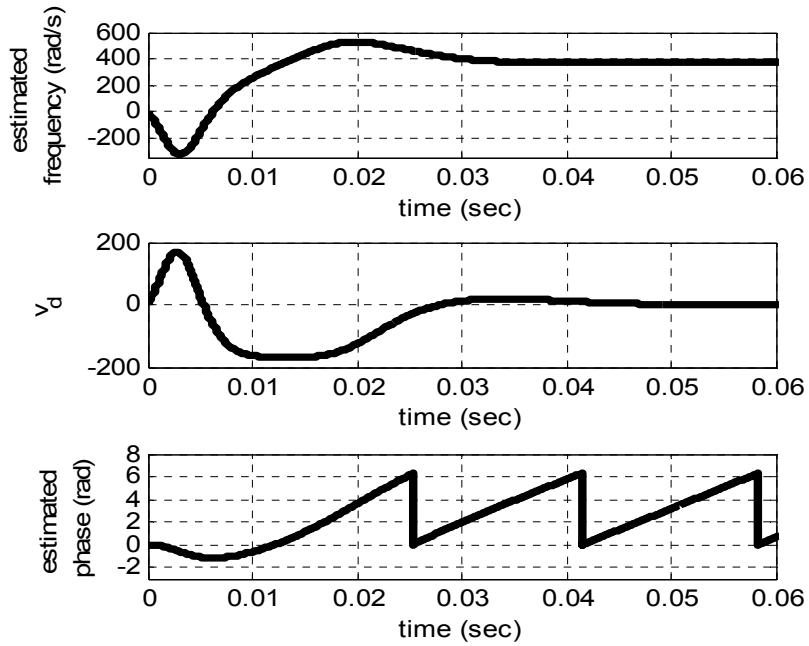

Figure 4.8. Dynamic performance of PLL with BW of 188 rad/s

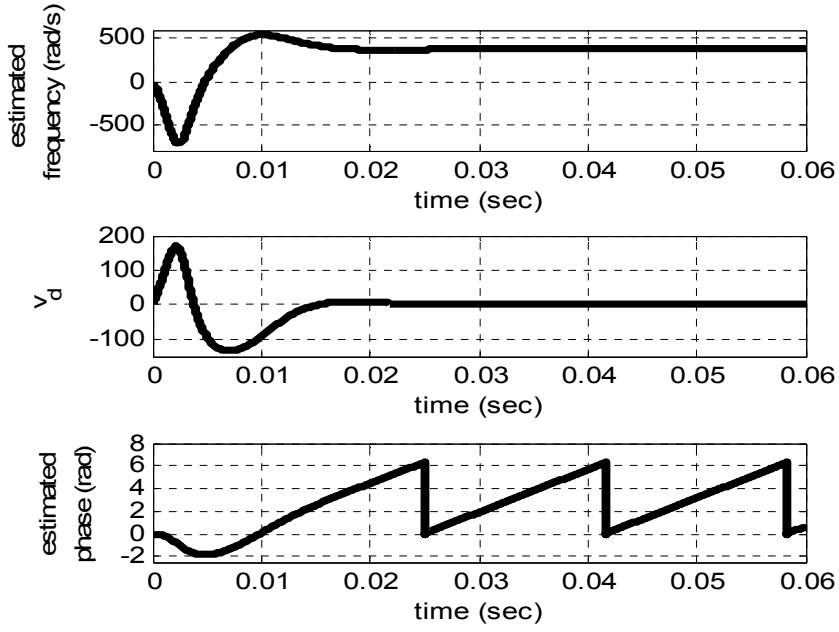

Figure 4.9. Dynamic performance of PLL with BW of 377 rad/s

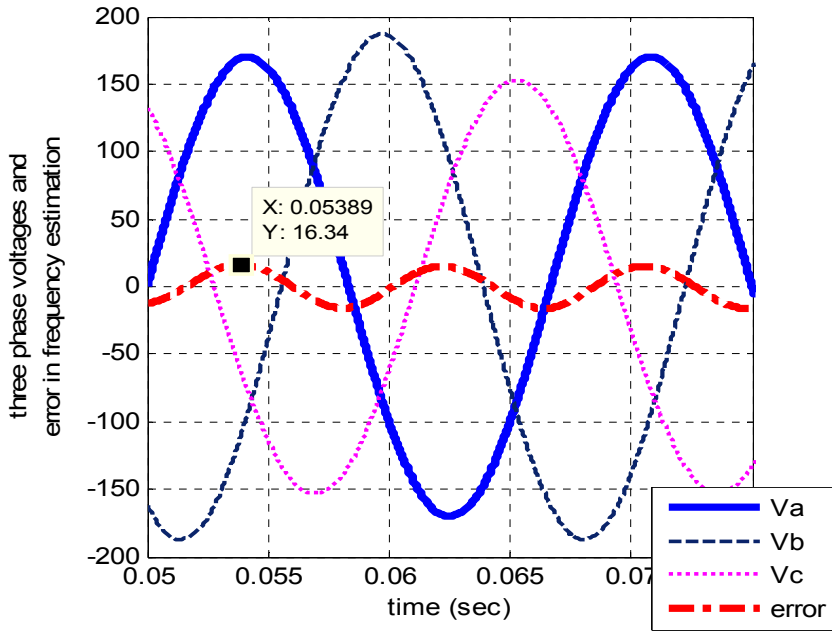

Figure 4.10. Frequency estimation error in unbalanced voltage condition with BW of 188 rad/s

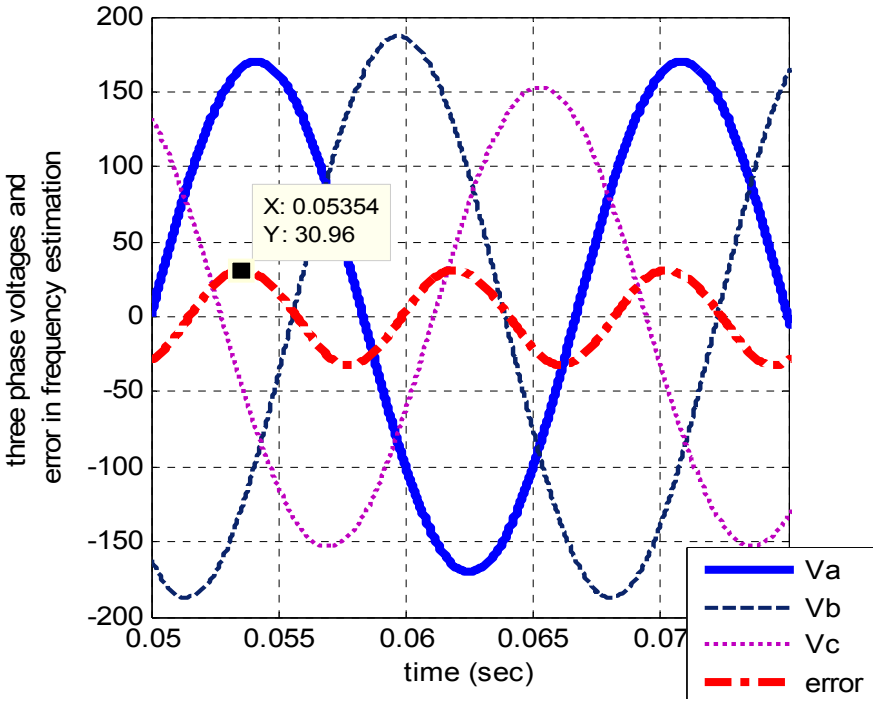

Figure 4.11. Frequency estimation error in unbalanced voltage condition with BW of 377 rad/s

If odd harmonics exist in grid voltage, it appears as even harmonics in direct axis voltage v_d which causes an error in frequency or phase estimation. As shown in Fig. 4.12, the grid voltage contains 5th and 7th harmonics of magnitude 5% and 3% of the fundamental. These harmonics appear as 6th harmonic in v_d.

The amount of phase deviation $(\theta - \varphi)$ increases with the increase of harmonic content in the grid voltage. In Fig. 4.13, the phase deviation of conventional SRL-PLL is shown for different amount of 5th harmonic content in grid voltage. As it is seen from this figure, the phase deviation is higher for higher 5th harmonic content. Also phase deviation for different harmonic content is quantified and shown in the bar chart of Fig. 4.13. Here the amount 5th, 7th, 11th and 13th harmonic content are considered to be 8%, 5%, 5% and 3% of the fundamental component respectively. Bandwidth is set as 377rad/s for both operation of SRF-PLL.

Fig. 4.14 shows the direct axis voltage v_d before and after the harmonic elimination when grid voltages are unbalanced and have 5th and 7th harmonics at the same time. The harmonic elimination block extracts v_d out of 2nd and 6th harmonics and the loop filter makes it zero to match the actual phase. Fig. 4.15 shows the estimated frequency and phase angle using harmonic elimination with BW of 377 rad/s. It is evident from Fig. 4.15 that the frequency estimation error is negligible with harmonic elimination while it is significant without harmonic elimination as shown in Fig. 4.11.

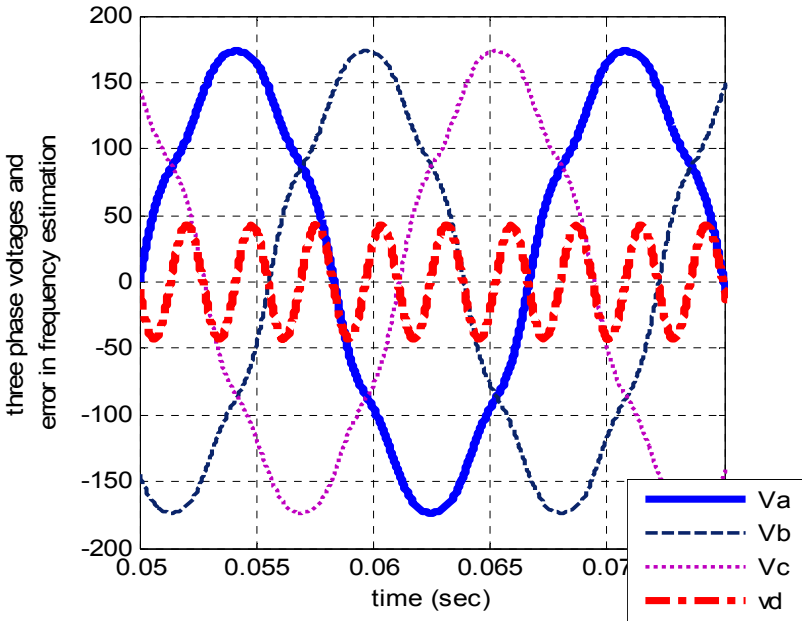

Figure 4.12. Frequency estimation error with 5th and 7th harmonics present in the grid voltage

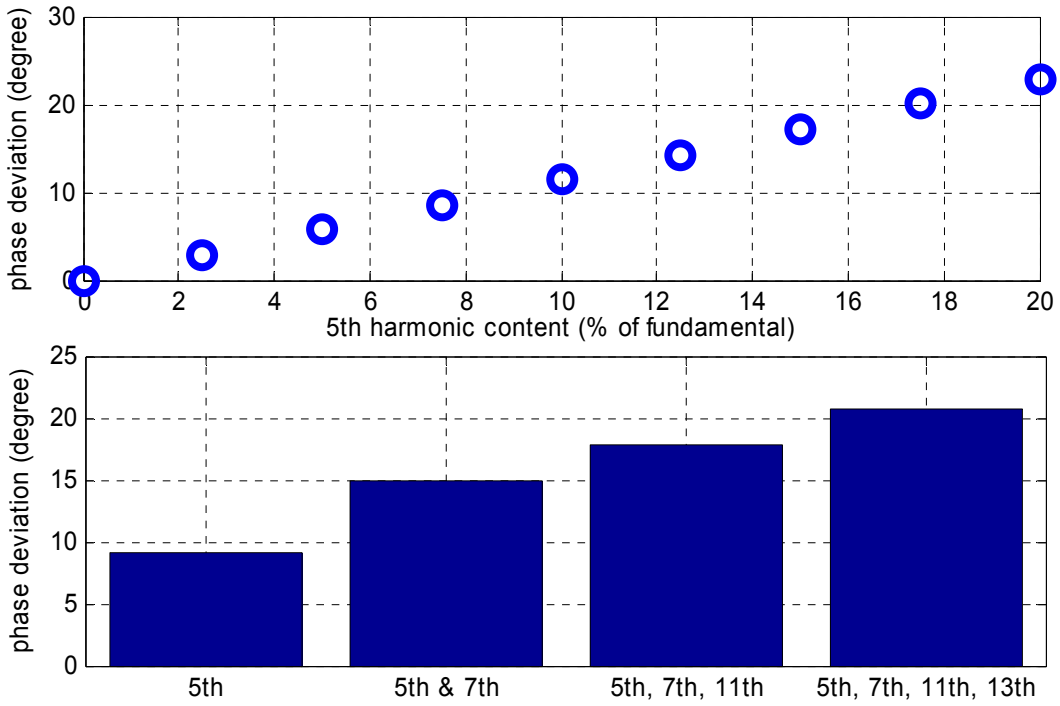

Figure 4.13. Phase deviation $(\theta - \varphi)$ for different harmonic content

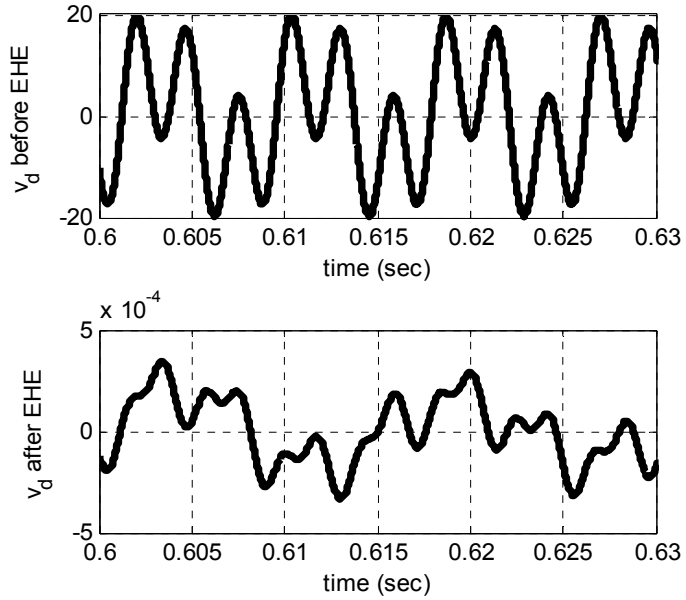

Figure 4.14. Effect of even harmonic elimination (EHE) on direct axis voltage

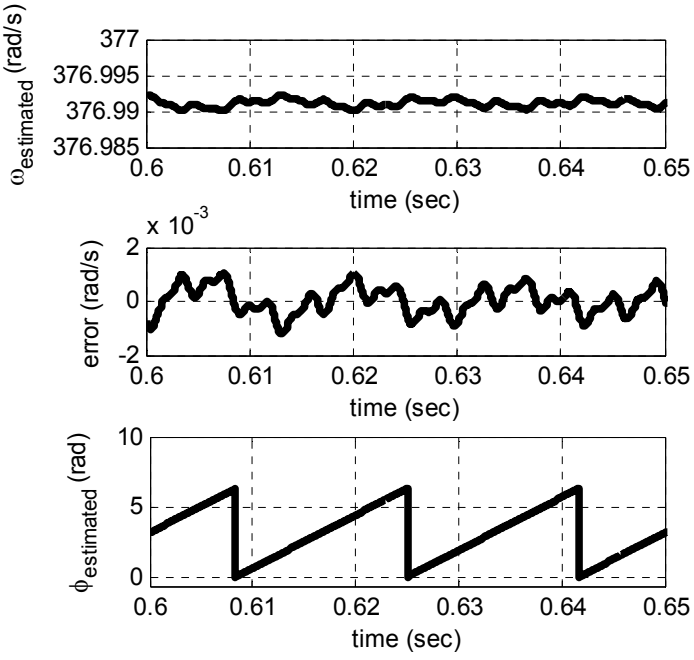

Figure 4.15. Effect harmonic elimination on frequency and phase estimation

4.6 Experimental Results

The proposed algorithm for single phase and three phase PLL is verified experimentally using Microchip DSP dsPIC33FJ256MC710A and Microchip Explorer-16 development board. Programmable AC voltage source is used to generate single phase and three phase voltages with harmonics and voltage unbalance.

4.6.1 Single Phase PLL

A single phase voltage of amplitude 120V rms at fundamental frequency 60Hz is considered. The voltage signal contains 3^{rd} harmonic of 21.21% of the fundamental component. Harmonic elimination method presented in section 4.4.3 is used to this signal. The original 3^{rd} harmonic contaminated grid voltage is passed through the 3^{rd} harmonic elimination block shown in Fig. 4.3 and then fed to the PLL. Fig. 4.16 shows the grid voltage before and after the harmonic elimination method is used. As seen from Fig. 4.16, harmonic elimination block can extract the fundamental component and gives output of pure sinusoidal voltage of 60Hz.

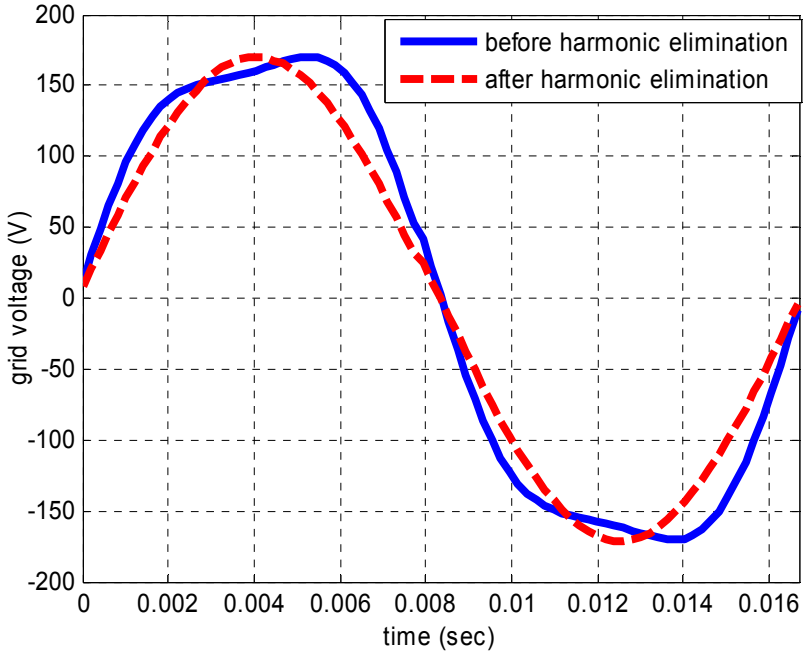

Figure 4.16. Single phase voltage signal before and after harmonic elimination

4.6.2 Three Phase PLL

In the first experiment of three phase PLL, proposed algorithm is tested with a harmonic contaminated three phase voltage of amplitude 120V rms at fundamental frequency 60Hz. This voltage signal contains the 5th and 7th harmonics of 2.42% and 7.39% of the fundamental component respectively. The three phase voltage is shown in Fig. 4.17. A 6th harmonic component appears in the direct axis voltage v_d due to the 5th and 7th harmonic component in three phase voltage. Therefore harmonic elimination block D1 is used as shown in Fig. 4.4 to remove the 6th harmonic component from v_d. The effect of harmonic elimination from v_d is shown in Fig. 4.18. As seen from Fig. 4.18, direct axis voltage v_d is free of 6th harmonic oscillation after the harmonic elimination and close to zero which indicates the estimated phase is locked with the actual phase. Fig. 4.19 shows the frequency estimation error before and after

the harmonic elimination. The estimated frequency before harmonic elimination has ripple of more than 5% based on actual frequency 377 rad/s due to the 6th harmonic component in v_d. On the other hand, frequency estimation error is below 0.5% after the harmonic elimination.

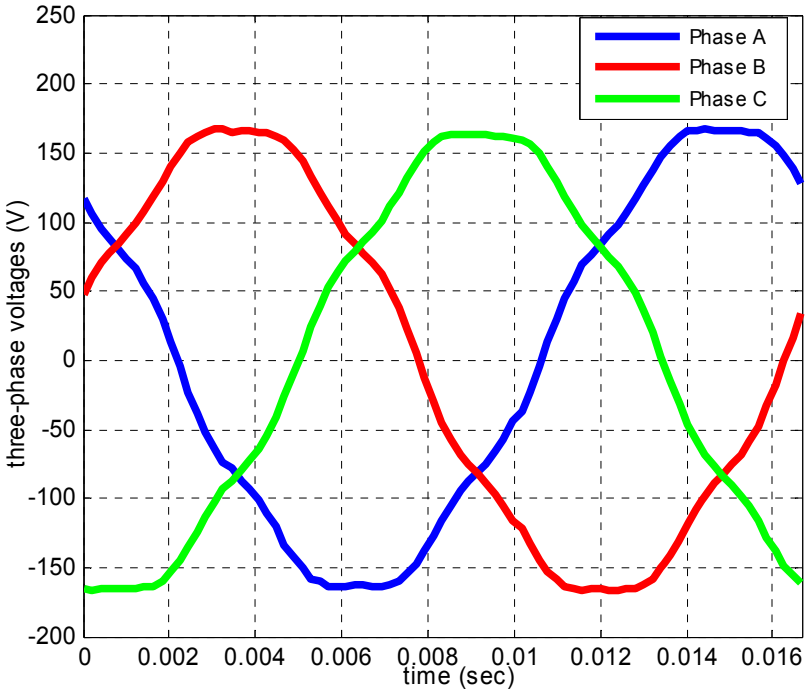

Figure 4.17. Three phase voltage contaminated by 5th and 7th harmonics

In the second experiment proposed three phase PLL is tested with an unbalanced three phase voltage. The amplitude of phase 'a' is considered as 120V rms while the amplitude of phase 'b' and 'c' are considered as 110% and 90% of phase 'a' respectively. Fig. 4.20 shows the unbalanced three phase voltage for this experiment.

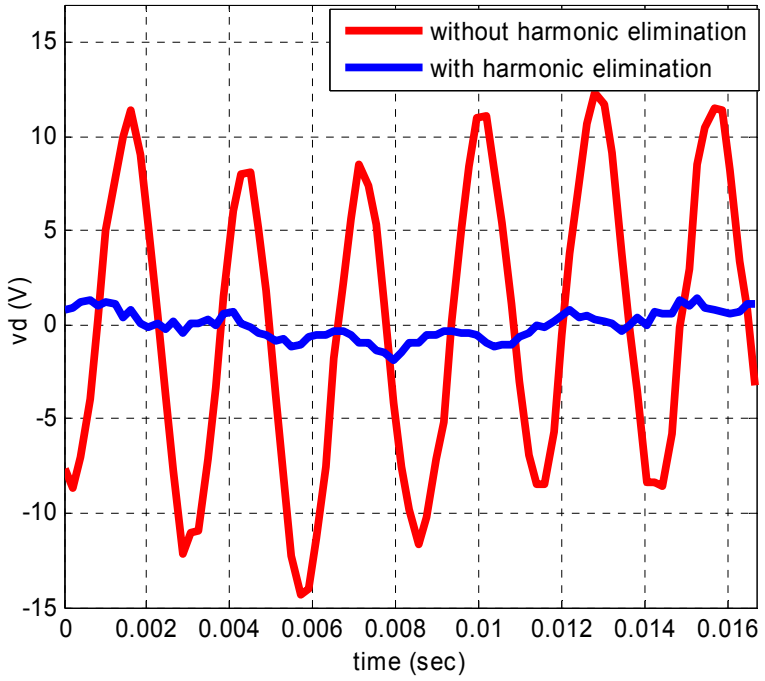

Figure 4.18. Direct axis voltage v_d for three phase harmonic contaminated voltage with and without harmonic elimination

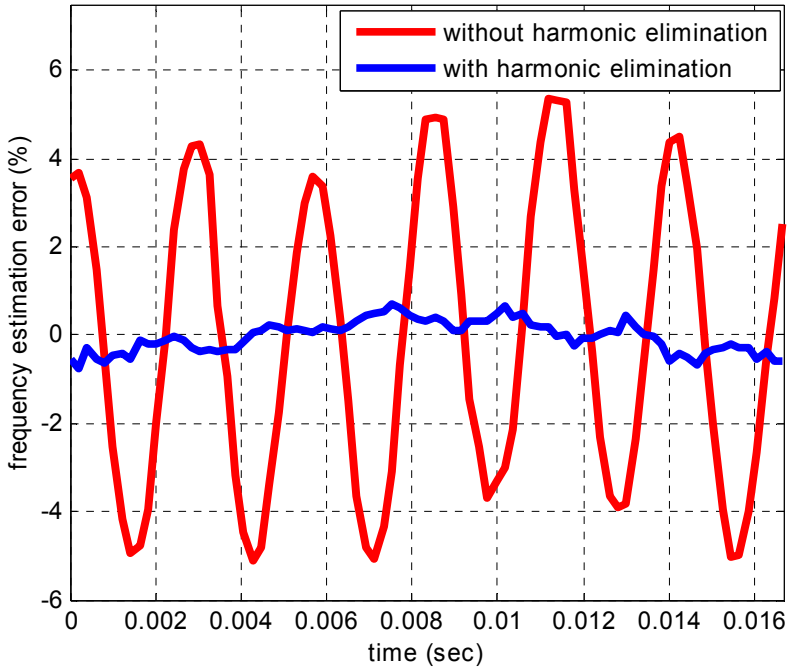

Figure 4.19. Frequency estimation error from three phase PLL for harmonic contaminated voltage with and without harmonic elimination

Fig. 4.21 shows the direct axis voltage v_d for unbalanced three phase voltage with and without harmonic elimination. As seen from this figure, a second harmonic oscillation appears in v_d due to the unbalanced voltage in three phase. Therefore harmonic elimination block D1 is used as shown in Fig. 4.4 to remove the 2nd harmonic component from v_d. Also v_d is close to zero after harmonic elimination which indicates phase locked loop can accurately track the phase angle of the grid voltage. Fig. 4.22 shows the frequency estimation error with and without harmonic elimination from v_d. Frequency estimation error is negligible and PLL works perfectly when 2nd harmonic term is eliminated from v_d using the proposed harmonic elimination block D1.

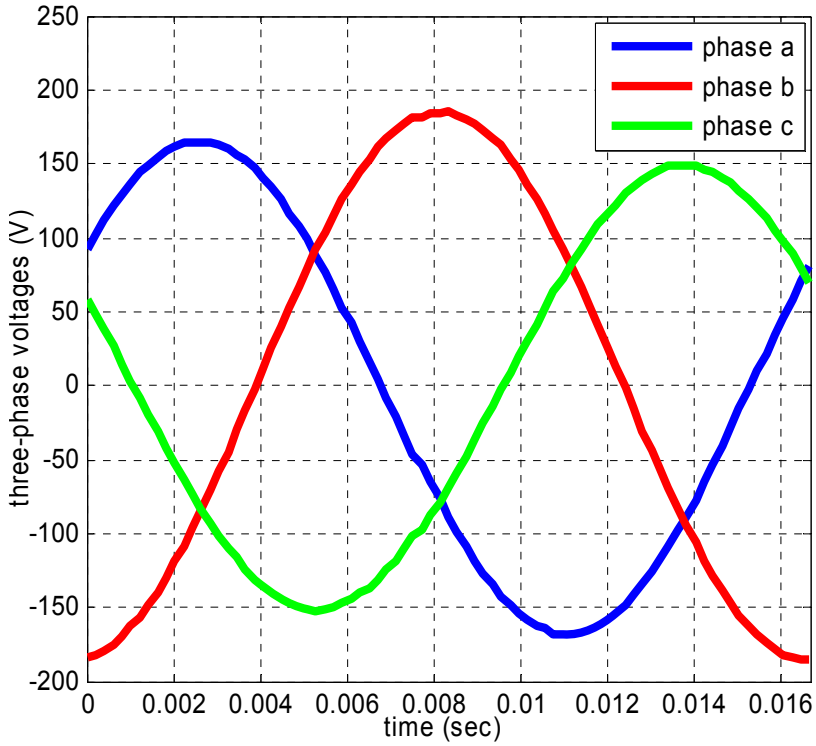

Figure 4.20. Three phase unbalanced voltage

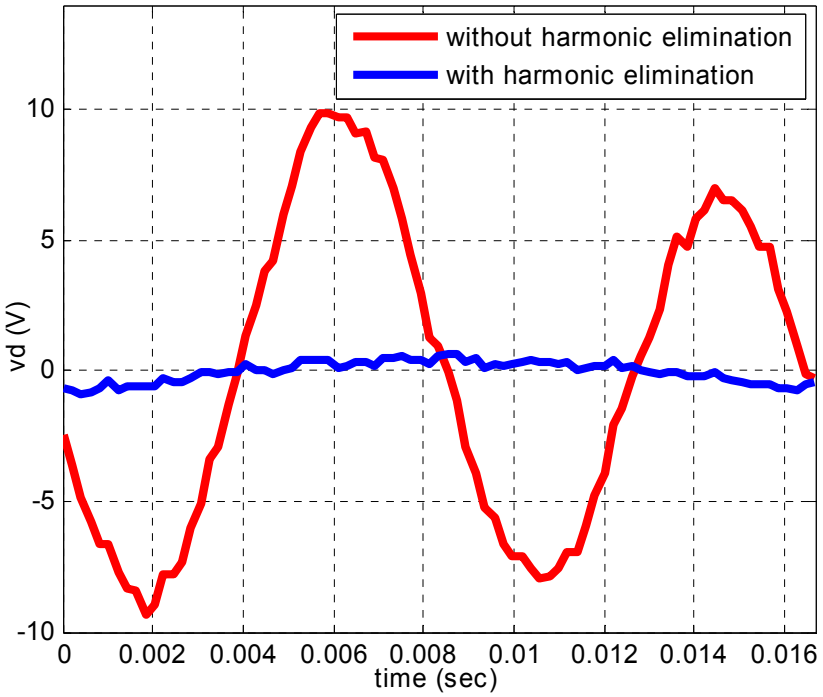

Figure 4.21. Direct axis voltage v_d for unbalanced three phase voltage with and without harmonic elimination

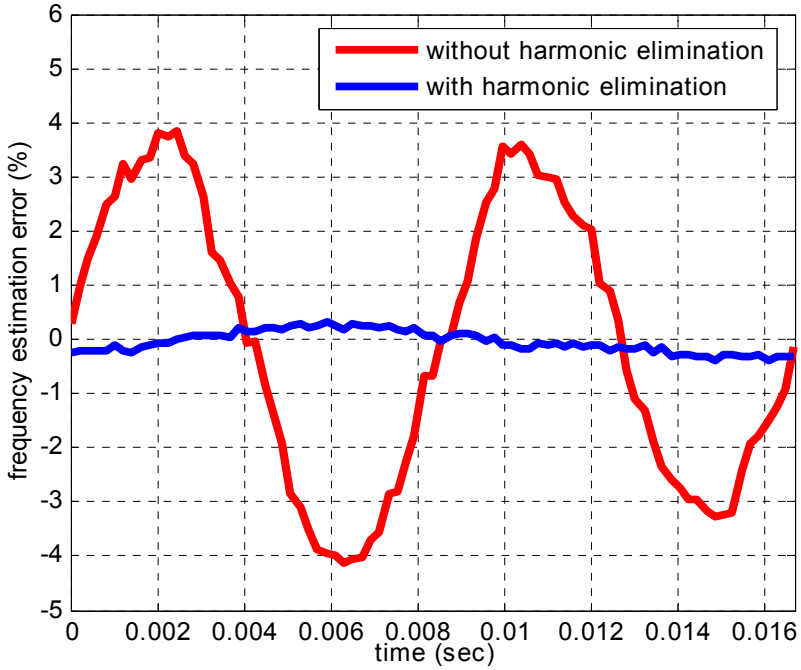

Figure 4.22. Frequency estimation error from three phase PLL for unbalanced voltage with and without harmonic elimination

4.7 Contribution

- A harmonic elimination method has been proposed for single phase PLL to eliminate any harmonics by using cascaded harmonic elimination blocks.
- A method of removing three phase grid voltage harmonics and unbalanced voltage effect has been presented to improve the three phase PLL performance in weak grid. The proposed method incorporates a harmonic elimination method in direct axis voltage v_d to remove the impurity effects.
- The harmonic elimination algorithm for both single phase and three phase PLL is implemented using trigonometric operations and does not require any external filters. It is easy to implement and does not suffer from filtering delay.
- As the sources of steady state error is eliminated, single phase or three phase PLL can be operated at high BW to ensure better dynamic performance in case of any frequency fluctuations.
- Simulation results and experimental validation have been presented to ensure better PLL performance for weak or distorted grid.

4.8 Conclusion

Grid synchronization for renewable energy source requires advanced algorithms when impurities such as harmonics and unbalanced voltage conditions are present in the grid. Real and reactive power control for DES is highly dependent on performance of PLL. For single phase grid, odd or even harmonics in grid voltage degrades the steady state performance of the

conventional SRF-PLL. A harmonic elimination method has been proposed to improve the performance of the single phase SRF-PLL in presence of harmonics. The proposed harmonic elimination technique incorporates cascaded blocks to eliminate both odd and even harmonics present in the grid. The processed voltage signal free of harmonics is fed into the PLL for $\alpha\beta$ and dq transformation.

The odd harmonics present in the three-phase grid appear as even harmonic components and unbalance grid voltage creates 2nd harmonic component in the direct axis voltage v_d when the three-phase grid voltage is transformed into dq rotating reference frame for PLL implementation. A modified SRF-PLL has been developed to enhance the robustness and accuracy of three-phase grid synchronization. The even harmonic elimination algorithm with minimum number of cascaded blocks applied to v_d removes the impurity effects of the grid to enable the PLL to track the phase and frequency with a loop filter of higher bandwidth. Simulation results and experimental verification for both single phase and three-phase PLL with high bandwidth have been presented.

Chapter 5: Electrical System Design and Grid Connection of Off-Shore Wave Energy System

5.1 Introduction

The research and development activity on energy harvesting from the ocean has been limited despite its vast potential for renewable energy. One advantage of wave power over wind power is the low profile of wave energy devices relative to the ocean surface, which results in less aesthetic impact. Renewables such as wind and wave present challenges due to their diurnal variability and weather dependence. The intermittency of energy sources poses a great challenge for their dispatch on the electric grid. The intermittency of the renewable energy sources is a significant drag on the economic value of these renewable energy resources compared to base-load fossil sources of energy. In addition, offshore renewable energy generation parks are typically located away from the shoreline, which poses transmission, grid interconnection and control requirements. These concerns are addressed in this research by analyzing an electrical system design concept of power generation by wave energy converters with bulk storage.

The integration of wave energy to the utility grid introduces significantly different challenges to the most other renewable technologies such as solar photovoltaic, onshore wind, hydroelectricity, biomass etc. [79]. All the renewable energy sources have unique nature and scalability. Most of the aforementioned technologies readily lend themselves to local small-scale and even domestic distributed generation. Some of the challenges associated with the

control and grid integration of distributed energy sources have been addressed in the previous chapters. However, development of the renewable energy technology has been gradually moved from small scale distributed sources towards the large scale production of off-shore wind and wave energy. Also, designing an off-shore wave park is economically viable only when it is of the utility scale. The deployment of such large scale power generation introduces economic and technical challenges on the transmission and grid integration. The grid code for distribution system sets regulatory limits on the technical performance of generators connected to the distribution network. If the power levels of wave park are several hundreds of megawatt, connection points of such wave park migrate to the transmission network. The grid code for transmission systems will then become the appropriate regulatory documentation.

One of the major challenges of the transmission of wave energy is to overcome the requirement of high reactive power due to the cable capacitance of high voltage submarine cable. Also power smoothing is an important concern for grid connection in order to reduce the impact of intermittency of wave energy. One way to smooth the power fluctuation is to use external storage. In order to reduce the impact of intermittency of renewable energy sources, applications have been suggested to make the economics of these resources more attractive; for example, an offshore wave energy generation has been proposed to drive desalination plants [47]. Controls techniques have also been proposed to reduce the effect of intermittency. Rotational speed control of the generator reacts with the short term changes of the turbine speed and average power can be adjusted accordingly [48]. A promising approach for energy storage is ocean-based compressed air storage system (OCAES) [54]. The primary approach of OCAES is to use the energy generated by an ocean energy source to compress air and store

it in tanks located on the sea floor. The compressed air is later used to generate electricity when it is needed. A key aspect of this concept entails the control of not only randomly oscillating power output of the ocean energy devices but also the flow of power to and from the OCAES.

This chapter discusses the electrical power transmission, grid connection and control aspects of the OCAES. Preliminary sizing issues from electrical aspects are also addressed. System design concepts, control strategies adopted and system simulation results are presented in this chapter.

5.2 Ocean Renewable Energy Generation

The extractable power from wave park is highly variable both in the short term and in the long term [80]. The short term variation is related to seconds or hourly variation, while long term variation means monthly to yearly variation. . However, wave energy is relatively more predictable than the other renewable energy sources such as solar or wind. The short term fluctuation of wave generated power has to be processed before transmission and grid connection since, otherwise, it may pose serious concern when it comes to the delivery of the power to electrical network. The use of a large number of wave energy converters (WEC) to form a wave park reduces the average power to peak power ratio [49], [80]. Appropriate spatial distribution of the WEC is proposed in [50] such that one WEC in the wave park can produce power when other produces zero power. An experimental result from aggregated WECs has been presented in [84]. To quantify the smoothing effect of aggregation of power, two of the

WECs at the wave energy research site outside Lysekil were operated during 88 min in a sea state of 4.6kW/m during 25 May 2009. It has been found that the electric power from array of directly driven point absorber is smoother than that from individual array members. It has been shown that the standard deviation reduces with the number of WECs in the array up to three WECs and that standard deviation of array power seems to be independent of sea state parameters for sea states above ~2kW/m. Also energy storage techniques have often been suggested as the means for load-levelling. At the utility scale, battery energy storage and compressed energy storage are popular emerging technologies [52]-[54]. Two simultaneous storage devices of battery and super capacitor have been used in [51]. Super capacitor removes the instantaneous or short term fluctuation of power while batteries remove the long term fluctuation of power. Therefore, power smoothing can be accomplished by the use of any or all of following means [79]:

a) Power extraction device can be designed to be capable of using its inherent storage such as hydraulic accumulators [81] or reservoirs [82].
b) Inertial storage through variable speed generator control in conjunction with system inertia.
c) Natural power smoothing by using large number of WECs and proper spacing of them.
d) Use of super capacitor at the power electronic conversion stage to remove the short term fluctuation of wave energy.

Electrical system configuration and grid connection of multi-megawatt off-shore wave park has been presented in [83]. A comparison of the permanent magnet generators (PMG) and

induction generators (IG) has been presented for wave energy extraction. PMG has been found more attractive option than IG, because of its smaller size (with multiple poles) and no requirement for a step-up gearbox considering the relatively small velocity of wave. A detailed analysis on different machines and drives used for wave energy generation and oscillating application has been presented in [77]. It has been found that the efficiency of the machine increases in oscillation while the efficiency of the drives decreases. But the increase in efficiency in oscillation for the machines is greater than the decrease for the drive, resulting in a net increase in system efficiency in oscillating operation.

For transmission of wave generated power from off-shore wave park to onshore grid, transmission voltage has to be boosted up to 33kV or 132kV. This requires an off-shore substation close to the wave park. The design, construction, deployment and operation of an offshore underwater substation have been discussed in [85]. One of the major issues related to the design of offshore substation is the cost. Also placement or anchoring the substation is a big challenge.

The ultimate goal of the wave energy research is to transmit the power to grid. A significant design and cost consideration have to be dedicated to subsea transmission of electric power from offshore wave park to onshore grid. A cost effective and reliable transmission system is required for grid integration of offshore power. The design of electrical transmission system affects the initial cost, maintenance cost, and electric loss of the system [85]. For large offshore wind or wave farms, two transmission options are available – one is high voltage alternating current (HVAC) transmission and another is high voltage direct current (HVDC) transmission.

A number of studies are there for the comparison between these two options [86]-[89]. HVAC transmission is more efficient and economic up to a certain distance [85] and HVDC is for longer transmission distance. The topology for HVAC [89]-[91] requires an offshore substation, subsea transmission cables, an onshore substation, reactive compensation, filters, and switchgear. Most of the existing transmission systems are HVAC and also the required reactive compensation devices, filters and switchgears are also available for HVAC transmission. The primary disadvantage of the HVAC transmission is the decreasing capacity to transmit active power at long distances because of the high voltage submarine cable's capacitance. This requires additional reactive power compensating devices. HVDC system consists of an offshore converter station, subsea DC cables, and an onshore converter station [92], [85]. The primary advantage of HVDC transmission over HVAC is the lower cable losses for long distances, improved fault response, and control over active and reactive power. The main disadvantage of the HVDC application is approximately 2% loss in each conversion stage [89], [93]. Moreover HVDC switchgear and protection scheme is still a vast area of research.

Another interesting research on offshore transmission is the optimization of transmission capacity. For offshore wind or wave energy, transmission system faces zero power transmission for a significant amount of time throughout the year. California offshore wind farms could generate zero power for over 1000h per year and wave farms for over 200h [85], [94]. A combined transmission for offshore wind and wave is proposed in [85] which not only reduce the zero power transmission duration over the year but also costs associated with submarine cables by proper optimization. Due to the relative proximity of the conductors and the dielectric insulator separating them, HVAC submarine cables have a much higher

capacitance per unit length compared to conventional overhead lines [95]. This high capacitance requires high reactive power compensation which cannot be supported by the distributed WECs alone. In [95], a combined approach of using reactive power from both distributed WECs in wave park and reactive power compensation devices at offshore substation has been proposed based on cost optimization.

5.3 State of Art for Ocean Energy Storage

The storage technology plays an important role to tie the renewable energy sources to the grid. There are several well established and also some developing technologies for energy storage. The storage should be economically viable, robust, and efficient to overcome the challenges of energy fluctuations delivered by the offshore renewable generation. The characteristics of bulk storage for offshore wind or wave energy are discussed in [63]. The energy storage technologies can be divided into four categories, namely, mechanical, electrical, thermal and chemical storage types [64]. The mechanical energy storage option includes storage in terms of potential and kinetic energy. Compressed air energy storage (CAES) is based on the elastic potential of the compressed air. Compressed air energy storage has the minimum investment risk to the cost per kilowatt generation; also, the levelized cost for CAES is low [65]. Capital cost of the CAES system depends on the volume of the air energy storage and infrastructure. Underground CAES system is the most economically viable option for offshore wave energy extraction that has the potential to store energy up to 400 MW at 8-26 hour of discharge [64], [66]. However, long construction time, large capital cost requirement

and low energy density make it suitable only for large scale and long transmission systems [67], [68].

Underground pumped hydro is another attractive option for large scale energy storage [69], [70]. It is based on pumping water from one reservoir to another at higher elevation during low power demand and releasing it to lower reservoir through hydroelectric turbine during high demand of power. It has outstanding robustness, high longevity and cycle efficiency of 80% [63]. However, it also has low energy density like CAES and the response time is approximately 15sec which is good for smoothing long term fluctuations.

The storage technologies of battery, fly-wheel, and ultra-capacitor have good energy density and fast response time [65], [71], [72]. Quick charge-discharge time is expected to smooth out short term fluctuations. The expected charge-discharge time for short term fluctuation is about 5-20 seconds and for long term fluctuation it is about 4-6 hours [73]. Therefore, different storage technologies should be considered to address the two different fluctuation patterns.

There are utility scale land-based compressed air energy storage systems that are currently in operation in Europe and USA. However, the ocean based version is a relatively new concept that has not been studied in detail nor proven feasible. As such there is no OCAES either currently being designed or in operation anywhere. The OCAES concept was proposed by Seymour in 1998 [54]. The concept proposes to use the energy generated off-shore from ocean wave energy device or offshore wind turbines to compress air and store the compressed air in containers (bags or concrete tanks) on the ocean floor. On the ocean floor at certain depth, the air pressure would be in equilibrium with the water pressure, and therefore, the differential

pressure is almost zero and the dominant load is buoyancy. Therefore, these containers do not need to be pressure vessels, which is advantageous for their design. However, there are several other design challenges including anchoring, storage capacity, site selection, turbo machinery selection, pipeline design, etc. Also, during the compression stage, heat is generated and there is need to evacuate this heat from the system. On the other hand, during expansion, the air is cooled and there is need to add heat to the system prior to using the air for electricity generation. These issues and related challenges are the subject of intense current research and are not addressed here [63]-[65]. The focus of this chapter is on the power transmission aspect.

5.4 Conceptual Overview

The grid connection is an important component of the OCAES system because the stored energy is ultimately converted to electricity. In this regard, the experiences in the connection of offshore wind are important lessons. Indeed, offshore wind and ocean wave energy converters are the two major sources of ocean renewable energy source for the OCAES. The power electronics enabling technologies for transmission and grid interconnection of these energy sources are practically similar, but there are some differences between these energy sources that present different challenges for grid inter-connection. For example, while wind generators use mostly conventional generators, the current commercially proposed wave energy converters (WECs) use conventional generators and unconventional generators such as linear generators for their power take off. Also the intermittency of wind output and WEC outputs are significantly different, and therefore, the power processing requirements of these

sources need to be considered separately. Fig. 5.1 shows the overall conceptual diagram of the interconnection of the OCAES. There are two main interfaces that connect the storage system to the grid on one end and to the energy sources on the other end.

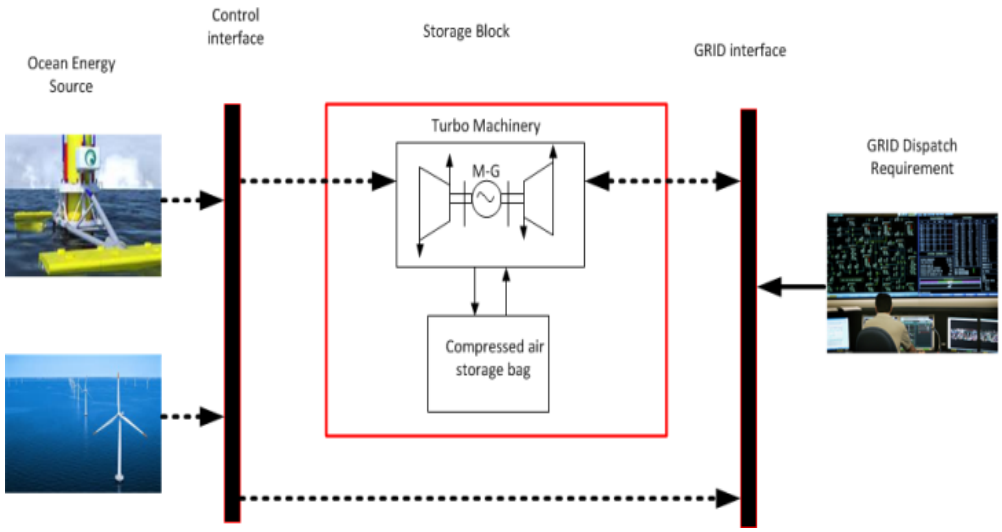

Figure 5.1. Conceptual configurations of transmission and grid connection system of the OCEAS

The arrows in the figure denote transmission lines of various design features such as length, voltage type, etc. The energy source control interface considers the issues involved in processing the output of the renewable energy source. The issues of interest here include the intermittency and power output processing requirements, power transmission to turbo compressor and/or grid, transmission distance (land or sea based turbo-machinery), system losses and VAR support, response time and storage duration. Some of the issues listed are not obvious from Fig. 5.1 but they become apparent if the interface is further expanded. Fig. 5.2 shows a further breakdown of the energy source control interface, showing banks of sources with Source Bank #1 further expanded into generating units.

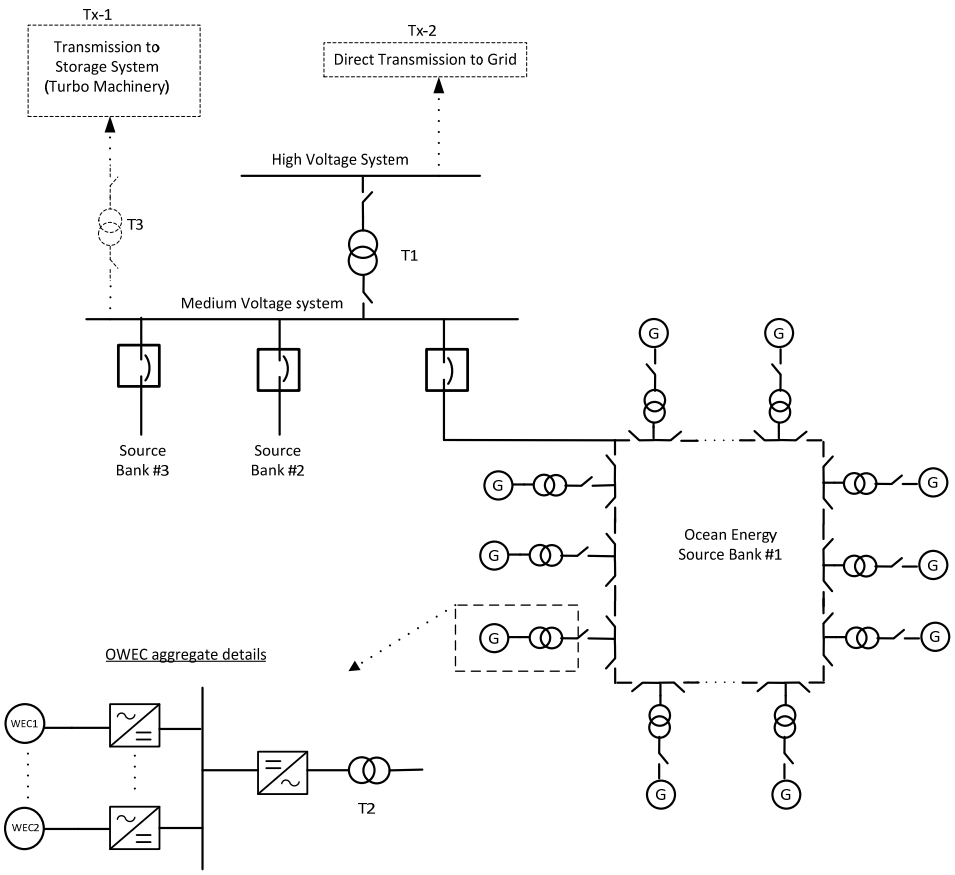

Figure 5.2. Conceptual configuration of energy source control interface of the OCEAS system

For example, Bank#1 could be a wave park of renewable energy sources as conceptualized in [55] or a series of generating units in close proximity. Each generating unit denoted with G is also an aggregation of several small devices as shown under "OWEC aggregate details''. Here, the output of the devices is rectified to a dc bus. The inverter converts the power on the dc bus into ac power and the output is transformed by the unit transformer T2. It can be noted that in Fig. 5.2 there are a number of devices aggregated into a generating unit for a given source. This arrangement is important because the WEC devices are currently of modest rating compared to wind turbines. The largest unit output of a commercial device is about 750kW,

reported for the Pelamis [56]. Other devices that have been sea tested or are at the commercial deployment stage have lower output. It is the opinion of the investigators that in the near term unit outputs might be lower rather than higher for various reasons. The optimal storage capacity is one of the subjects of research investigations. However, in order to create a storage system that would be economically competitive the capacity should be large – perhaps of the order of several megawatts. Because of this, it is needed to aggregate a large number of units to obtain a utility scale economic output that would be required for the OCAES. These units may not be physically located at one point in the ocean and would have to be interconnected.

One way of connecting the units together is through a ring circuit. With the ring circuit, one or more units can be taken out easily without impacting the operation of the rest of the units, thereby ensuring high availability. The ring circuit configuration is one of several alternative configurations depending on the capacity of the source bank. Radial connections are often a good start for the configuration which can be expanded into ring circuits when the number of units contributing to the source increases. The WECs indicated could be representative of a large number of devices that are radially connected to busbars forming the MV network.

The transmission requirements of the energy source control interface are described by blocks Tx-1 and Tx-2 of Fig 5.2. The requirements for transmission block Tx-1 depends on the location of the turbo machinery which can be on land or in the ocean. If the turbomachinery is located on land, the transmission distance from the energy sources to the turbomachinery would be longer than if it was offshore. The location of the turbo machinery for a particular

geographical location is a subject of detailed investigations. In this research, the turbo machinery location is assumed offshore, rather than on land, since the generating devices and storage tank are both located offshore. In this case, the transmission distance from the ocean energy source to the turbo-machinery would be relatively small.

The control interface should also be designed to allow for the direct transmission of power from the ocean energy source to the grid, under specified conditions. The transmission capacity of the Tx-2 line would be sized to match the percentage of the output that is transmitted, and this percentage must be carefully chosen. On one hand, if Tx-2 is sized to carry the full output of the source, the line may be underutilized due to the intermittency and the direct transmission to grid undermines the benefits of storage. The direct transmission to grid is linked from the high voltage bus as shown in block Tx-2. The direct transmission to grid helps to meet system demand when required or to transfer energy when storage capacity is full.

The grid interface deals primarily with transmitting the electric power generated by the turbo-machinery back to the grid as well as the direct feed from the ocean energy sources. The grid interface issues include the tracking of the frequency and phase angle of the grid voltage for grid synchronization. The Phase locked loop (PLL) technique has been presented in detailed in chapter 4. The amount of power provided by the WECs is controlled by the current controller in the power converter. The challenges associated with transmission of power from off-shore wave park to the onshore grid are presented in next section.

5.5 Transmission and Grid Connection

The primary challenge of HVAC transmission is to overcome the high reactive power requirement due to the high capacitance of submarine cables. Reactive power compensating devices such as static VAR compensator can be used at offshore substation for reactive power compensation. But incorporating a large VAR which is required for high power wave park increases the installation and maintenance cost. Also it increases the weight of the offshore substation which also increase the implementation cost of offshore collection platform. As the size of the offshore wave park and their distance from the shore increase, HVDC transmission can be considered. However, DC transmission comes with gigantic structure incorporating converters and protections in offshore platform. Though extensive research is going on for HVDC transmission in offshore power, but still the cost of transmission cable and structure have not been dropped. Therefore, it is important to increase the capability of classical HVAC submarine cables with increased controllability to overcome the challenges [114].

The excess capacity power electronic inverter associated with each WEC module can be incorporated to produce reactive power as shown in chapter 2. But to mitigate the huge amount of total reactive power, the inverter has to be oversized a lot which would not be economical solution. But combination of VAR compensating device and distributed compensation by inverters will reduce the device cost, inverter oversizing cost and structural cost for offshore platform. In [95] similar approach of combined operation of concentrated compensation and distributed compensation has been presented. This paper discusses about the optimization of the two compensation methods to minimize the cost function. This paper considers the array

of wind or wave energy converter and the proposed method incorporates only few of the inverters in a column to reduce the number of variables in optimizing equations. However, this may make some of the inverters unutilized even if they have some reactive power capacity.

5.6 Simulation of 200MW Wave Park

Models of a 2MW wave park and a 200MW wave park systems have been built and simulated with Matlab and SimPower Systems. In the 2MW system, the effect of number of WECs and their spatial distribution on the intermittency of the power production from the wave park is analyzed. Also the control for turbo-machinery of the OACES for 2MW generation is presented. Then the wave park of 200MW capacity has been considered for system level simulation. The system simulation block diagram for the wave energy park is shown in Fig. 5.3. The transmission and distribution system for the wave energy park is shown in Fig. 5.4.

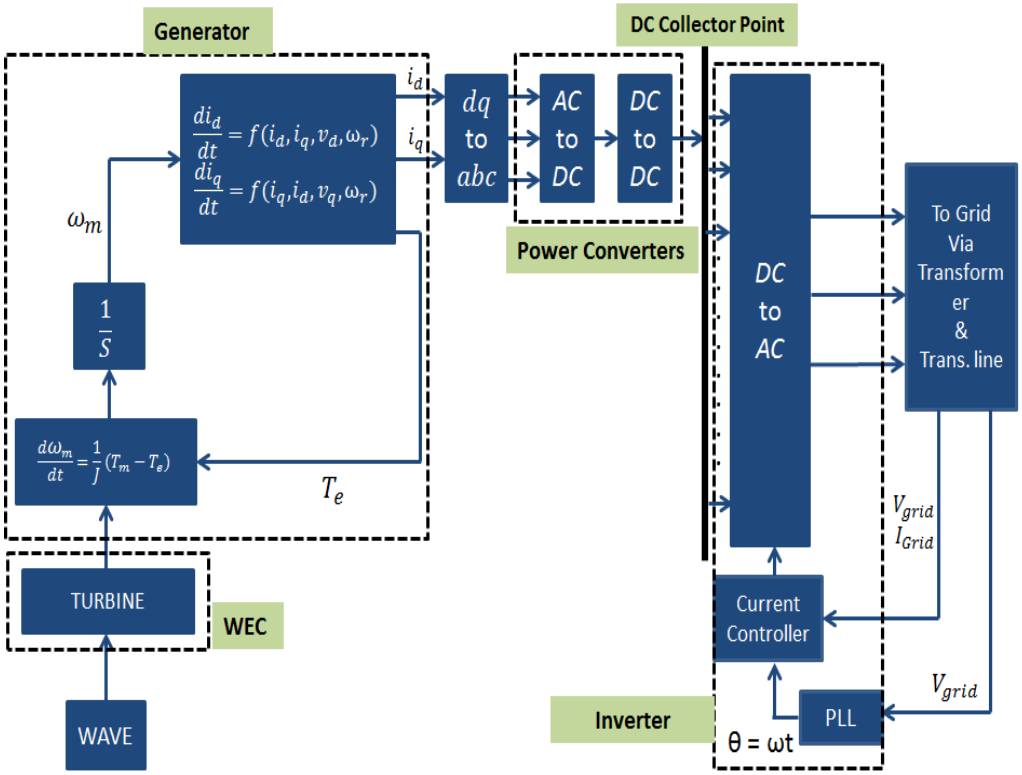

Figure 5.3. System simulation block diagram

5.6.1 2MW Wave Park System

The wave park evaluated consists of two modules, with each having four WECs placed at different locations in the ocean. The WEC consists of a turbine and a generator. Ocean wave power is converted to electric power and through power electronic devices and transmission cables it goes to the turbo machinery for storage and/or grid. The size of each WEC is considered to be capable of producing 250kW power, omitting the capacity factor. Therefore, two modules in the transmission and distribution system shown in Fig. 5.4 are connected to the 11kV collector point to make the output capacity of the wave park 2MW. The DC bus

voltage is 1100V [74]. The grid can be supplied both from the wave park and the OCAES. The transformer ratings are given in Table 5.1.

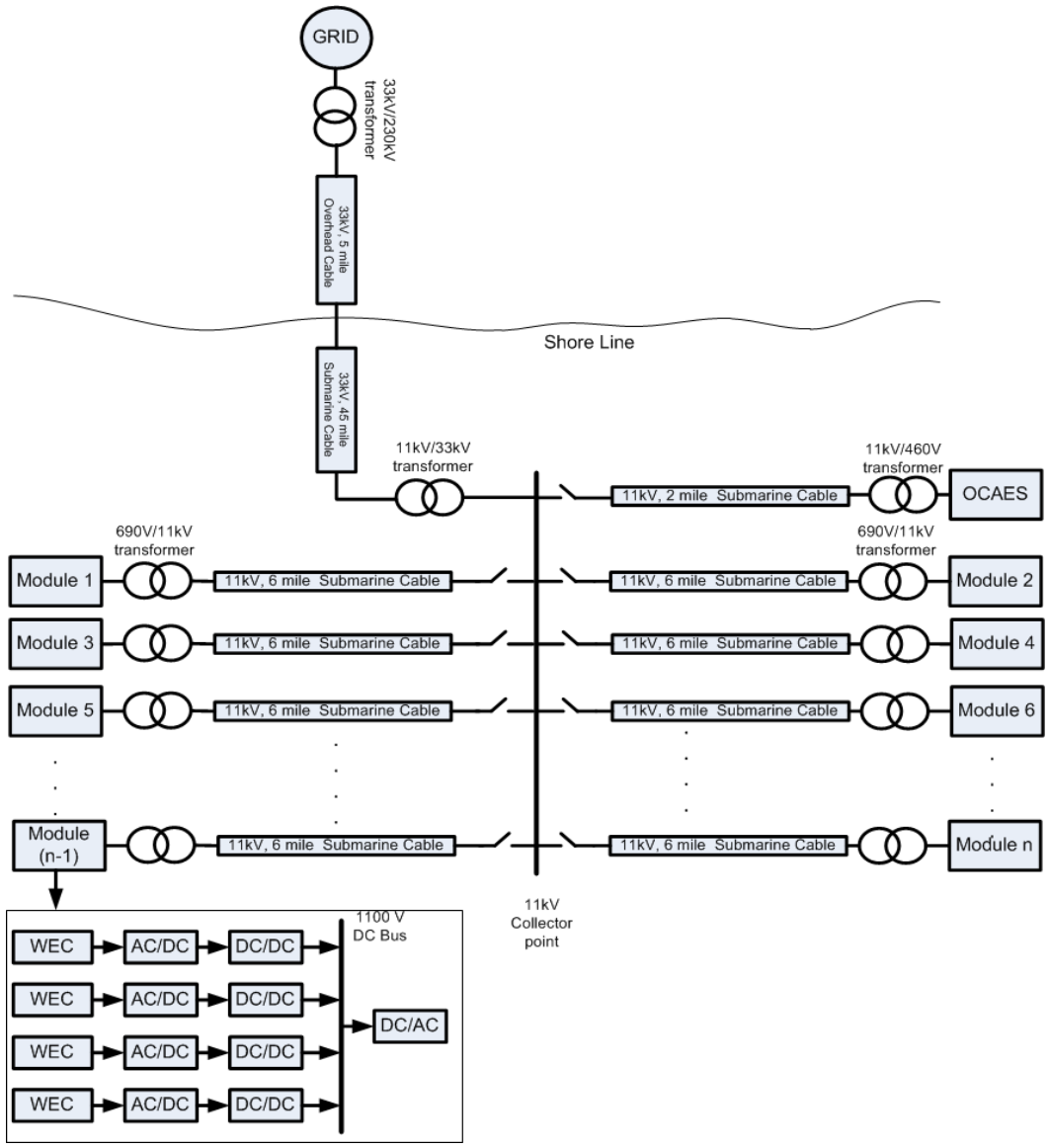

Figure 5.4. Transmission and distribution system for the wave park

Table 5.1. Transformer Ratings

Rating	**Power**
690V/11kV	1 MW
11kV/33kV	2 MW
33kV/230kV	2 MW
11kV/460V	1 MW

The reference i_d and i_q are determind by the total real and reactive power required by the system, respectively. An induction machine is used as turbomachinary which drives or is being driven by OCAES depending on the amount of power generated by wave park and power demand for grid. To demonstrate the effect of wave velocity on intermittency of the generated power, the wave velocities shown in Fig. 5.5 have been considered on the generator of different WECs of module 1. Wave velocities are taken as sine waves [77]. Similarly wave velocities of module 2 are phase shifted sine waves from each other. The intermittency of the power produced by the wave park is highly dependent on the different wave velocities. Proper spatial distribution and high number of WECs reduce the possibility of getting low velocities on most of the WECs at the same time. Spatial distribution places WECs in different wave conditions with the possibility of different wave heights and phases thereby leveling the power output. Table 5.2 shows the effect of wave velocities on power generation. Fig. 5.6 shows the variation of the power going to grid for different phase difference of wave velocities on different WECs. The worst case happens when phase difference of sinusoidal wave velocities on different WECs is $\frac{\pi}{12}$ as all WECs have peak velocity almost at the same time. Here the power variation is calculated as

$$Power\ variation = \frac{crest\ value - trough\ value}{crest\ value}\ X\ 100 \quad (5.1)$$

Table 5.2. Effect of Spatial Distribution of Waves on Four WECs

Wave Phase Difference	Total Crest Power (MW)	Total Trough Power (MW)	Power Variation
$\pi/12$	0.9986	0.565	43.4%
$\pi/4$	0.945	0.578	38.8%
$\pi/2$	0.830	0.815	negligible

Along with the wave velocity, number of WECs in a wave park also has an effect on power variation. If the wave park has higher number of WECs, the effect of varying wave velocities on power production will be decreased. Table 5.3 shows the decrease of power variation with the increase of the number of WECs while wave velocities on WECs follow the same pattern. Fig. 5.7 shows the effect of number of WECs on power variation.

Table 5.3. Effect of Number of WECs in Wave Park

Number of WECs	Total Crest power (MW)	Total Trough power (MW)	Power variation
4	0.945	0.565	43.4%
6	0.958	0.773	19.3%
8	0.955	0.935	negligible

Wave velocities can alternatively be modeled as a composition of several sinusoidal wave of different frequency and amplitude as shown in Fig. 5.8. Random wave velocities as shown

in Fig. 5.8 are considered for both module 1 and 2 for more practical scenario to show how power produced by the wave park is transmitted to the OCAES and grid. The output voltage of the AC/DC converter follows envelop of the peak of the generator AC output. The DC-DC boost converter is controlled to produce a constant 1100V for DC bus. Fig. 5.9 shows the output of the AC/DC converter of one WEC in module 1 and DC bus voltage of module 1.

Fig. 5.10 shows the grid voltage and current when total power produced by the Wave Park is delivered to the grid. It has been assumed that the grid is demanding only real power. The real power can be calculated from the voltage and current as

$$P_{total} = P_{grid} = \sqrt{3} V_{grid} I_{grid} cos\theta = 1.89MW \quad (5.2)$$

here, V_{grid} and I_{grid} is the RMS grid voltage and grid current, respectively. The transmission cable draws very little amount of reactive power for 2MW system and power factor is almost equal to 1.

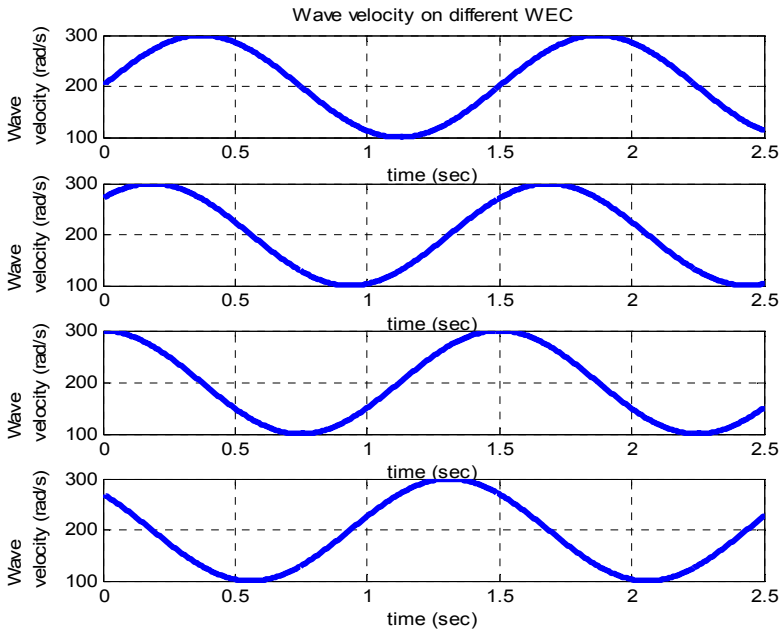

Figure 5.5. Wave velocity at different WECs of module 1

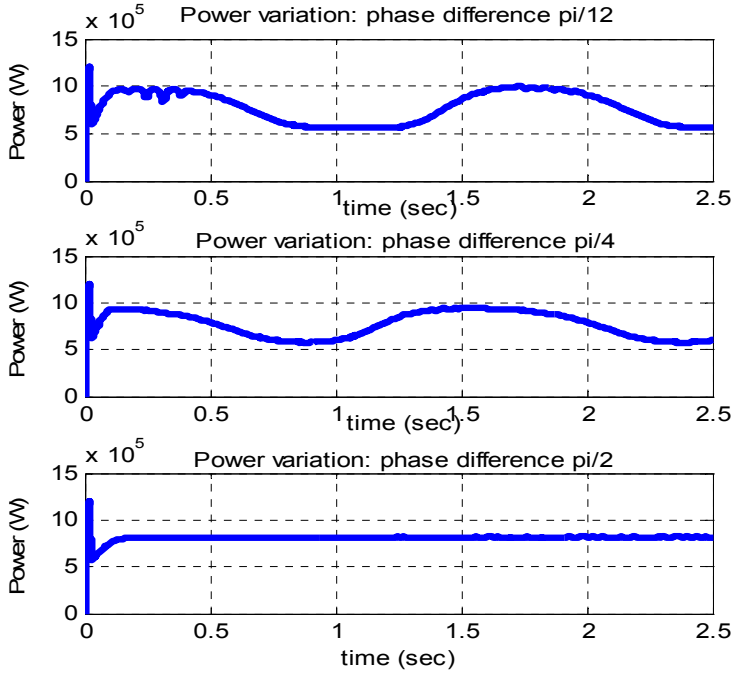

Figure 5.6. Power variation for phase difference of wave velocities on different WECs

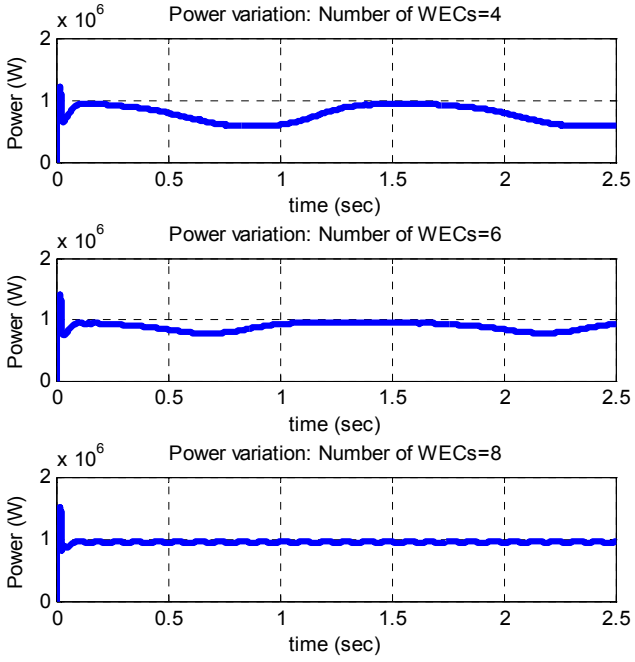

Figure 5.7. Power variation for number of WECs in the Wave Park

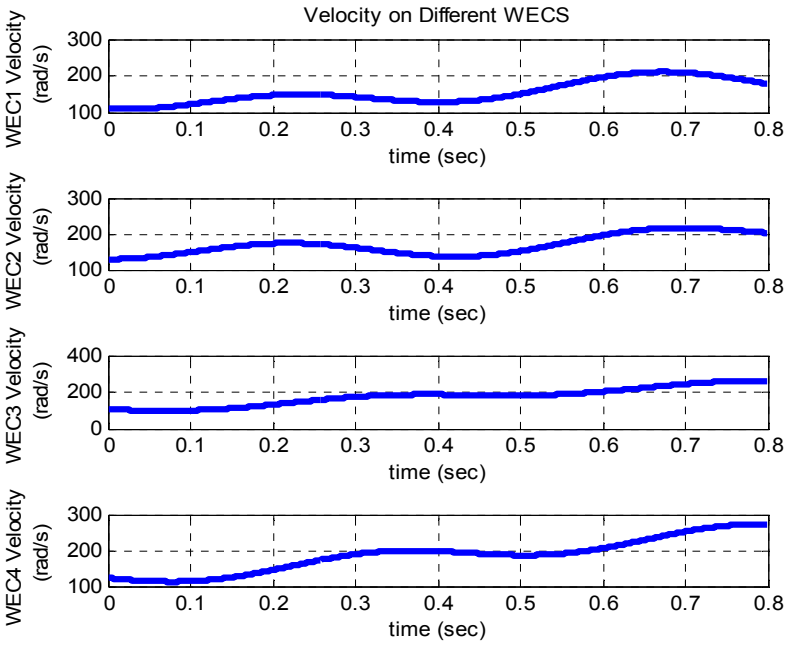

Figure 5.8. Wave velocity with composition of different sine wave at module 1

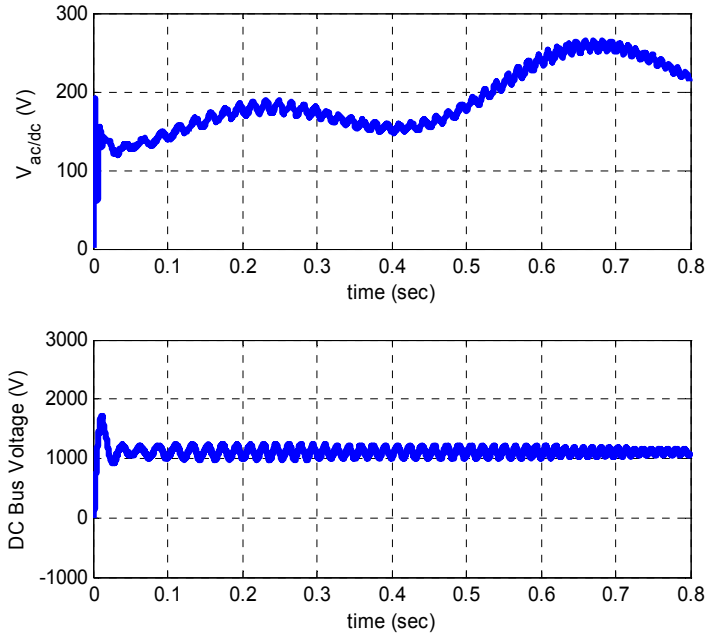

Figure 5.9. Output of AC/DC and DC/DC converter of module 1

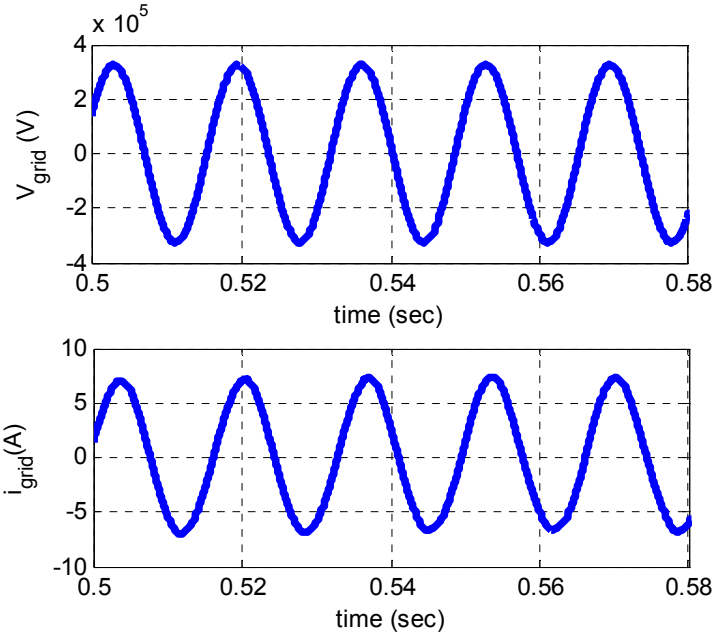

Figure 5.10. Grid voltage (L-L) and current of grid connected Wave Park

Due to the intermittent nature of the wave energy, sometimes energy produced by the Wave Park is higher than the grid demand and sometimes lower than the grid demand. Offshore storage system is used to supply required power to the grid using OCAES. An induction machine (IM) drive has been used for compression and expansion of the air in the OCAES system. Thus, the turbo-machinery is represented by an IM. When the wave generated power is higher than the grid demand, the induction machine works as a motor and compresses the air to store energy. But when the grid demand is higher than wave generated power, the induction machine works as a generator. In this case, the compressed air that was previously stored is expanded in the turbine connected to the IM to drive the machine as generator. Fig. 5.11 shows the overview of power flow to and from the storage system with the IM operating in motoring and generating regimes.

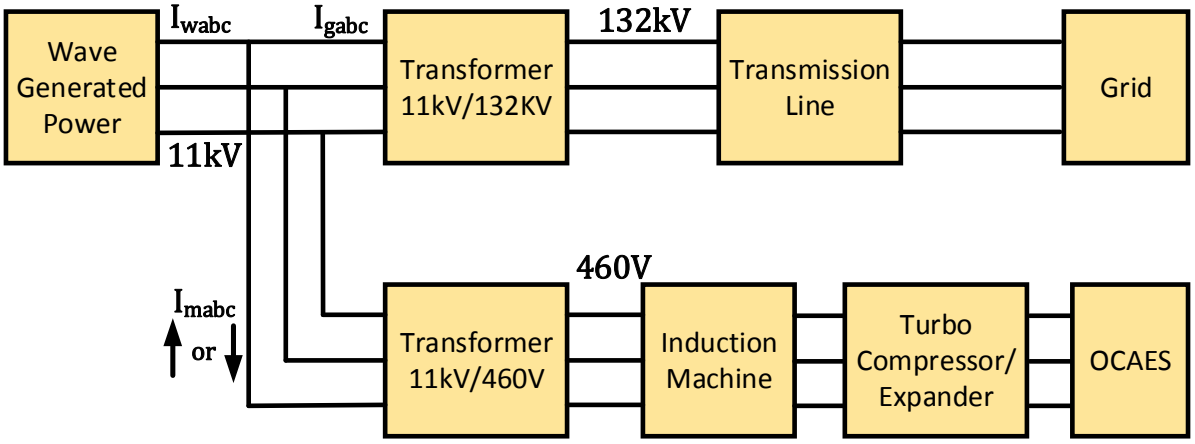

Figure 5.11. Wave park power flow among WECs, grid and storage

The grid may demand both real and reactive power. The real and reactive power generated by the wave park is controlled by the current controller. The induction machine power controller is shown in Fig. 5.12. Depending on the grid demand and wave park generated

power, the current command for IM is determined and the corresponding torque command is calculated. Figs. 5.13 and 5.14 show the simulation results with IM in OCAES.

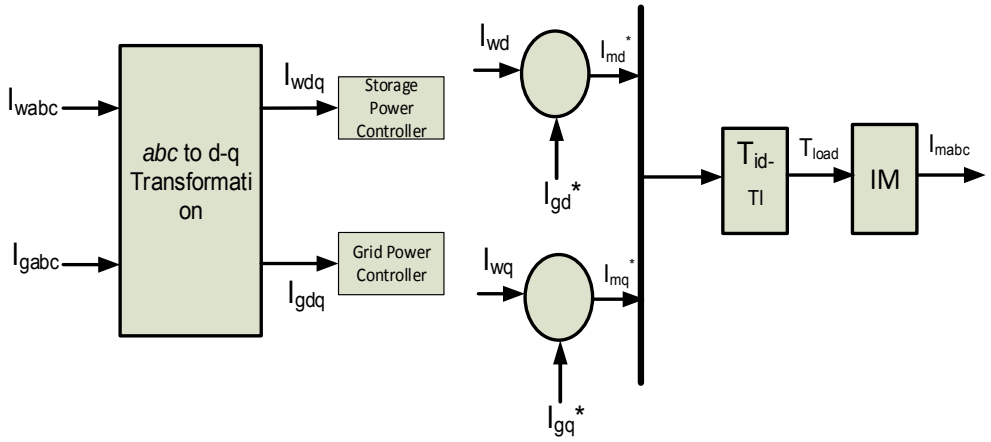

Figure 5.12. Induction machine power controller.

All currents are measured from 11kV lines. The *d*-axis currents are a measure of real power flow and *q*-axis currents are measure of reactive power flow. For example, in Fig. 5.13, *d*-axis current from the wave park $I_{wd} = 70A$ and *d*-axis current going to grid which is the measure of real power demand for grid, $I_{gd} = 50A$. Therefore, the wave park produces more real power than the grid demand and excess power goes to the IM which works as a motor to drive the OCAES by compressing the air. The *d*-axis current going to the IM in this case is $I_{md} = 20A$. If grid demand increases and becomes higher than the power produced by wave park, then additional power has to be supplied to the grid by the OCAES. This is achieved by expanding the previously stored air to drive the IM as a generator. Fig. 5.13 also shows the sudden increase of grid real power demand to 90A and thereby OCAES supplies additional 20A to meet the

demand. Here, the negative sign of I_{md} indicates that IM is working as generator as shown in Fig. 5.13. The corresponding q-axis components of currents for this scenario are shown in Fig. 5.14.

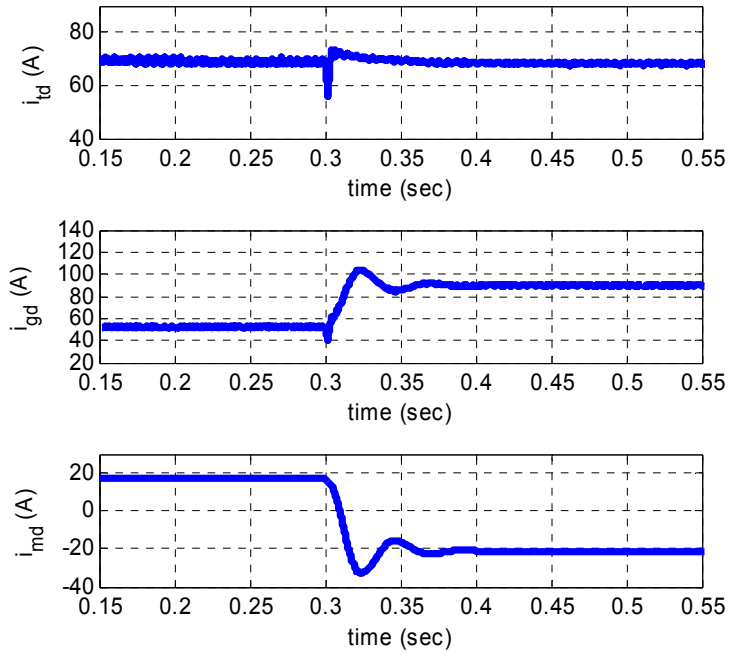

Figure 5.13. *d-axis* current when IM works as motor/generator.

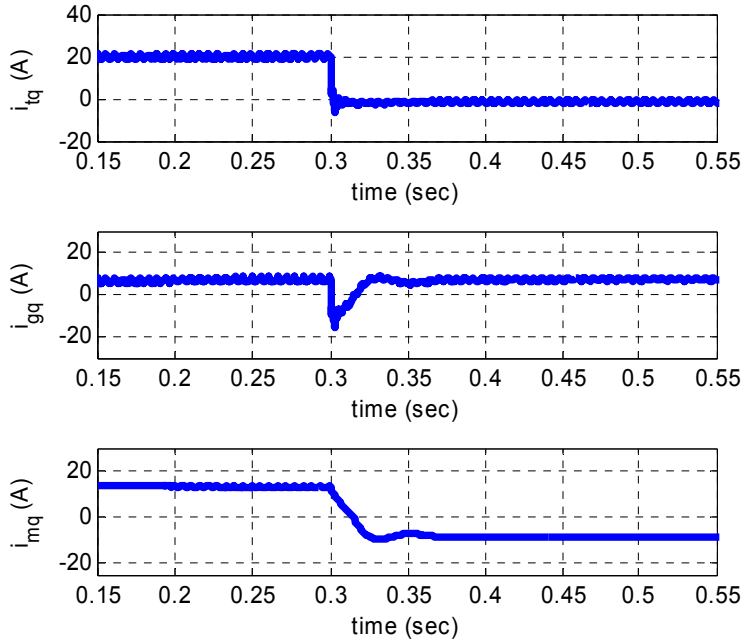

Figure 5.14. *q-axis* current when IM works as motor/generator

5.6.2 200MW Wave Park System

A Wave Park of capacity 200MW is considered for system level simulation. For a 200MW Wave Park, 200 of the WEC modules presented earlier with four 250kW WECs in a module are required. The transmission line and submarine cable capacity has to be changed to transmit higher amount of power. Transmission cables rating and specification for both 2MW and 200MW systems are presented in Table 5.4 [75]-[76]. The main challenge with a large Wave Park of 200MW is to overcome high reactive power requirement due to the high power transmission at higher voltage from offshore collector point to the onshore grid. For a 2MW system with longest submarine cable of 33kV requires less amount of reactive power as shown in Fig. 5.4 and inverter of the wave park and OCAES could meet the reactive power

requirement without oversizing the inverter. But for 200MW system with longest submarine cable of 132kV requires higher amount. In high voltage transmission system cable capacitance demands a large amount of charging current which worsen the power factor [78]. In this case static VAR compensator has been used to produce reactive power which also regulated the voltage at PCC. Fig. 5.15 shows the line to line voltage and phase current at grid tie point.

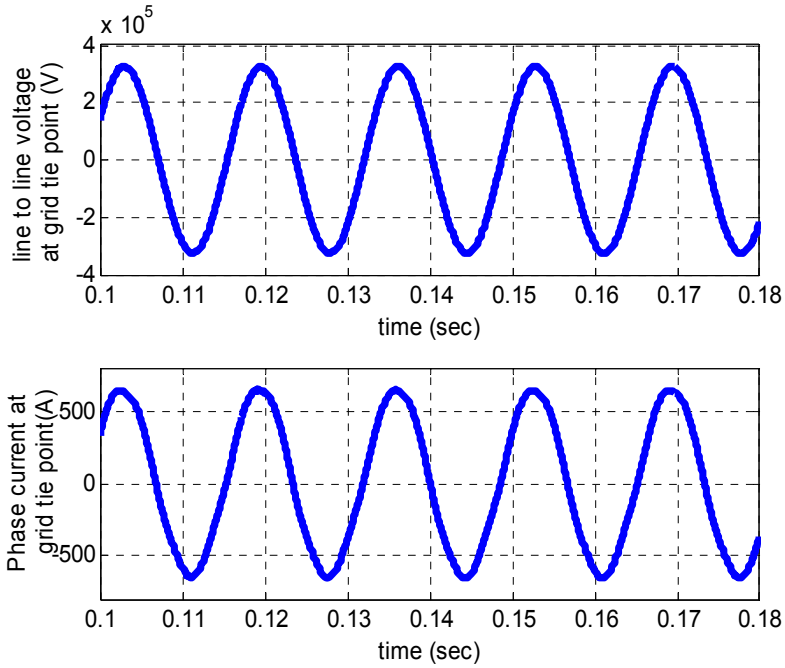

Figure 5.15. Grid voltage (L-L) and current of grid connected Wave Park

Table 5.4. Transmission Cable

System	Voltage Rating	Cable	Cross Section (mm^2)	Current Rating (Amp)	Comment
2 MW	11 kV Submarine Cable	XLPE 3 core cable of Copper Conductor	95	300	ABB XLPE cable. Larger cross section reduces the cable resistance.
	33 kV Submarine Cable	XLPE 3 core cable of Copper Conductor	95	300	ABB XLPE cable. Larger cross section reduces the cable resistance.
	33 kV Land Cable	Three core cable of Copper Conductor	95	270	ABB land cable.
200 MW	11 kV Submarine Cable	XLPE 3 core cable of Copper Conductor	95	300	ABB XLPE cable. Same as 2 MW system as each module rating is still 1MW.
	132 kV Submarine Cable	XLPE 3 core cable of Copper Conductor	500	655	For 200 MW this cable carries higher current. So voltage rating is higher than 2MW system to reduce transmission loss.
	132 kV Land Cable	Single core cable of Copper Conductor	500	655	Single core cables are formed in trefoil formation to minimize the sheath circulating currents induced by the magnetic flux linking the cable conductors

5.7 Conclusion

The chapter presents a new concept of ocean based energy storage system for load levelling of offshore wave energy devices. Basic system design concepts for the electrical connection

and grid control have been discussed. The challenges associated with the transmission have been discussed. A detailed description of the system simulation with grid connection and power flow control is provided. The simulation analysis provides an insight into the configurations that are the most suitable for achieving the optimal operational performance of the OCAES system. Although wave energy generation is used as an example in the simulation, the system can easily applied to other renewable sources such as wind energy.

Chapter 6: Summary and Future Work

This chapter provides a summary of the dissertation and proposes some future work on this research.

6.1 Summary

The present dissertation can be summarized as follows:

- In chapter 2, distributed voltage regulation using reactive power from the distributed inverters has been presented.
- A reactive power scheduler (RPS) has been proposed to produce reference reactive power for different distributed inverters based on the real power generation dictated by MPPT algorithm.
- The RPS has the ability to detect the reactive power capacity of each inverter in the system dynamically. The reactive power capacity may change with the change in environmental condition. In the perturbation state of RPS, this change can be monitored and used for new reactive power reference.
- The objective of the RPS is to regulate the voltage of the distribution node by using reactive power capacity of the RES after meeting the real power demand in such a way so that none of the inverters get overstressed and share the total reference reactive power in a balanced way. In this algorithm, inverters among the system have no communication with them but have minimum communication only with the RPS.

- In chapter 3, critical bus concept of a radial distribution system and sensitivity of the distributed inverters to the critical bus voltage has been considered.
- During high PV penetration critical bus inverter has to absorb high reactive power. There is a possibility that the critical bus inverter becomes saturated with its capacity and cannot absorb reference reactive power generated by existing methods.
- An improved central reactive power management system has been proposed in chapter 3 for overvoltage protection of radial distribution system during high PV penetration by effective utilizing the reactive power capacity of high sensitive inverters.
- The control of real and reactive power presented in chapter 2 and 3 requires proper estimation of phase angle and frequency of the grid voltage. An improved phase-locked loop (PLL) algorithm has been presented in chapter 4 for phase detection in case of impurity presents in the utility grid.
- Grid harmonics and unbalanced voltage are common impurities of the grid, typically for rural or distant distribution system. Impurity elimination technique has been presented for single phase and three-phase PLL grid synchronization. The proposed algorithm improves the PLL performance by reducing the phase estimation error even with high bandwidth of loop filter which ensures better dynamic performance as well.
- Apart from the distributed low scale renewable sources, large scale production has been considered these days to overcome the rapidly increasing energy demand of the world. This leads to the implementation of utility scale offshore wind or wave energy system. As the power levels of wave parks are usually several hundreds of megawatt and may

even increase into the future, connection points of such wave park migrate to the transmission network.

- A detailed analysis of offshore wave energy system has been presented in chapter 5. The technical challenges of transmission and grid connection of the energy coming from wave park have been discussed. Also, simulation results showing some solution for the intermittency reduction for 2MW and 200MW wave park were shown.

6.2 Future Work

- The voltage regulation work can be further extended by incorporating optimization algorithm in CRPMS method. The reference reactive power can be generated for each inverter in the system by the optimization of its sensitivity and remaining current carrying capacity at a certain moment. Also power factor should not go below the allowable range. The optimization may ensure better utilization of inverters reactive power capacity and reduced amount of reactive power flow in the system.

- A wireless communication can be considered in RPS algorithm for the communication between the scheduler and the inverters. Improved two way communication method has been introduced for smart grid operation with much reduced cost. It may be worth to investigate the feasibility of using this communication for RPS as it incorporates only two way communication between inverters and scheduler.

- The proposed grid synchronization algorithm is capable of removing unbalanced voltage effect from three-phase grid. In future work, fault ride through (FRT) operation can be studied using or modifying the proposed algorithm.

- In chapter 5, a large wave park of 200MW has been simulated and technical challenges have been pointed out for transmission of high power high voltage electricity to the grid through submarine cable. One of the solution to overcome high reactive power requirement may be to incorporate optimization of reactive power from concentrated sources such as VAR compensator and distributed reactive power sources. This will reduce the size of the concentrated source in offshore substation by utilizing the current capacity of the inverters associated with the WECs.

- A cost optimization for the proposed reactive power solution can also be considered in future research.

REFERENCES

[1] C. Whitaker, J. Newmiller, M. Ropp, B. Norris, "Renewable Systems Interconnection Study: Distributed Photovoltaic Design and Technology Requirements," SANDIA Report, SAND 2008-0946 P.

[2] Hiroyuki Hatta, Satoshi Uemura, Hiromu Kobayashi, "Demonstrative Study of Control System for Distribution System with Distributed Generation", *Power Systems Conference and Exposition, 2009.* PSCE '09. IEEE/PES, pp 1 – 6.

[3] A. Rahmati, A. Abrishamifar, and E. Abiri, "An DSTATCOM for compensating different abnormal line voltage and nonlinear load," in *IEEE International Conf. on Indus. Tech., ICIT 2006*, December 2006, pp. 756 – 761.

[4] N. G. Hingorani and L. Gyugyi, *Understanding FACTS: Concepts and Technology of Flexible AC Transmission Systems*, Wiley-IEEE Press, 2000.

[5] E. Twining and D. G. Holmes, "Voltage compensation in weak distribution networks using multiple shunt connected voltage source inverters," in *Proc. 2003 IEEE Power Tech Conf.*, Bologna, June 2003., pp. 8.

[6] N. Mariun, H. Masdi, S. M. Bashi, A. Mohamed, and S. Yusuf, "Design of a prototype DSTATCOM using DSP controller for voltage sag mitigation," *IEEE Power India Conference*, April 2006, pp.6.

[7] Sudipta Chakraborty, Benjamin Kroposki, William Kramer, "Evaluation of VAR Control and Voltage Regulation Functionalities in a Single-Phase Utility-Connected Inverter for

Distributed Energy Applications", *Energy Conversion Congress and Exposition, 2009.* ECCE 2009. IEEE, pp 1753 – 1759.

[8] Amarnath Tamersi, Ghadir Radman , Mehriar Aghazadeh , " Enhancement of Microgrid Dynamic Voltage Stabilty Using Microgrid Voltage Stabilizer", *Southeastcon, 2011 Proceedings of IEEE,* pp 368 – 373.

[9] Yilmaz Sozer and David A. Torrey, "Modeling and Control of Utility Interactive Inverters", *Power Electronics, IEEE Transactions,* Nov. 2009*,* pp 2475 – 2483.

[10] P. M. Anderson and A. A. Fouad, *Power System Control and Stabily*, 2nd Edition, Wiley Interscience 2003

[11] G.-C. Hsieh and J. C. Hung, "Phase-locked loop techniques. A survey," *IEEE Trans. Ind. Electron.*, vol. 43, no. 6, pp. 609–615, Dec. 1996.

[12] Se-Kyo Chung, "A Phase Tracking System for Three Phase Utility Interface Inverters," *IEEE Transaction on Power Electronics,vol 15, no. 3, May 2000.*

[13] V. Kaura and V. Blasko, "Operation of a phase locked loop system under distorted utility conditions", *IEEE Trans. Ind. Appl.*, vol. 33, no. 1, pp. 58-63, Jan./Feb. 1997.

[14] Fran González-Espín, Emilio Figueres, Gabriel Garcerá, "An Adaptive Synchronous-Reference-Frame Phase-Locked Loop for Power Quality Improvement in a Polluted Utility Grid", *IEEE Transactions on Industrial Electronics, Vol. 59, June 2012.*

[15] G. Saccomando and J. Svensson, "Transient operation of grid-connected voltage source converter under unbalanced voltage conditions," in *Proc. 36th IAS Annu. Meeting IEEE Ind. Appl. Conf.*, Sep./Oct.4, 2001, vol. 4, pp. 2419–2424.

[16] F. Freijedo, J. Doval-Gandoy, O. Lopez, and E. Acha, “A generic open-loop algorithm for three-phase grid voltage/current synchronization with particular reference to phase, frequency, and amplitude estimation,” *IEEE Trans. Power Electron.*, vol. 24, no. 1, pp. 94–107, Jan. 2009.

[17] D. Yazdani, A. Bakhshai, G. Joos, and M. Mojiri, “A nonlinear adaptive synchronization technique for grid-connected distributed energy sources,” *IEEE Trans. Power Electron.*, vol. 23, no. 4, pp. 2181–2186, Jul. 2008.

[18] D. Yazdani, A. Bakhshai, and P. Jain, “A three-phase adaptive notch filter-based approach to harmonic/reactive current extraction and harmonic decomposition,” *IEEE Trans. Power Electron.*, vol. 25, no. 4, pp. 914–923, Apr. 2010.

[19] Yi Fei Wang, Yun Wei Li, “Grid Synchronization PLL Based on Cascaded Delayed Signal Cancellation”, *IEEE Transaction on Power Electronics,Vol 26, no. 7, July 2011.*

[20] P. Rodriguez, A. Luna, R. Teodorescu, and F. Blaabjerg, “Grid synchronization of wind turbine converters under transient grid faults using a double synchronous reference frame PLL,” in *Proc. IEEE Energy 2030 Conf. (ENERGY)*, Nov. 2008, pp. 1–8.

[21] P. Rodriguez, A. Luna, R. Teodorescu, F. Iov, and F. Blaabjerg, “Fault ride-through capability implementation in wind turbine converters using a decoupled double synchronous reference frame PLL,” in *Proc. 2007 Eur. Conf. Power Electron. Appl.*, Sep., pp. 1–10.

[22] N. Mohan, T. M. Undeland, and W. P. Robbins, *Power Electronics. Converters, Applications, and Design*, 3rd ed. Hoboken, NJ: Wiley, 2003.

[23] M. H. Rashid, *Power Electronics Handbook*. New York: Academic, 2007, pp. 1–1152.

[24] Ali Elrayyah, Ali Safayet, Yilmaz Sozer, Iqbal Husain, Malik Elbuluk, "Novel Harmonic and Phase Estimator for Grid-Connected Renewable Energy Systems", *Energy Conversion Congress and Exposition (ECCE),* pp. 4683 – 4689, September 2012.

[25] C.L. Masters, "Voltage rise the big issue when connecting embedded generation to long 11 kV overhead lines," *Power Engineering Journal*, Vol. 16, Issue.1, pp 5-12, 2002.

[26] M. E. Elkhatib, R. E. Shatshat, and M. M. A. Salama, "Decentralized reactive power control for advanced distribution automation systems," *IEEE Trans. Smart Grid*, vol. 3, no. 3, pp. 1482–1490, Sep. 2012.

[27] L. F. Ochoa, C. J. Dent, and G. P. Harrison, "Distribution network capacity assessment: Variable DG and active networks," *IEEE Trans. Power Syst.*, vol. 25, no. 1, pp. 87–95, Feb. 2010.

[28] A. Mehrizi-Sani and R. Iravani, "Online set point adjustment for trajectory shaping in microgrid applications," *IEEE Trans. Power Syst.*, vol. 27, no. 1, pp. 216–223, Feb. 2012.

[29] A. Tamersi, G. Radman, and M. Aghazadeh, "Enhancement of microgrid dynamic voltage stabilty using microgrid voltage stabilizer," *Proc. IEEE Southeastcon*, pp. 368–373, Mar. 17–20, 2011.

[30] Mohamed Shawky El Moursi, , H. H. Zeineldin, James L. Kirtley, Jr., and Khaled Alobeidli, "A Dynamic Master/Slave Reactive Power-Management Scheme for Smart Grids With Distributed Generation," *IEEE Transactions On Power Delivery*, Vol. 29, No. 3, June 2014.

[31] Seyedmostafa Hashemi, Jacob Østergaard, andGuangya Yang, "Effect of Reactive Power Management of PV Inverters on Need for Energy Storage," *IEEE 39th Photovoltaic Specialists Conference (PVSC)*, June2013; Tampa, FL.

[32] T. Hazel, N. Hiscock, and J. Hiscock, "Voltage regulation at sites with distributed generation," *IEEE Trans. Ind. Appl*., vol. 44, no. 2, pp. 445–454, Mar./Apr. 2008.

[33] J. C. Vasquez, R. A. Mastromauro, J. M. Guerrero, and M. Liserre, "Voltage support provided by a droop-controlled multifunctional inverter," *IEEE Trans. Ind. Electron.*, vol. 56, no. 11, pp. 4510–4519, Nov. 2009.

[34] M. H. J. Bollen and A. Sannino, "Voltage control with inverter-based distributed generation," *IEEE Trans. Power Del.*, vol. 20, no. 1, pp. 519–520, Jan. 2005.

[35] J. Smith, W. Sunderman, R. Dugan, and B. Seal, "Smart inverter volt/var control functions for high penetration of PV on distribution systems," in *Proc. Power Syst. Conf. Expo. (PSCE)*, Phoenix, AZ, USA, 2011, pp. 1–6.

[36] E. Demirok, D. Sera, R. Teodorescu, P. Rodriguez, and U. Borup, "Evaluation of the voltage support strategies for the low voltage grid connected PV generators," *in Proc. Energy Convers. Congr. Expo. (ECCE*), Atlanta, GA, USA, 2010, pp. 710–717.

[37] R. Tonkoski, L. A. Lopes, and T. H. El-Fouly, "Coordinated active power curtailment of grid connected PV inverters for overvoltage prevention," *IEEE Trans. Sustain. Energy*, vol. 2, no. 2, pp. 139–147, Apr. 2011.

[38] P. Tenti, H. K. M. Paredes, and P. Mattavelli, "Conservative power theory, a framework to approach control and accountability issues in smart microgrids," *IEEE Trans. Power Electron.,* vol. 26, no. 3, pp. 664–673, Mar. 2011.

[39] S. Alyami, Y. Wang,, C. Wang, J. Zhao, and B. Zhao, "Adaptive Real Power Capping Method for Fair Overvoltage Regulation of Distribution Networks With High Penetration of PV Systems," *IEEE Transactions On Smart Grid*, Vol. 5, No. 6, November 2014.

[40] Y. Wang, P. Zhang, W. Li, W. Xiao, and A. Abdollahi, "Online Overvoltage Prevention Control of Photovoltaic Generators in Microgrids," *IEEE Transactions On Smart Grid*, Vol. 3, No. 4, December 2012.

[41] Li Yu, Dariusz Czarkowski, and Francisco de León, "Optimal Distributed Voltage Regulation for Secondary Networks With DGs," *IEEE Transactions On Smart Grid*, Vol. 3, No. 2, June 2012.

[42] J.-W. Choi, Y.-K. Kim and H.-G. Kim, "Digital PLL control for single-phase photovoltaic system," *Electric Power Applications, IEE Proceedings*, Volume:153, pp. 40-46, January 2006.

[43] D. Abramovitch, "Phase-locked loops: A control centric tutorial," in *Proc. Amer. Control Conf.*, Anchorage, AK, USA, 2002, vol. 1, pp. 1–15.

[44] P. Rodriguez, A. Luna, R. S. Muñoz-Aguilar, I. Etxeberria-Otadui, R. Teodorescu, and F. Blaabjerg, "A stationary reference frame grid synchronization system for three-phase grid-connected power converters under adverse grid conditions," *IEEE Trans. Power Electron.*, vol. 27, no. 1, pp. 99–112, Jan. 2012.

[45] R. Pereira, C. Da Silva, and L. Da Silva, "New strategies for application of adaptive filters in active power filter," *IEEE Trans. Ind. Appl.*, vol. 47, no. 3, pp. 1136–1141, May/Jun. 2011.

[46] P. Mattavelli, "A closed-loop selective harmonic compensation for active filters," *IEEE Trans. Ind. Appl.*, vol. 37, no. 1, pp. 81–89, Jan./Feb. 2001.

[47] P.A. Davies, "Wave-powered desalination: resource assessment and review of technology", Desalination (186) pp. 97-109, Elsevier, 2006.

[48] M. Alberdi, M. Amundarain, A. J. Garrido, I. Garrido, O. Casquero, and M. De la Sen , "Complementary Control of Oscillating Water Column-Based Wave Energy Conversion Plants to Improve the Instantaneous Power Output", *Energy Conversion, IEEE Transactions, Vol. 26,* pp. 1021-1032, Dec 2011.

[49] M. Molinas, O. Skjervheim, P. Andreasen, T. Undeland, J. Hals, T. Moan, B. Sorby, "Power electronics as grid interface for actively controlled wave energy converters", *Clean Electrical Power, 2007. ICCEP '07. International Conference*, May 2007, pp. 188-195.

[50] C.E. Jones, S.J. Finney, C.S. Parry, "Regulating DC link voltage fluctuations on a grid connected wave power system using energy storage", *Renewable Power Generation (RPG 2011), IET Conference on*, Sept. 2011, pp. 1-6.

[51] Zanxiang Nie, Xi Xiao, Hu Yi, Qing Kang, "Direct drive wave energy converters integrated with a composite energy storage system", *Electrical Machines and Systems (ICEMS), 2011 International Conference*, Aug. 2011, pp. 1-5.

[52] M. Vahedipour Dahraie, H. R. Najafi R. Nasirzadeh Azizkandi M.R. Nezamdoust, "Study on compressed air energy storage coupled with a wind farm", *Renewable Energy and Distributed Generation (ICREDG), 2012 Second Iranian Conference*, March 2012, pp. 147 – 152.

[53] V. Vongmanee, V. Monyakul, "A new concept of small-compressed air energy storage system integrated with induction generator ", *Sustainable Energy Technologies, 2008. ICSET 2008. IEEE International Conferenc*e, Nov. 2008, pp. 866 – 871.

[54] R. Seymour, "Undersea Pumped Storage for Load Leveling", *Proceedings, California and the World's Oceans*, '97, San Diego, CA, pp. 158-163.

[55] A. von Jouanne, Ted Brekken, "Overview of wave energy activities at Oregon State University", available: www.oregonstate.edu.

[56] R. Yemm, "Pelamis", in Ocean Wave Energy , Ed. J. Cruz , pp 304-321, Springer 2008.

[57] Shek J.K.H., Macpherson D.E., Mueller M.A., Xiang J., "Reaction force control of a linear electrical generator for direct drive wave energy conversion*," IET Renew. Power Gener.*1, pp. 17‐24, 2007.

[58] T. Ackermann, N. N. Barberis, J. Todorovic, and L. Lazaridis, "Evaluation of electrical transmission concepts for large offshore wind farms," in *Proc. Copenhagen Offshore Wind Conf. Expo.*, Copenhagen, Denmark, 2005.

[59] E. Twinning and D. G. Holmes, "Grid current regulation of a three phase voltage source inverter with an LCL input filter," *IEEE Trans. Power Electron.*, vol. 18, no. 3, pp. 888–895, May 2003.

[60] H. Tao, J. L. Duarte, and M. A. M. Hendrix, "Control of grid-interactive inverters as used in small distributed generators," in *Proc. IEEE 42nd Annu. Meeting Ind. Appl. Conf.*, Jun. 2008, pp. 1498–1502.

[61] R. Krismadinata, N. A. Rahim, and J. Selvaraj, "Implementation of hysteresis current control for single-phase grid connected inverter," *in Proc. 7th Int. Conf. Power Electron*. Drive Syst., Nov. 2007, pp. 1097–1101.

[62] T. Ahmed, "Electrical Technologies for Grid Integration of Ocean Wave Power into the UK National Grid," *Journal of Power Electronics*, vol.3, no. 10, May 2010

[63] Pickard W F., Shen A Q., Hansing N J., "Parking the power: Strategies and physical limitations for bulk energy storage in supply–demand matching on a grid whose input power is provided by intermittent sources*", Renewable and Sustainable Energy Reviews* 2009;13:1934-1945.

[64] Evans A, Strezov V, Tim J. Evans, "Assessment of utility energy storage options for increased renewable energy penetration", *Renewable and Sustainable Energy Reviews* 2012;16:4141-4147.

[65] Rastler D. Electric energy storage technology options: a white paper primer on applications, costs, and benefits. Palo Alto, CA: EPRI; 2010.

[66] Zweibel K, Mason J, Fthenakis V. A solar grand plan. Sci Am 2008;298:64–73.

[67] Kondoh J, Ishii I, Yamaguchi H, Murata A, Otani K, Sakuta K, et al. "Electrical energy storage systems for energy networks". Energy Convers Manage 2000;41:1863–74.

[68] Honghai K, Zhengqiu W. "Research of super capacitor energy storage system based on DG connected to power grid". *In: International Conference on Sustainable Power Generation and Supply*, 2009. SUPERGEN '09. IEEE. 2009. pp. 1–6.

[69] Yang C-J, Jackson RB. "Opportunities and barriers to pumped-hydro energy storage in the United States", *Renew Sustain Energy Rev* 2011;15:839–44.

[70] Dursun B, Alboyaci B. "The contribution of wind-hydro pumped storage systems in meeting Turkey's electric energy demand". *Renew Sustain Energy Rev* 2010;14:1979–88.

[71] Fang X, Kutkut N, Shen J, Batarseh I. Analysis of generalized parallelseries ultracapacitor shift circuits for energy storage systems. Renew Energy 2011;36:2599–604.

[72] Vazquez S, Lukic SM, Galvan E, Franquelo LG, Carrasco JM. Energy storage systems for transport and grid applications. *IEEE Trans Ind Electron* 2010; 57:3881–95.

[73] Zhou Z, Benbouzid M, Charpentier J F, Scuiller F, Tang T, "A review of energy storage technologies for marine current energy systems", *Renewable and Sustainable Energy Reviews* 2013;18:390-400.

[74]] Ho, T.C.Y. , Li Ran, "A study on the electrical system arrangement for offshore wind turbines and factors influencing the voltage level choice", *Power Electronics for Distributed Generation Systems (PEDG*), 2012 3rd IEEE International Symposium, June 2012, pp. 442-449.

[75] ABB, "XLPE cable systems user's guide," [Online]. Available: http://www.abb.com

[76] ABB, "HVDC light, submarine and land cables," [Online]. Available: http://www.abb.com

[77] Ted K. A. Brekken, Hannes Max Hapke, Chad Stillinger, Joe Prudell, "Machines and Drives Comparison for Low-Power Renewable Energy and Oscillating Applications", *IEEE Transactions on Energy Conversion*, Vol. 25, no. 4, December 2010, pp. 1162-1170.

[78] Takahiro Kase, Yasuhiro Kurosawa, Hidenari Amo, "Charging Current Compensation for Distance Protection", *IEEE Transactions on Power Delivery*, Vol. 23, no. 1, January 2008, pp. 124-131

[79] D.L. O'Sullivan, G. Dalton, A.W. Lewis, "Regulatory, technical and financial challenges in the grid connection of wave energy devices," *IET Renew. Power Gener.*, Vol. 4, Iss. 6, pp. 555–567, 2010

[80] Molinas M., Skjervheim O., Sørby B., Andreasen P., Lundberg S., Undeland T., "Power smoothing by aggregation of wave energy converters for minimizing electrical energy storage requirements," *European Wave and Tidal Energy Conf.*, Porto, 2007.

[81] Henderson R.. "Design, simulation, and testing of a novel hydraulic power take-off system for the Pelamis wave energy converter," Renew. Energy, 31, pp. 271–283, 2006

[82] Kofoed J.P., Frigaard P., Friis-Madsen E., Sørensen H.C., "Prototype testing of the wave energy converter wave dragon", Renew. Energy, 31, pp. 181–189, 2006.

[83] P. Igic, Z. Zhou, W. Knapp, J. MacEnri, H.C. Sørensen, E. Friis-Madsen, "Multi-megawatt offshore wave energy converters - electrical system configuration and generator control strategy," *IET Renew. Power Gener.*, Vol. 5, Iss. 1, pp. 10–17, 2011.

[84] M. Rahm, O. Svensson, C. Bostrom, R. Waters, M. Leijon, "Experimental results from the operation of aggregated wave energy converters," *IET Renew. Power Gener.*, Vol. 6, Iss. 3, pp. 149–160, 2012.

[85] Eric D. Stoutenburg and Mark Z. Jacobson, "Reducing Offshore Transmission Requirements by Combining Offshore Wind and Wave Farms*," IEEE Journal Of Oceanic Engineering*, Vol. 36, No. 4, October 2011.

[86] I. M. de Alegría, J. L. Martín, I. Kortabarria, J. Andreu, and P. I. Ereño, "Transmission alternatives for offshore electrical power," *Renew. Sustain. Energy Rev.*, vol. 13, no. 5, pp. 1027–1038, 2009.

[87] W. L. Kling, R. L. Hendriks, and J. H. den Boon, "Advanced Transmission Solutions for Offshore Wind Farms," *IEEE Power and Energy Society General Meeting - Conversion and Delivery of Electrical Energy in the 21st Century*, 2008.

[88] B. van Eeckhout, D. van Hertem, M. Reza, K. Srivastava, and R. Belmans, "Economic comparison of VSC HVDC and HVAC as transmission system for a 300 MW offshore wind farm," *Eur. Trans. Electr. Power*, vol. 20, no. 5, pp. 661–671, Jul. 2010, DOI: 10.1002/etep.359.

[89] T. Ackermann, N. Barberis Negra, J. Todorovic, and L. Lazaridis, "Evaluation of electrical transmission concepts for large offshore wind farms," presented at the Copenhagen Offshore Wind-Int. Conf. Exhib., Copenhagen, Denmark, Oct. 2005.

[90] L. Lazaridis, "Economic comparison of HVAC and HVDC solutions for large offshore windfarms under special consideration of reliability," M.S. thesis, Dept. Electr. Eng., Royal Inst. Technol., Stockholm, Sweden, 2005.

[91] A. Reidy and R. Watson, "Comparison of VSC based HVDC and HVAC interconnections to a large offshore wind farm," in *IEEE Power Eng. Soc. General Meeting*, 2005, DOI: 10.1109/PES.2005.1489081.

[92] ABB AB Grid Systems—HVDC, "It's time to connect—Technical description of HVDC Light® Technology," 2010 [Online]. Available: http://www.abb.com/industries/db0003db004333/add2081b520d929ac12574810034c0c4.aspx

[93] P. Bresesti, W. L. Kling, R. L. Hendriks, and R. Vailati, "HVDC connection of offshore wind farms to the transmission system," *IEEE Trans. Energy Conv.*, vol. 22, no. 1, pp. 37–43, Mar. 2007.

[94] E. D. Stoutenburg, N. Jenkins, and M. Z. Jacobson, "Power output variations of co-located offshore wind turbines and wave energy converters in California," *J. Renew. Energy*, vol. 35, pp. 2781–2791, 2010, DOI: 10.1016/j.renene.2010.04.033.

[95] G. Guidi, and O. B. Fosso. "Investment Cost of HVAC Cable Reactive Power Compensation Off-shore," 2nd IEEE ENERGYCON Conference & Exhibition, 2012.

[96] Erhan Demirok, Pablo Casado Gonz´alez, H. B. Frederiksen, Dezso Sera, Pedro Rodriguez, and Remus Teodorescu, "Local Reactive Power Control Methods for

Overvoltage Prevention of Distributed Solar Inverters in Low-Voltage Grids,*" IEEE Journal Of Photovoltaics*, Vol. 1, No. 2, December 2011.

[97] R. Aghatehrani and R.Kavasseri, "Reactive powermanagement of a DFIG wind system in microgrids based on voltage sensitivity analysis," *IEEE Trans. Sustainable Energy,* vol. 2, no. 4, pp. 451–458, Oct. 2011.

[98] Hen-Geul Yeh, Dennice F. Gayme, and Steven H. Low, "Adaptive VAR Control for Distribution Circuits With Photovoltaic Generators," *IEEE Trans. on Power Systems,* Vol. 27, No. 3, pp. 1656–1663, August 2012.

[99] M. E. Baran and F. F.Wu, "Optimal Capacitor Placement On Radial Distribution Systems," *IEEE Trans. Power Del.,* vol. 4, no. 1, pp. 725–734, Jan. 1989.

[100] M. E. Baran and F. F. Wu, "Optimal Sizing Of Capacitors Placed On A Radial Distribution System," *IEEE Trans. Power Del.,* vol. 4, no. 1, pp. 735–743, Jan. 1989.

[101] J. Carrasco,L.Franquelo, J. Bialasiewicz,E.Galván, R. P. Guisado,M. M. Prats, J. León, and N. Moreno-Alfonso, "Power-electronic systems for the grid integration of renewable energy sources: A survey," *IEEE Trans. Ind. Electron*., vol. 53, no. 4, pp. 1002–1016, 2006.

[102] M. Farivar, C. R. Clarke, S. H. Low, and K.M. Chandy, "Inverter VAR control for distribution systems with renewables," *in Proc. Int. Conf. Smart Grid Communication*, 2011.

[103] Maher Abdelkhalek Azzouz, Mostafa F. Shaaban and Ehab F. El-Saadany, "Real-Time Optimal Voltage Regulation for Distribution Networks Incorporating High Penetration of PEVs," *IEEE Trans. On Power Systems*, Vol. 30, No. 6, pp. 3234-3245, November 2015.

[104] Q. Zhou and J. W. Bialek, "Generation curtailment to manage voltage constraints in distribution networks," *Generation Transm. Distribution*, vol. 1, no. 3, pp. 492–498, May 2007.

[105] Gustavo Valverde and Thierry Van Cutsem, "Model Predictive Control of Voltages in Active Distribution Networks," *IEEE Trans. On Smart Grid*, Vol. 4, No. 4, pp. 2152-2161, December 2013.

[106] Hany E. Farag, Ehab F. El-Saadany, and Ravi Seethapathy, "A Two Ways Communication-Based Distributed Control for Voltage Regulation in Smart Distribution Feeders," *IEEE Transactions On Smart Grid*, Vol. 3, No. 1, pp. 271-281, March 2012

[107] Baosen Zhang, Albert Y.S. Lam, Alejandro D. Domínguez-García, and David Tse, "An Optimal and Distributed Method for VoltageRegulation in Power Distribution Systems," *IEEE Transactions on Power Systems*, Vol. 30, No. 4, pp. 1714-1726, July 2015.

[108] Petra Solar RFI Response Document Innovative Renewable Distributed Energy Technology. South Plainfield, NJ, USA, May 30, 2012. Available on: http://www.nyenergyhighway.com/Content/documents/115.pdf

[109] American National Standard for Electric Power Systems and Equipment, ANSI C84.1, 1995.

[110] Ali Safayet, Iqbal Husian, Yilmaz Sozer, “Reactive power scheduler for voltage regulation of distributed energy systems,” *Energy Conversion Congress and Exposition (ECCE),* pp. 2996–3002, Denver, CO, 2013.

[111] J. Zhao, D. Shi and R. Sharma, "Microgrid Reactive Power Management During and Subsequent to Islanding Process," *2014 IEEE PES Transmission and Distribution Conference and Exposition*, Apr. 2014.

[112] Ali Safayet, Iqbal Husain, Ali Elrayyah, Yilmaz Sozer, “Grid harmonics and voltage unbalance effect elimination for three-phase PLL grid synchronization algorithm,” *Energy Conversion Congress and Exposition (ECCE),* pp. 3299–3304, Denver, CO, 2013.

[113] Ali Safayet, Poria Fajri, Iqbal Husain, “Reactive Power Management for Overvoltage Prevention at High PV Penetration in Low Voltage Distribution System,” *Energy Conversion Congress and Exposition (ECCE)*, pp. 1988–1994, Montral, Canada, 2015.

[114] Emmanuel Agamloh, Iqbal Husain, Ali Safayet, “Investigation of the Electrical System Design Concept and Grid Connection of Ocean Energy Devices to an Offshore Compressed Energy Storage System,” *Energy Conversion Congress and Exposition (ECCE),* pp. 2819–2826, Raleigh, NC, 2012.